University of California, Los Angeles
Mechanical, Aerospace and Nuclear Engineering Department

DESIGN OF A SCIENTIFIC PROBE FOR OBTAINING MARS SURFACE MATERIAL

FINAL REPORT

Participating Students (Term #1):

Miles Baker
Eric Deyerl
Tim Gibson
Bob Langberg
Terrance Yee, Report Editor

Instructor:

R. X. Meyer, Adjunct Professor

Sponsored by NASA/USRA

June 15, 1990

MSP SPECIFICATIONS

OBJECTIVE: Return 1Kg martian soil sample from the surface of mars to a mothership in a 600km mars orbit.

STRUCTURE:

overall height : 1.2 meters (touchdown configuration)
1.5 meters (stowed/descent configuration)
overall width : 0.66 meters (touchdown configuration)
1.5 meters (stowed/descent configuration)
maximum gross vehicle mass: 110.25 Kg (after mothership separation)
mass at return: 2.00Kg (includes 1Kg sample)
planform: 3-legged layout with hexagonal bus
materials: Beryllium(launch rings, sample retrieval system, heat shield backing, landing gear main struts)
Magnesium (shock absorbers, landing gear secondary struts, bus frame)
Aluminum (bus platform, vehicle skin)

PROPULSION

deorbit/descent/ascent: 1 single restartable liquid propellant motor,pressure fed, using 50%UDMH, 50%Hydrazine as a fuel and nitrogen tetroxide as oxidizer
apogee kick(rendezvous): solid propellant motor
maneuvering: (8) thrusters using UDMH as propellant

MISSION PROFILE

0 - 1

This mission begins with detachment from the mother ship, the Mars Orbiting Vehical (MOV) of the designed spacecraft, the Mars Surface Probe (MSP). After separation the MSP determines its position and the relative position of the landing sight and initiates a short burn which will cause the MSP to be at our optimum position for deorbit within seven days. During this time the ship is in a dormant mode with occasional systems checks made by a monitoring microcomputer. Adjustments to the precession orbit are periodically made. When the MSP is in the correct location to descend with a minimum fuel expendature and no plane change, the main motor fires, deccelerating the ship.

1 - 2

The MSP turns around to face its heat shield toward the direction of flight. When the atmosphere is encountered at about 200-150km altitude the ship releases a kind of "drogue chute" for passive stability during descent.

2 - 3

The MSP sheds velocity during reentry, protected by its heatshield and a multilayer insulation. At 1km above the actual ground surface a parachute is deployed to slow the craft even further. The heat shield is jettisoned with explosive bolts. After slowing to 42 m/s and drifting to within 100 meters of the surface the chute is released and the main motor fires to bring the craft to a standstill 5 meters above the surface.

3 - 4

After stopping 5 meters above the surface the main motor shuts down and the MSP falls freely to avoid contamination of soil samples. Once safely on the ground a shovel type mechanism deploys and begins collecting sample soil.

4 - 5

Once the sample has been collected and stored the ship waits for half a martian day until the MOV orbit will be nearly overhead. The MSP ascent stage separates from the hexagonal descent stage leaving spent fuel tanks, the sample collector, the landing gear, and other used parts.

5 - 6

The ascent stage climbs out of the atmosphere using the main liquid motor for the last time.

6-7

The ascent stage burns out. The computer points the rendevous stage in the right direction, spins it up and releases it. There is no active guidance on the rendevous stage.

7-8

The rendevous stage makes its solid motor burn and activates its beacon for the MOV to find it. Its orbit differs slightly from the MOV so the two will eventually pass each other.

8-9

The MOV catches up to the rendevous stage and brings it inside the docking bay which originally held the full MSP and then secures it for the return trip.

MSP Mission Scenario

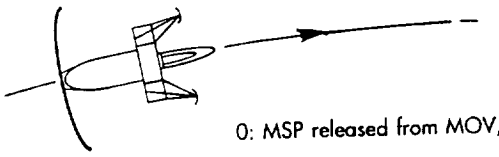

0: MSP released from MOV, main liquid motor burn

1: End of burn, reorientation of MSP

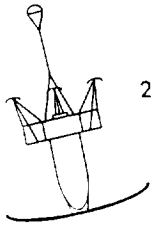

2: Descent through atmosphere, deployment of guide/drogue chute

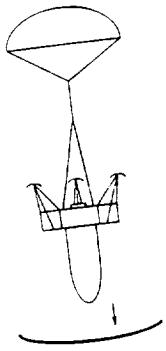

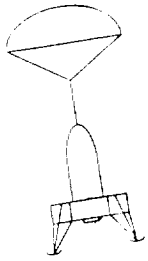

3: Chute release, main engine retro firing

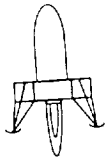

4: Sample acquisition

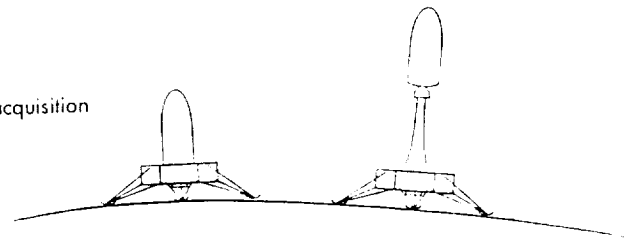

5: Ascent stage separation

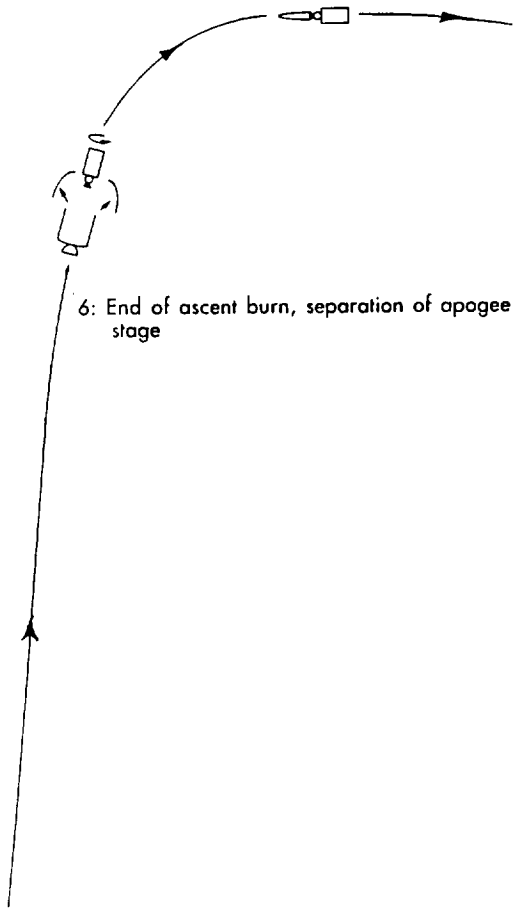

6: End of ascent burn, separation of apogee stage

7: Solid apogee motor burn and orbital insertion

Mass:	Final (on orbit):	
	Dirt:	1.00 (kg)
	Sample Container:	0.10 (kg)
	Apogee Engine Case:	0.25 (kg)
	Beacon:	0.30 (kg)
	Batteries/solar cells:	0.15 (kg)
	Structure:	0.20 (kg)
	Total:	2.00 (kg)
	Before Separation:	
	Apogee Stage:	2.00 (kg)
	Apogee Fuel:	0.73 (kg)
	Apogee Stage Support:	0.90 (kg)
	Fuel and Helium Tanks:	3.10 (kg)
	Valves and Regulators:	0.50 (kg)
	Aeroshell:	1.80 (kg)
	Guidance and Control:	2.00 (kg)
	Batteries:	0.10 (kg)
	Liquid Engine and Plumbing:	2.00 (kg)
	Engine Structural Support:	0.90 (kg)
	Thermal Insulation:	0.50 (kg)
	Attitude Control:	0.50 (kg)
	Total:	15.03 (kg)
	Ascent Stage Before Liftoff:	
	Ascent Stage Dry Mass:	15.03 (kg)
	Ascent Fuel (5% ullage):	44.17 (kg)
	Total:	59.20 (kg)
	Mass on Mars:	
	Ascent Stage:	59.20 (kg)
	Descent Tanks and Plumbing:	1.50 (kg)
	Landing Gear:	1.50 (kg)
	Payload Scoop:	15.00 (kg)
	Batteries:	0.80 (kg)
	Laser Range Finder:	1.00 (kg)
	Landing Computer:	1.00 (kg)
	Attitude Control:	0.50 (kg)
	Thermal Insulation:	1.50 (kg)
	Structure:	7.55 (kg)
	Total:	89.55 (kg)
	Mass at Re-entry:	
	Landing Mass:	89.55 (kg)
	Retro Fuel:	3.00 (kg)
	Parachute:	2.00 (kg)
	Parachute Canister:	0.30 (kg)
	Heat Shield and Supports:	5.00 (kg)
	Drogue Basket:	2.00 (kg)
	Total:	101.85 (kg)
	Initial (On-Orbit) Mass:	
	Re-entry mass:	101.85 (kg)
	Descent Fuel:	7.57 (kg)
	Orbital Maneuvering Fuel:	0.83 (kg)
	Total:	110.25 (kg)

Table (
MSP Mass Estimates

Contents

Section A: **Structural Design and Component Placement**
Eric Deyerl

Section B: **Thermal Control and Guidance**
Terrance Yee

Section C: **Propulsion Systems**
Myles Baker

Section D: **Orbital Mechanics**
Bob Langberg

Section E: **Specialized Structures**
Tim Gibson

Section A:

Structural Design and Component Placement

Eric Deyerl

1. Goal

To provide the most compact (space and weight efficient) structure to unite, protect, and allow effective operation of all spacecraft components.

2. Development

2.1 Research

Much research was accomplished, mainly through the perusal of large amounts of NASA technical reports (see References). Here, the designer focused his attention on reports that dealt with landing gear and spaceframe studies. Most specifically, there were two NASA projects that provided the most insight in these areas; those were the Surveyor and Apollo programs. (Figures 1 and 2).Although both of these missions were lunar in objective, they had similar parameters in their missions, and so were valuable in the information they provided.

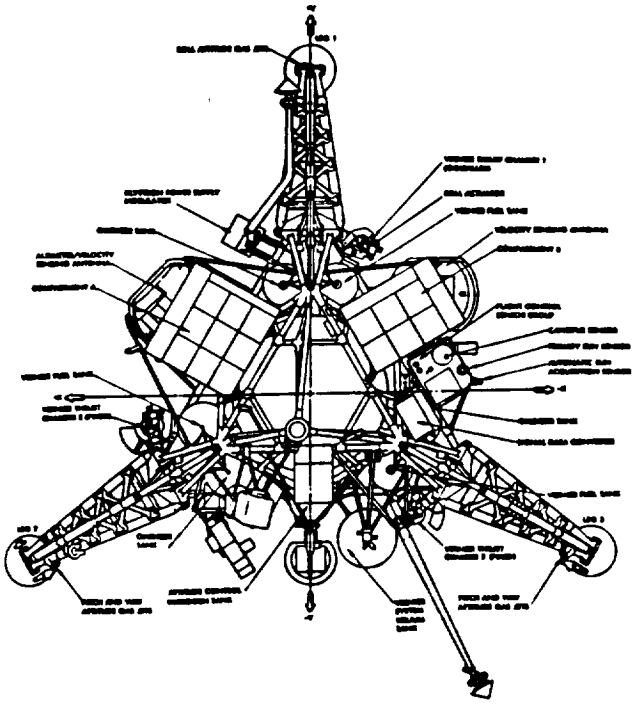

Figure 1: Surveyor spacecraft

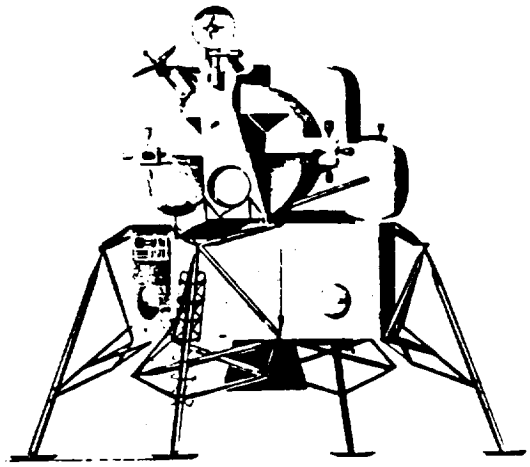

Figure 2: Apollo lunar lander

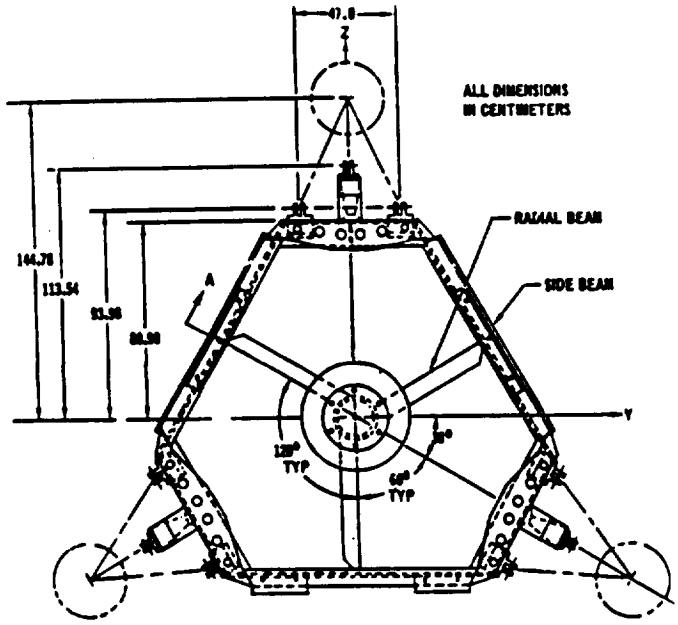

Figure 3: Generic three-legged lander planform

The surveyor three-legged layout was inspirational for the MSP designer. It is simplistic and effective, and had been used successfully in the Viking mission to Mars. (Refer to Figures 3 and 4) With three legs, one can be sure that all footpads will be in contact with the Martian soil upon landing. The three-legged design also allowed nicely for a structural-rigid hexagonal bus structure. Finally, it is also a stable platform whose shape makes it difficult for surface winds to catch a broad side of the craft and topple it.

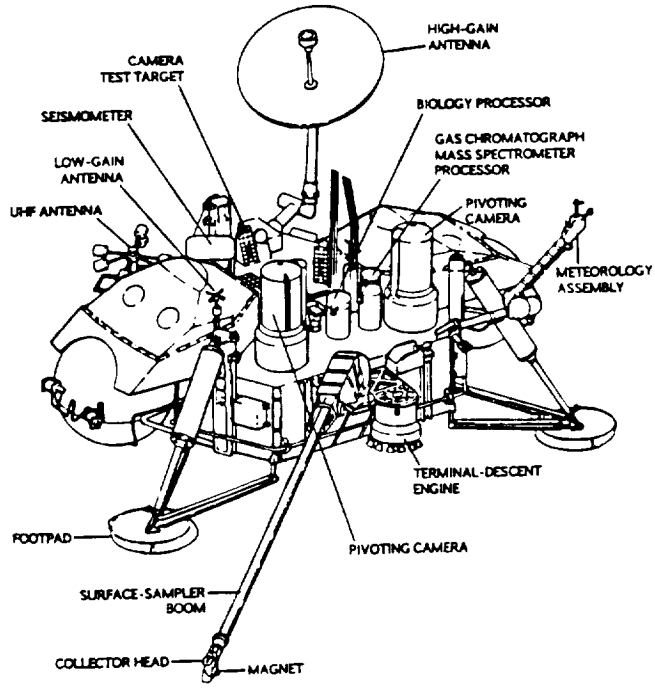

Figure 4: Viking spacecraft

The surveyor project also gave valuable insight into landing gear and shock absorber design, in conjunction with the placement of crushable honeycomb material. (Figure 5)

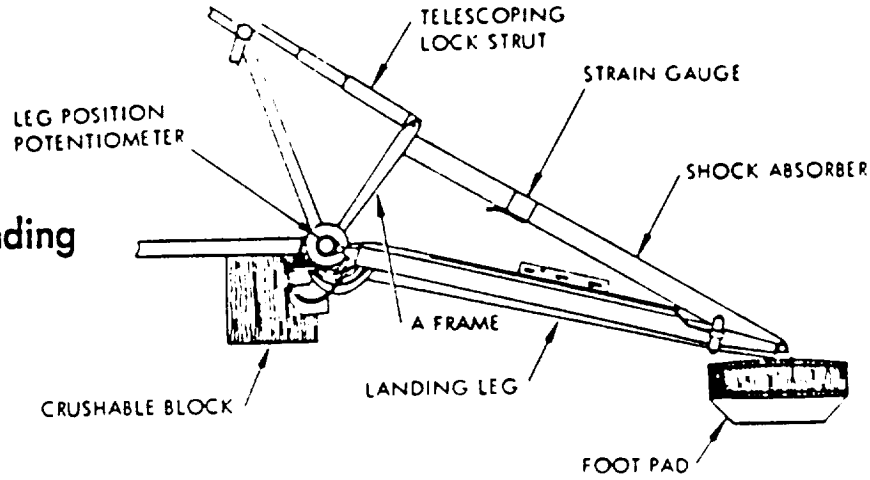

Figure 5: Surveyor landing gear leg

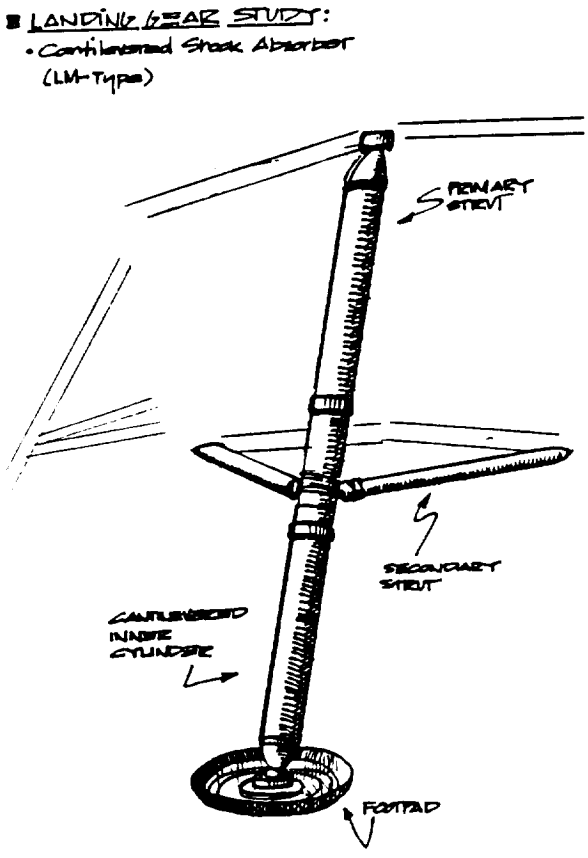

Figure 6: Apollo lunar lander landing gear leg

The Apollo Lunar Module's landing gear was also studied in an effort to incorporate a similar retracting system on the MSP. This was later found unnecessary. A rendition of one of the "Eagle's" gear is found in Figure 6.

2.2 Preliminary Layout Studies

Prior to much of the research, preliminary sketches were made to seek out viable spacecraft layouts. Two early plans and some notes on each are given in Figures 7 and 8.

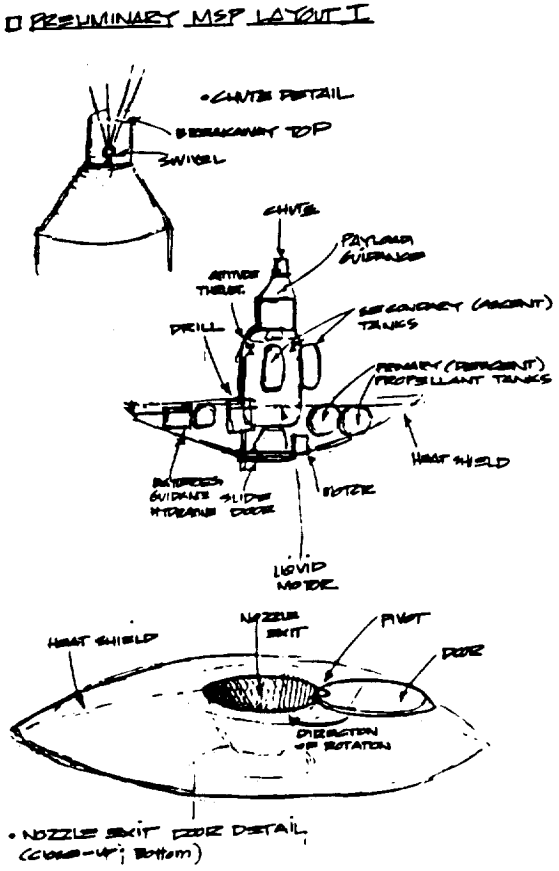

PRELIMINARY MSP I: COMMENTS

ASSETS:

1. Use of liquid main engine eliminates need for separate de-orbit, descent, and ascent solid motors
2. Bread-based heat shield allows for surface discontinuities, thus eliminating need for more complex landing structure (legs, shock absorbers, etc.)
3. Throttleable main engine can aid in descent so parachute may be cut early, preventing any interference with MSP.
4. Large shield allows for mounting of much hardware that can be left behind on Martian

LIABILITIES

1. Use of single liquid engine may incur weight penalties in form of additional hardware (tanks, plumbing, pumps)
2. Door in heat shield may not be feasible due to complexity and possible imperfect sealing.
3. Use of bread shield for landing may incur difficulties on a surface with large discontinuities.

Figure 7: First preliminary MSP layout sketch and comments

Figure 8: Second preliminary MSP layout sketch and comments

PRELIMINARY MSP II: COMMENTS

ASSETS:

1. Use of several small solid descent motors eliminates need for one large main.
2. Tri-pod type contact points assure contact with surface at all points
3. Use of solid descent motors eliminates need for liquid plumbing, tanks, pumps

LIABILITIES:

1. Possible interaction of solid descent motor outgassing with probe components.
2. Layout somewhat large; not best use of quality of material

PRELIMINARY MSP II LAYOUT

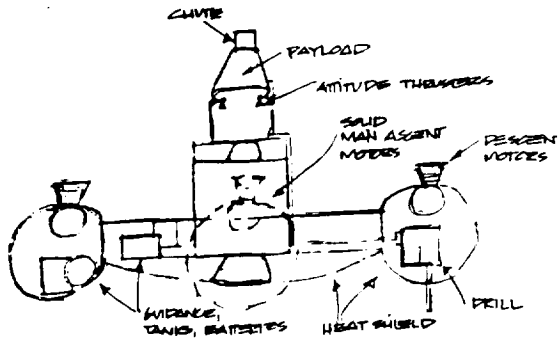

Later, after more propulsion studies and relative sizing of components had been undertaken, it was possible to produce more accurate and intermediate layouts, as shown in Figure 9.

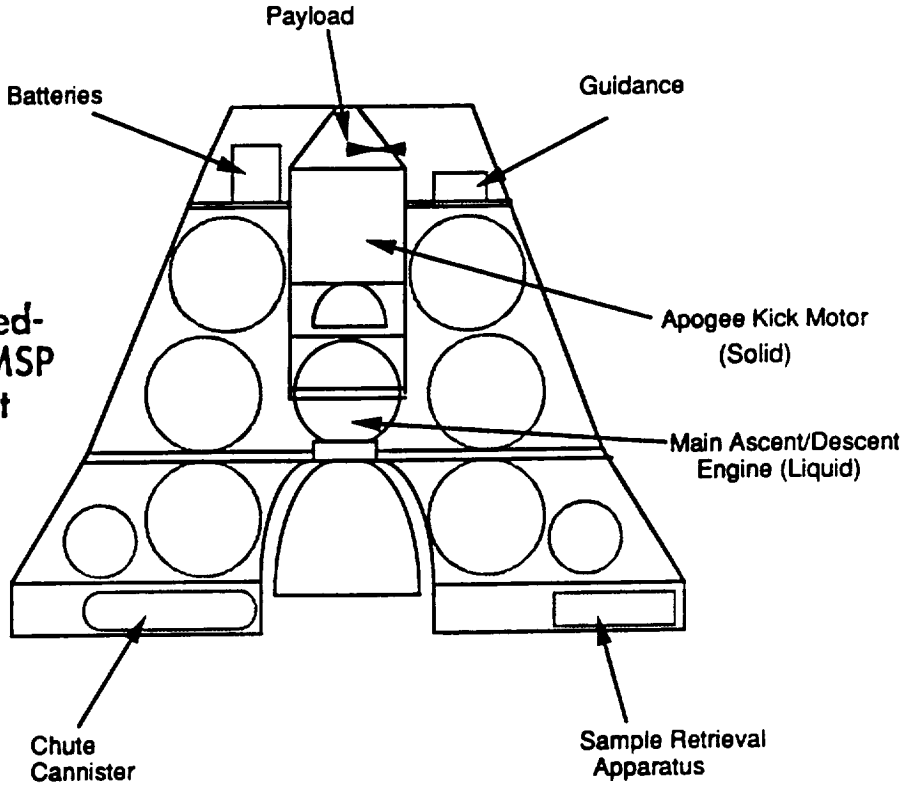

Figure 9: Intermediate MSP layout

It was at this point that the designer realized that the critical components, as far as space was concerned, were the fuel and oxidizer tanks. (which is usually the case with light aerospace vehicles). Thus, a fuel tank study was initiated, which (as shown in Figure 10) resulted in a possible toroidal tank configuration. This idea was later discarded due to complexity of purging, pressure containment, and the like.

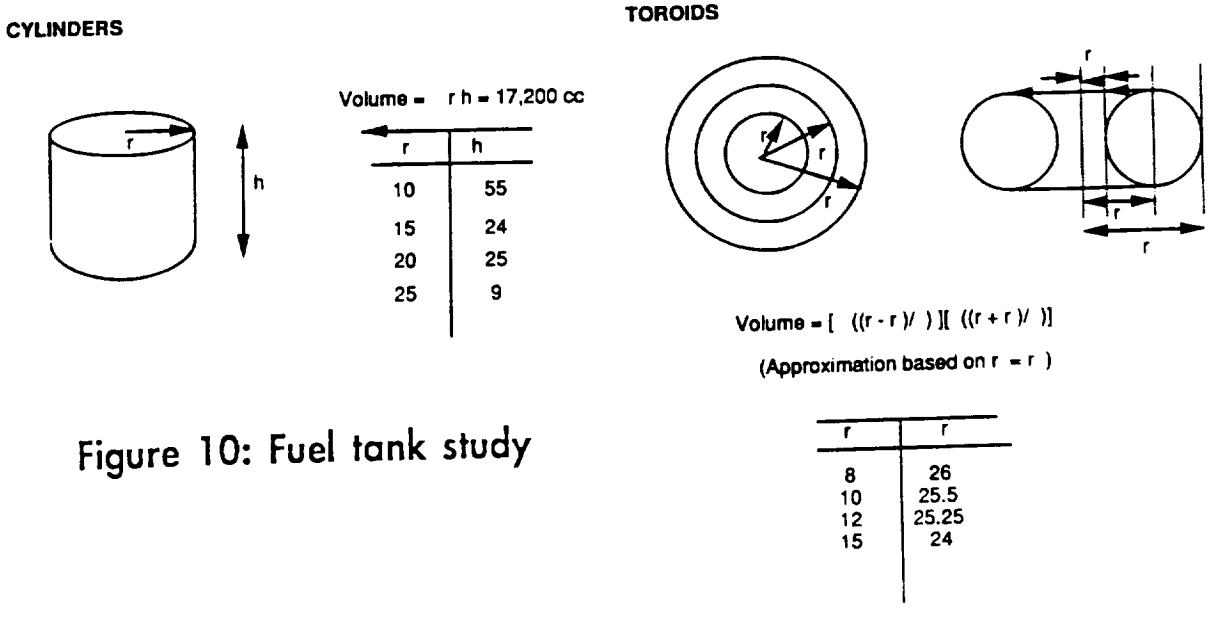

Figure 10: Fuel tank study

2.3 Final MSP Configuration

After many hours of conference, deliberation, and improvisation, the layout of the MSP was finalized to that shown in Figures 11 and 12.

It is a space efficient design, and yet tries to remain as simple as possible. The design is roughly axisymmetric, with the ascent vehicle able to clear all bus components.

3 Component Design

Following are the steps taken to design the critical components of the MSP, which include the landing gear, shock absorbers, bus frame and platform, and ascent and apogee stage launch rings.

Care was taken to use the lightest and (naturally) strongest materials possible, with thought given to their manufacture and interaction with the environments the MSP would be subjected to. It also was always desired to use a safety factor of at least 1.5. As will be shown, because of the generally small dimensions of the craft, this would never be a problem.

3.1 Landing Gear

It was chosen to use the landing gear configuration shown in Figures 13 and 14, with a main strut containing a shock absorber to cushion the vehicle at landing, and secondary struts for any torsional forces encountered by the gear. The following are the calculations made in the design of these components.

3.1.1 Loads on Gear

The mission scenario calls for the MSP to impact the Martian surface at 5.5 m/s. The force on one gear (considered in the extreme case of a one-legged landing) is given by

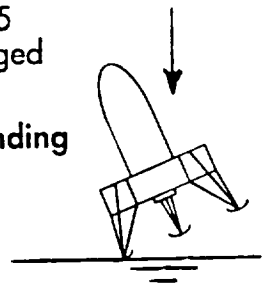

Figure 15: One-legged landing

$$F = ma$$

where $m = 73.9$ kg (at landing)

$a = (v^2/2s)$

where $v = 5.5$ m/s

$s = 0.20$ m (vertical gear travel)

Thus, the force on one leg (taken to be applied through the axis of the shock absorber in the case of a lopsided one-legged worst-case landing, depicted in Figure 15) is

Landing force on one leg = F = 5589 N

Figure 11.1:MSP Exterior Dimensions

(Descent Configuration)

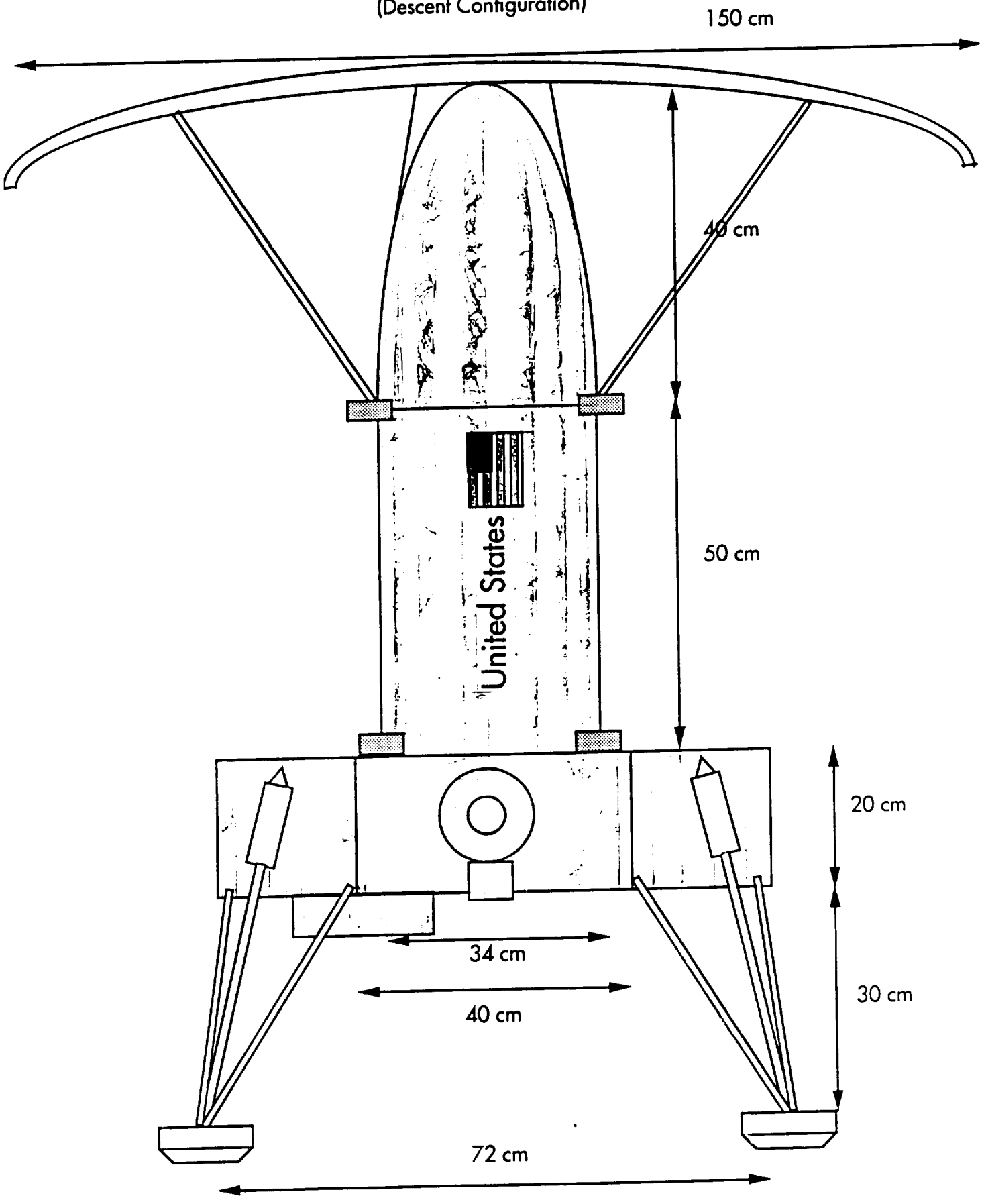

Figure 11: MSP Cutaway

(Descent Position)

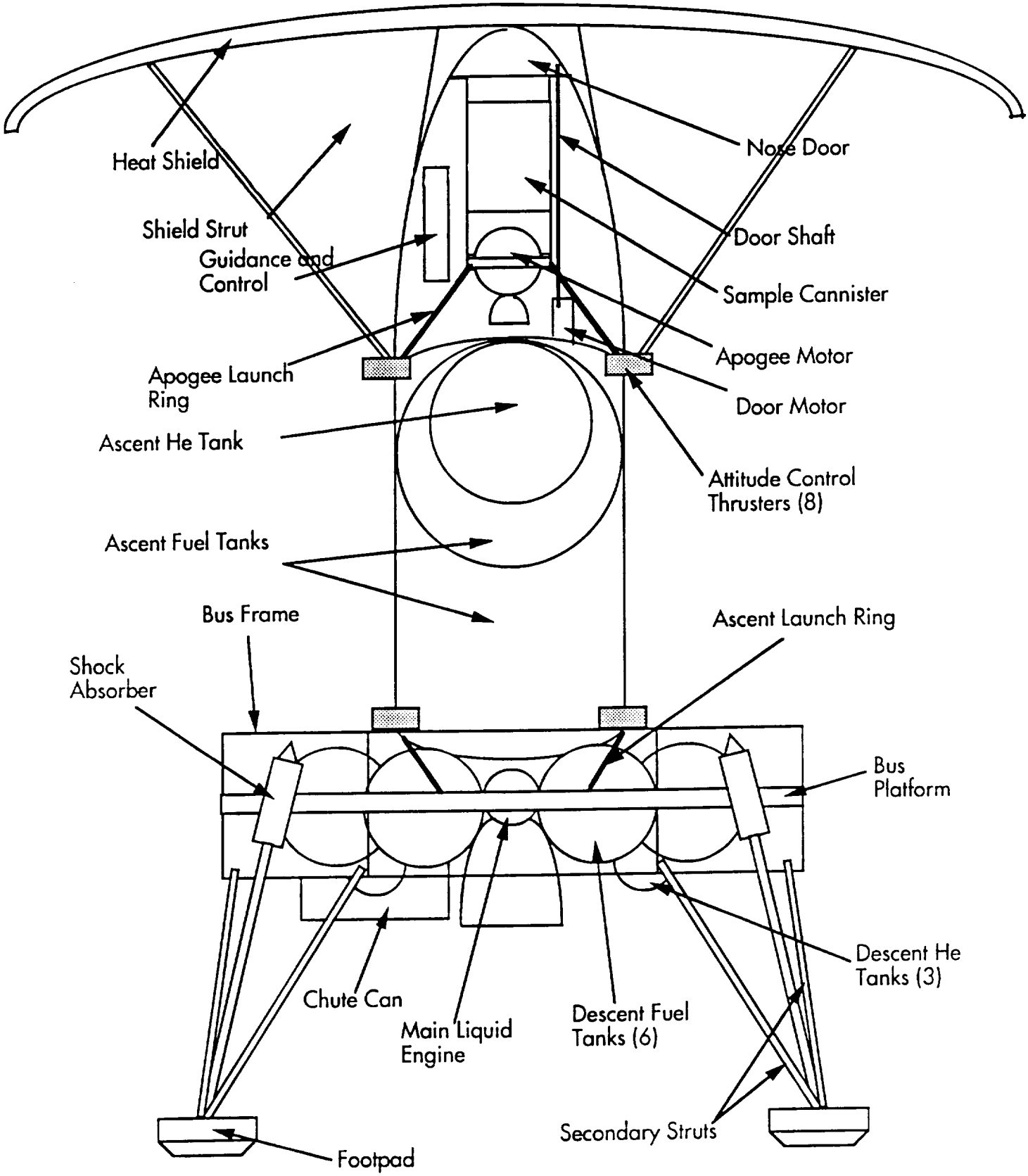

Figure 12.2: MSP Planform Exterior

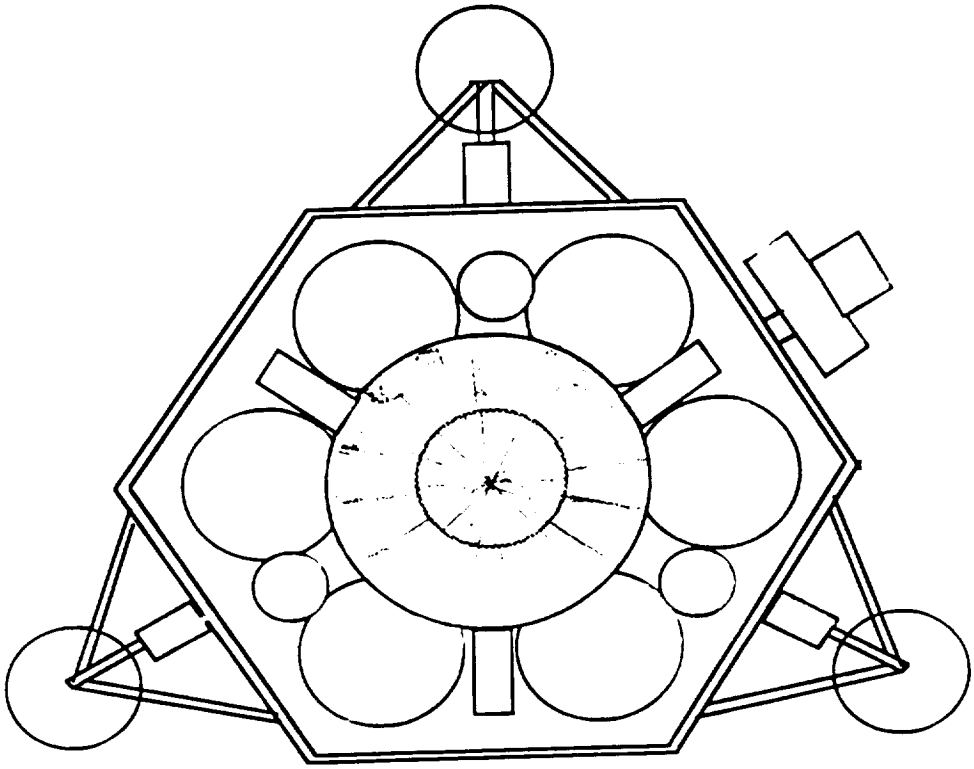

Figure 12: MSP Planform Cutaway

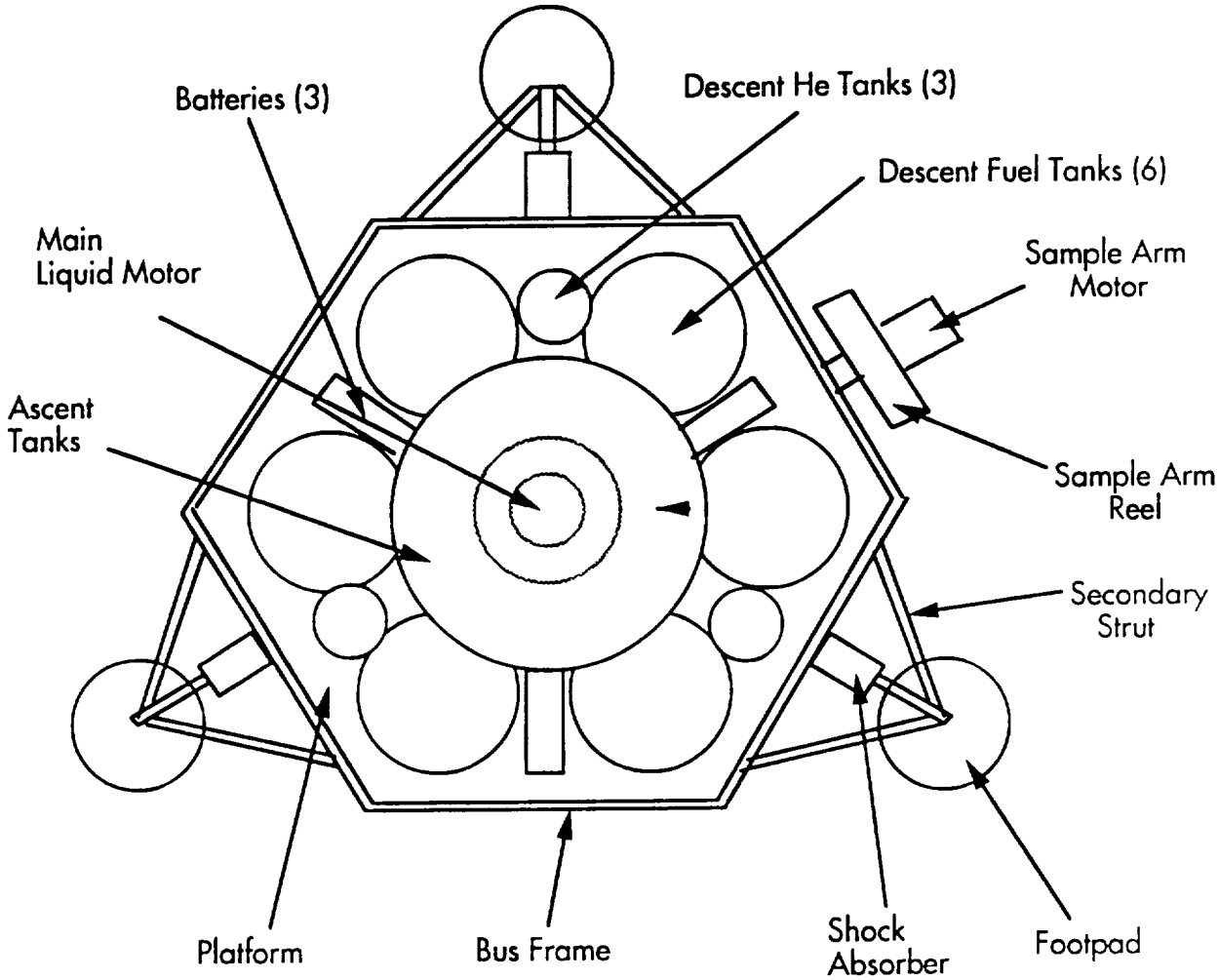

Figure 12.1: MSP Planform Dimensions

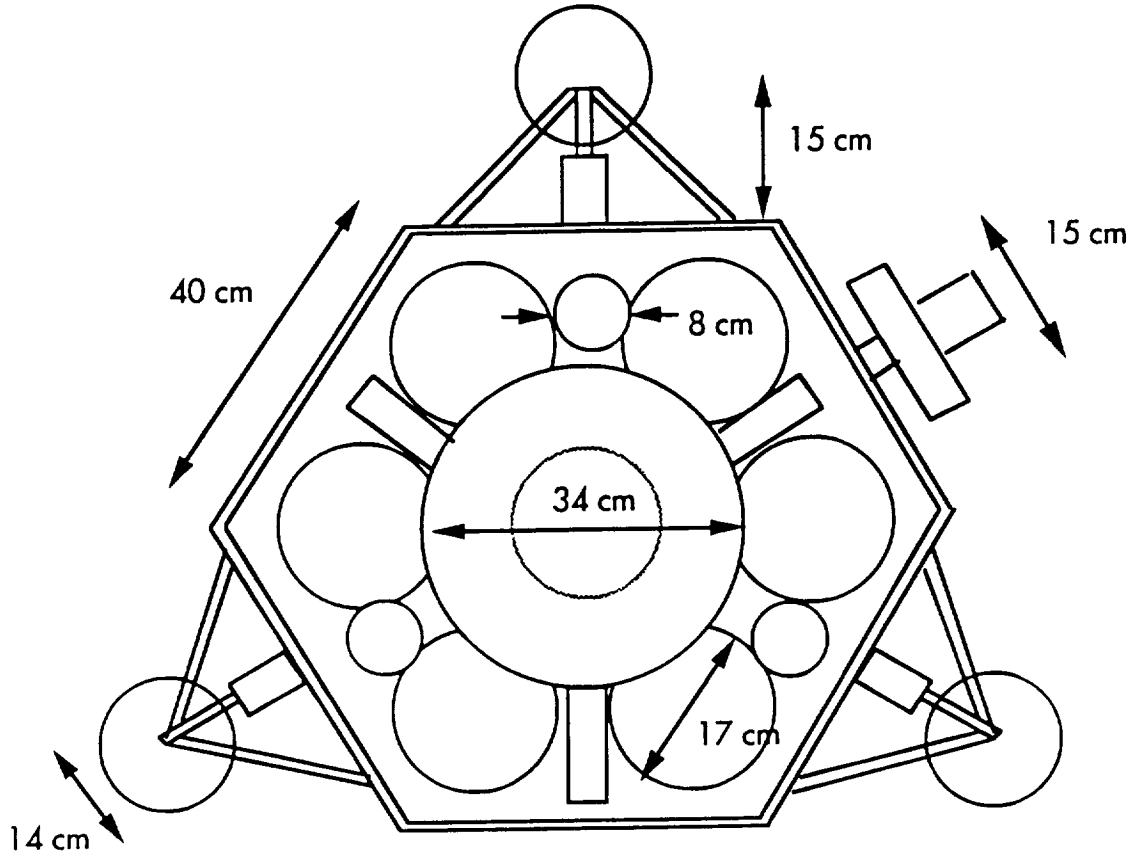

Figure 13: Landing Gear Geometry

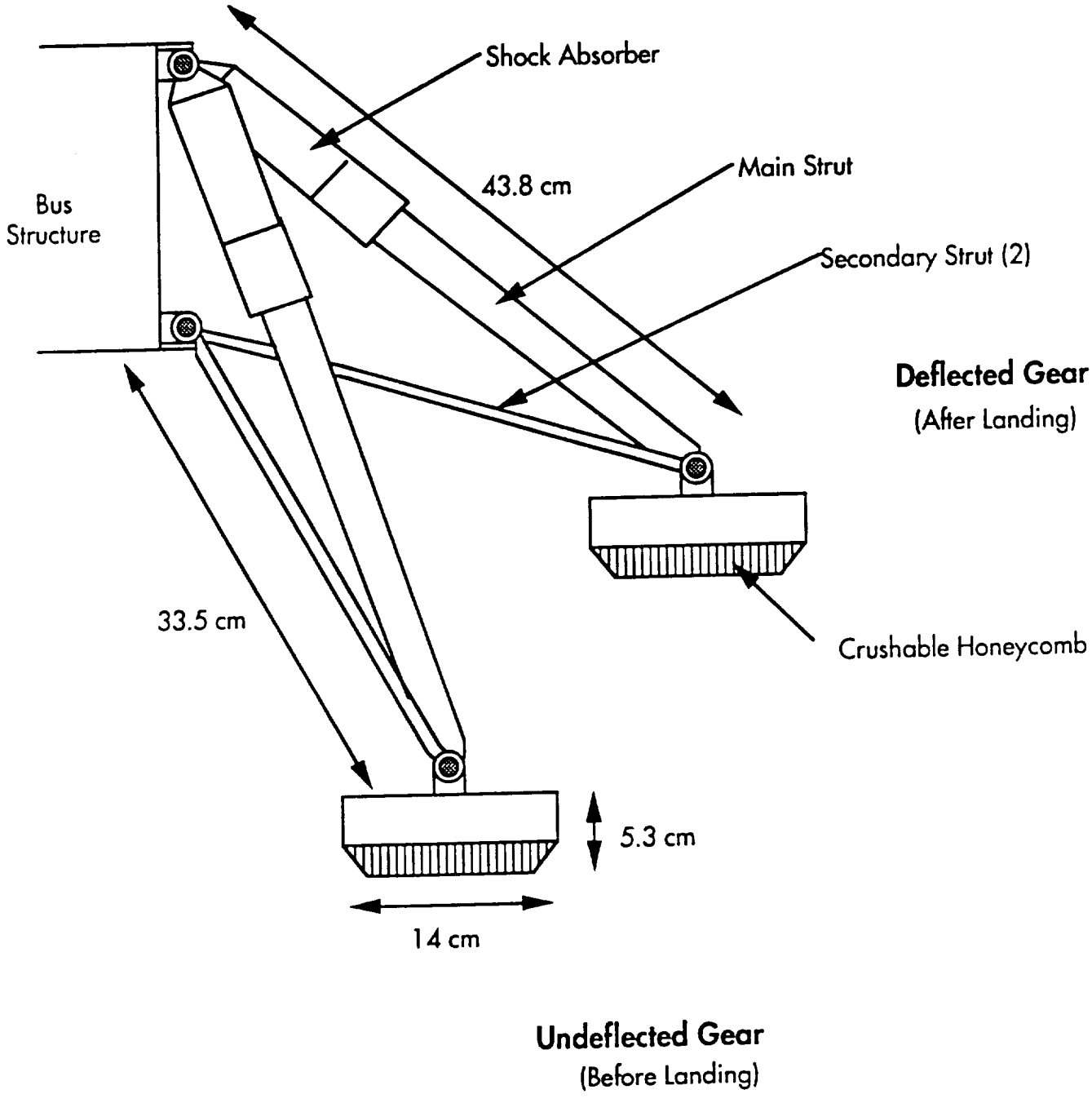

3.1.2 Shock Absorber

The shock absorber chosen was a fluid-filled type, in which the travel of the piston forces fluid through a small orifice in the piston, damping the spacecraft's motion. A cutaway of the MSP shock is given in Figure 16.

Figure 16: Shock Absorber Cutaway

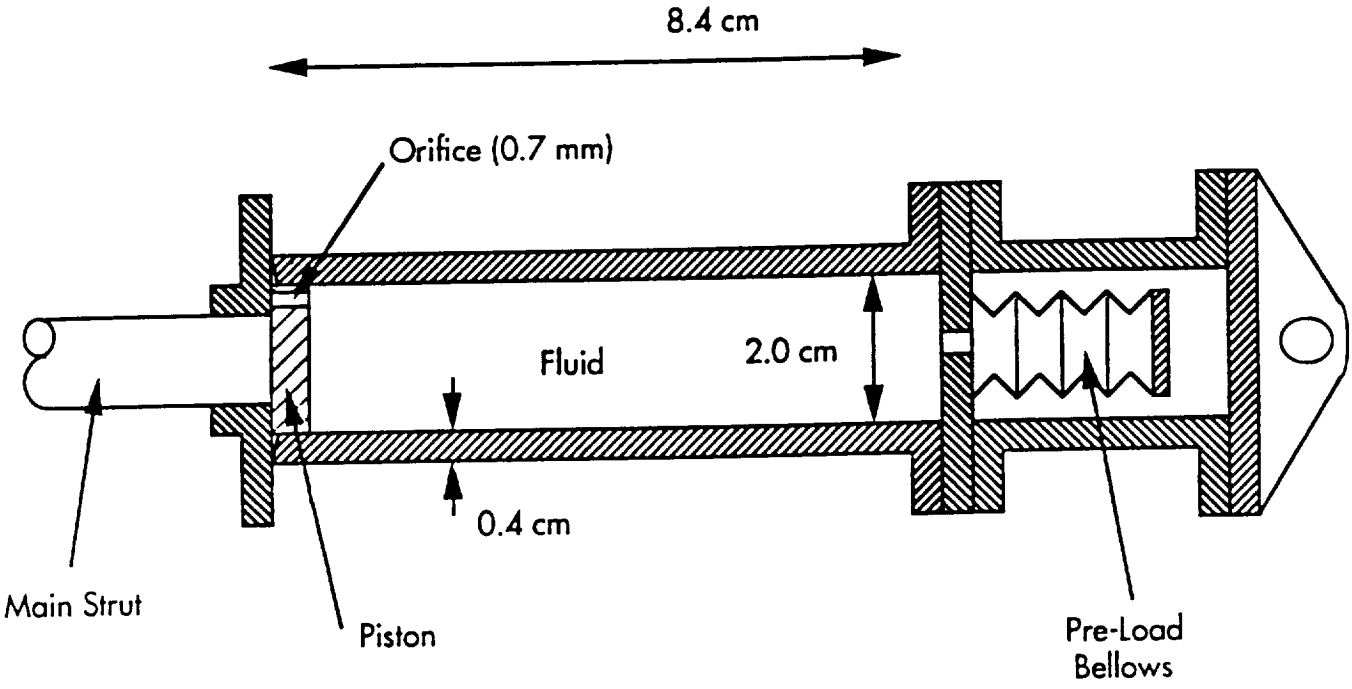

From the derivation given in class, which uses Bernoulli's principle to equate mass flow generated by the motion of the piston of area A to the resulting mass flow through the orifice of area A*, the following relation results:

$$A/A^* = (2F/\rho A)^{1/2} (1/v)$$

where $F = 5589$ N (landing force)
$\rho = 917$ kg/m^3 (assumed from SAE 30W oil)
$v = 5.5$ m/s (landing velocity)

which results in

$$A^* = (1.57)A^{3/2}$$

Then, for the sake of a compact design, choosing a piston radius of 1 cm gives

Piston area = $A = 3.14 \times 10^{-4}\ m^2$
Orifice area = $A^* = 8.74 \times 10^{-6}\ m^2$

From the geometry of the landing gear, it can be seen that to effect a 20 cm vertical deflection of the footpad, it is necessary to have

Piston stroke travel = 8.4 cm

To design the dimensions of the shock cylinder for strength, it was necessary to find the maximum pressure developed in the cylinder. Here, it was assumed that immediately upon impact, the maximum force of landing was transmitted to the shock absorber (this is obviously a more-stringent-than-reality assumption). So here, the pressure is given by

$$P = F/A$$

where again $F = 5589\ N$
$A = 3.14 \times 10^{-4}\ m^2$

Maximum pressure in shock cylinder = 43.76 atm
$(44.36 \times 10^5\ Pa)$

Finally, to find the maximum stresses occurring in the cylinder, we use the relations from Ugural,

$$\sigma_r = (r_i^2)(P)(1 - (r_o^2/r_i^2))/(r_o^2 - r_i^2)$$

$$\sigma_\theta = (r_i^2)(P)(1 + (r_o^2/r_i^2))/(r_0^2 - r_i^2)$$

$$\sigma_z = F/(p\ )(r_o^2 - r_i^2)$$

where here, $r_i = 0.01\ m$
$r_o = 0.014\ m$
$P = 44.36 \times 10^5\ Pa$

This results in the following

Maximum stresses in the shock cylinder

$\sigma_r = 4.44\ MPa$
$\sigma_\theta = 24.59\ MPa$
$\sigma_z = 18.53\ MPa$

As for the material chosen, at first Lockalloy, the Be-Al metal looked promising, but proved too heavy for original gear weight estimations, so the following metal was chosen (Bruhn):

Material for Landing Gear: AZ61A Magnesium
Ultimate Strength: 96.53 MPa
Density: 1791 kg/m^3

Obviously, our safety factors are well-satisfied, and as long as the Magnesium can be machined to 4 mm, there should be no problem. In fact, the weight savings are tremendous:

Mass of shock absorber:

Fluid = (stroke)(area)(density) = (0.084)(0.000126)(917) = 97.1 g
Cylinder = (length)(area)(density) = (0.10)(π)($0.012^2 - 0.01^2$)(2100)
= 29.0 g
TOTAL = 0.189 kg

In addition, the main strut must be checked for Euler buckling, where the critical load applied to the strut is given by

$$P_{cr} = \pi^2 EI/L^2$$

After performing this analysis once, it was found necessary to use Beryllium, where

Material for Landing Gear Main Struts: Lockalloy (Be-Al)
Young's Modulus: 2.9×10^{11} Pa
Yield Strength: 3.24×10^8 Pa
Density: 1826 kg/m3

$E = 2.9 \times 10^{11}$ Pa
$I = \pi r^4/4 = (\pi)(0.01)^4/4 = 7.85 \times 10^{-9}$ m^4
L = 0.40 m

And thus

Critical buckling load for main strut = 140,400 N

Which is well within the factor of 3 for safety used for most buckling and instability cases, considering that the applied load will be about 5900 N.

Mass of gear struts:

Braces (2) = (2)(length)(area)(density) = (2)(0.335)(π)(0.005^2)(1791)
= 94.2 g

Main Strut = (0.422)(π)(0.012)(1826) = 229 g

TOTAL/leg = 0.323 kg

Total mass of landing gear = (0.0189 + 0.154 + 0.0942)(3) + footpads = 1.50 kg

Figure 17: MSP Bus Construction

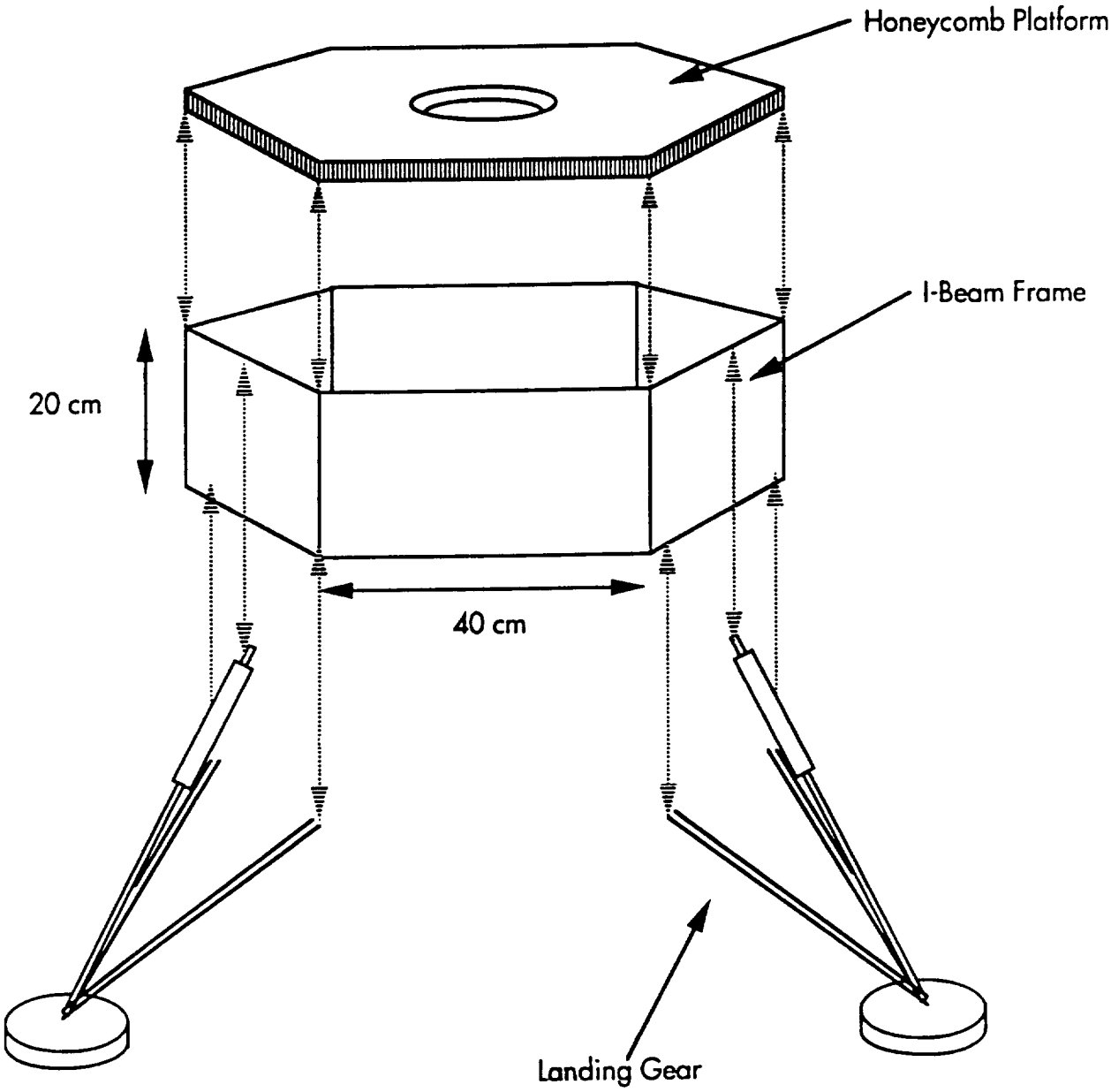

3.2 Bus Analysis

The construction of the main structure of the MSP is, as given in Figure 17, a hexagonal frame of I-beams with a center platform made from a composite hexagonal sandwich platform. The following is the analysis done for its design.

Figure 18: Analytical Modelling of Bus Shelf

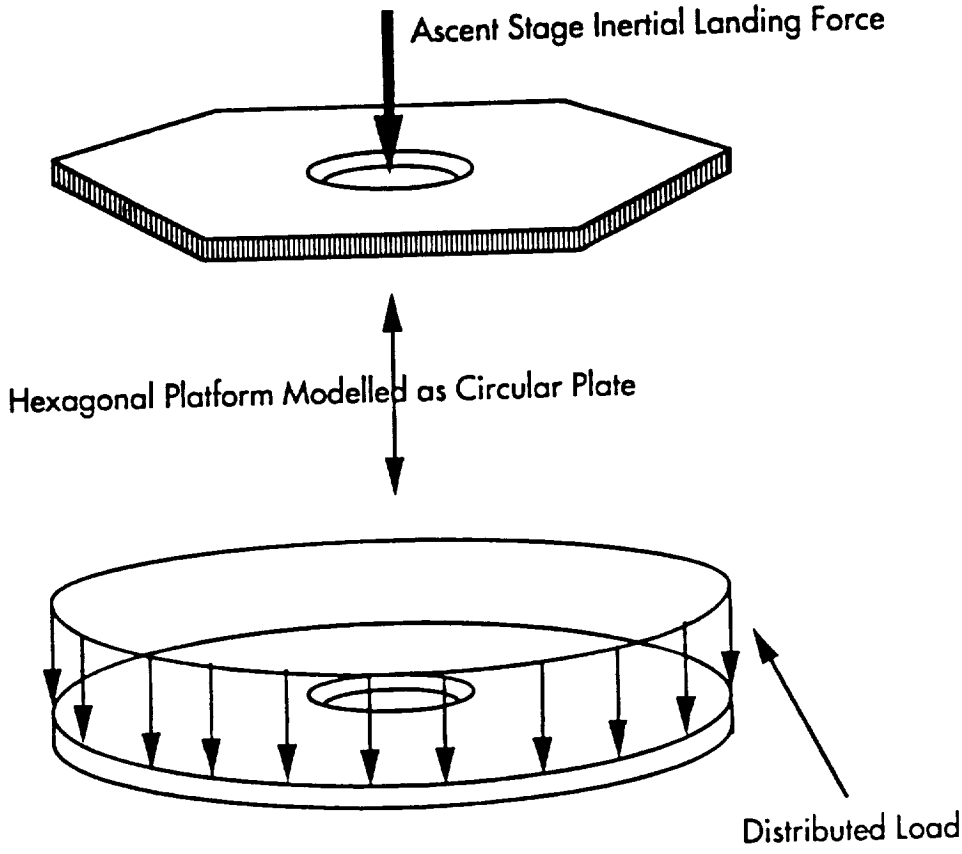

3.2.1 Platform Design

The bus platform encounters its main loading condition upon landing, when the inertial force of the ascent vehicle stack impinges upon the thrust ring at its center, as shown in Figure 18. Because of its hexagonal shape, the platform was modelled as a circlular plate under a distributed loading, as shown in Figure 18. From Urugal, we have

$$\sigma_{rmax} = (3/4)(P_o)(r^2)/(t^2)$$

where P_o = load/area = $(m_{asc})(a)/(\pi)(r^2)$
$= (45kg)(75.6m/s^2)/(\pi)(0.32m^2)$
$= 33.2$ KPa
t = thickness of plate = 0.025 m

Thus $\sigma rmax = (0.75)(33,200)/(\pi) = 7.64$ KPa

From Bruhn, we are able to find a honeycomb sandwich material as shown in Figure 19:

Material for platform: Al 5056 honeycomb
Flexural rigidity: approx 4.5 MPa
Density: 76.4 kg/m^3

So, for our needs, the platform will have a mass of

Platform mass = 0.71 kg

And obviously, well within the range of safety.

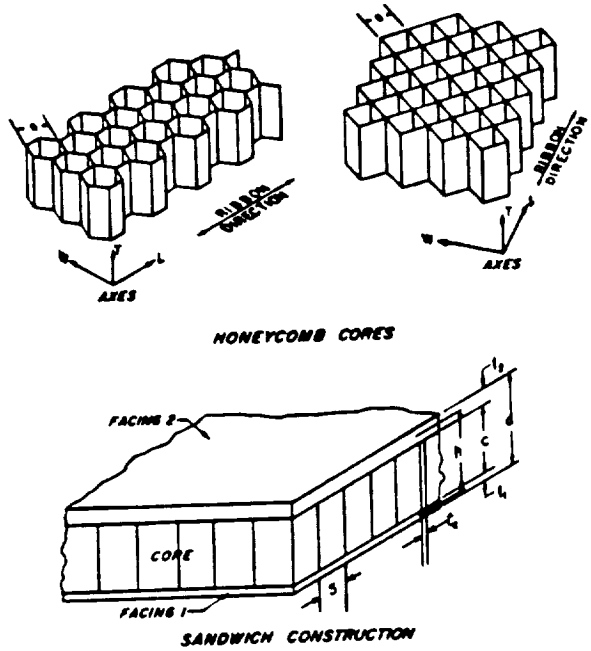

Figure 19: Platform material construction

3.2.2 I-Beam Design

The frame of the bus is constructed of I-beams, depicted in Figure 20. Here, the designer assumed a worst-case condition, in which a side beam is load with the total vertical force of landing transmitted through the shock absorber into the I-beam at midpoint.

Figure 20 : Analytical Modelling of Bus Frame I-Beams

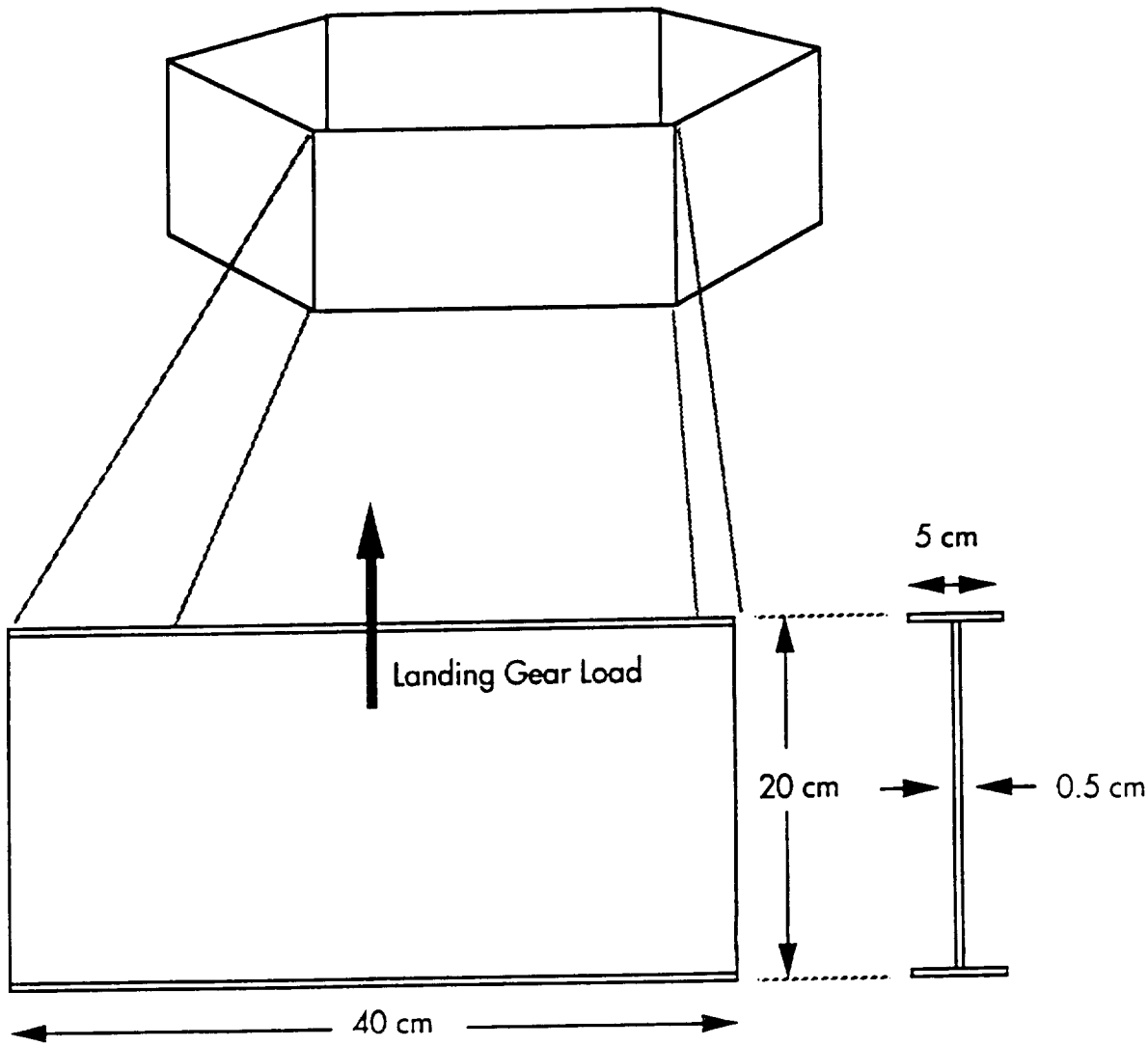

From the classical beam theory analysis, the maximum stress occurs from bending at midpoint in the beam, and is given by

$$\sigma_b = M(h/2)/I$$

Where M = moment applied = (landing force)(half of beam length)
= (5589N)(0.20m) = 1118 Nm
h = height of beam = 0.20 m

And where I for the beam is calculated by taking the moments of area each of the portions in Figure 21 separately, as is classically done. So, using the notations in Figure 21, we have

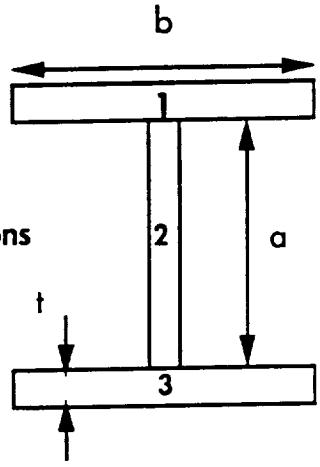

Figure 21: I-Beam Cross-Section Dimensions

Portion	Area	Arm	(Area)(Arm^2)	Own i
1	(t)(b)	(0.5)(a+t)	(t)(b)(1/4)(a+t)^2	(b)(t^3)/12
2	(t)(a)	0	0	(t)(a^3)/12
3	same as portion 1			

Inserting all the relevant dimensions gives

$$I_{section} = 7.61 \times 10^{-6}\ m^4$$

Which ultimately leads to

Maximum stress in beams = 14.7 MPa

Which is well below the same ultimate stress level of the Magnesium. As for the masses of the beams, we can use that

Mass = (cross-sectional area)(length)(density)
= [(2)(t)(b) + (a)(t)](L)(ρ)
= [(2)(0.005)(0.05)+(0.19)(0.005)](0.40)(1791)
= 1.04 kg/ beam

Total mass of frame = 6.24 kg

3.3 Launch Rings

The launch rings are located as shown in the cutaway of Figure 11. The lower, or ascent launch ring is designed to join the ascent stage to the bus frame, and the upper, or apogee launch ring is designed to join the apogee stage to the ascent stage. Both rings are to be strong enough to keep the craft together upon the two major vehicle forces of chute deployment and landing. The two rings are depicted in Figure 22.

Figure 22: Launch Rings

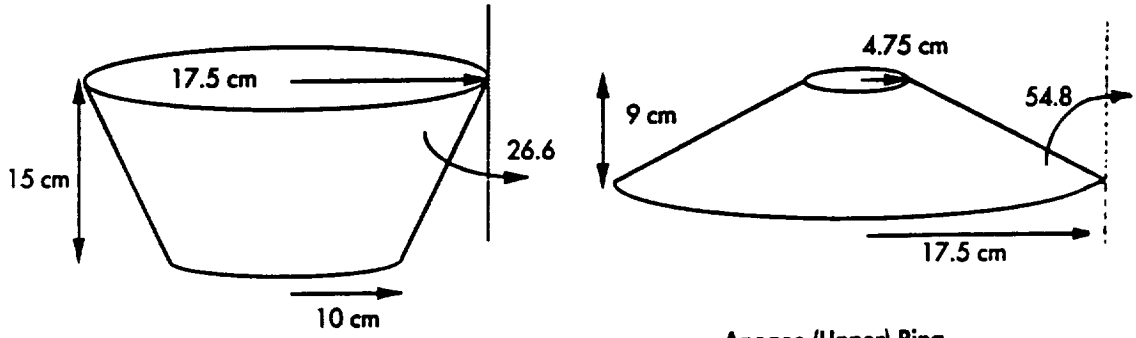

Naturally, the chute deployment is a condition that puts the rings in tension, while the landing phase puts both in compression. Roughly, both need to withstand joining the vehicle at 10g's in tension and 7.5g's in compression. Because the rings separate parts of the vehicle that have different masses, the forces each experiences will be different under the different conditions.

The resulting applied stress on each ring will be given by

$$\sigma app = F/A$$

where $F = ma$

where m = mass of the portion of the space-craft supported by the ring in ques tion under load
a = acceleration in question

The designer then compared this resulting applied stress to the critical stress for the case of a loaded truncated cone, which is given by

$$\sigma_{cr} = (\gamma)(E)(t)(\cos\alpha)/(r)[3(1 - \nu^2)]^{1/2}$$

where
γ = buckling safety factor = 0.33
E = Young's modulus = 2.9 x 1011 (Beryllium)
t = thickness of cone = 0.005 m
ν = Poisson's ratio = 0.33 (non ferrous)
r = smaller radius
α = cone half angle

The results for different loading conditions for the two Beryllium rings of Figure 22 are summarized as follows:

Ring	r (m)	α (deg)	Loading (g)	Supported Mass (kg)	σapp (Mpa)	σcr (Mpa)
Upper	0.0475	54.8	7.5 comp. (landing)	2.75	0.28	3550
Lower	0.100	26.6	7.5 comp. (landing)	45.0	2.17	2620
Upper	0.0475	54.8	10.0 tens. (chute)	87.0	11.44	3550
Lower	0.100	26.6	10.0 tens. (chute)	34.0	2.12	2620

Very obviously, the applied stresses in the rings are several orders of magnitude below the critical stresses, and therefore acceptable.

Mass of rings

Finally, we can roughly compute the masses of the rings, assuming that they are less in mass than a cylinder of similar radius and thickness.

M = (density)(volume) < $(\rho)(\pi)(D)(t)(h)$

where for each ring

ρ = 1826 kg/m3
D = 35.0 cm
t = 5.0 mm
hupper = 9.0 cm
hlower = 15.0 cm

Mass of upper launch ring = 0.90 kg
Mass of lower launch ring = 1.50 kg

4 Summary

This MSP structural design, then, represents a involved attempt to satisfy mission criteria for a spacecraft designed to return of a sample of Martian soil for Earthbound analysis.

Although at points overdesigned, and in some areas not detailed enough, the structure (or at least its critical components) have been shown to be able to withstand some of the major loads placed upon them by the harsh and varied environments the craft would encounter on its round trip to and from the Red Planet.

References

1. A.C. Urugal & S.K. Fenster, "Advanced Strength and Applied Elasticity", Elsevier, N.Y., 1987

2. E.F. Bruhn, "Analysis and Design of Flight Vehicle Structures", Jacobs, Indianapolis, 1973

Various NASA Technical Reports:

3. R.E. Hutton, "Mars Surface Soil Erosion Study", CR-100822

4. V.J. Blanchard, "Full-Scale Dynamic Landing Impact Investigation of Prototype Lunar Module Landing Gear", TN-D-5029

5. J.R. McGehee, "An Expandable Gas Bag Concept for a Stowable Omnidirectional Multiple-Impact Landing System", TM-X-59623

6. J.L. McCarty, "Experimental Study of Vertical Impacts of a Lunar-Module Type Landing Gear Assembly Under Simulated Lunar Gravity", TN-D-4711

7. O.R. Otto, "Analysis and Limited Evaluation of Payload and Legged Landing System Structures for the Survivable Soft Landing of Instrument Payloads", CR-111919

MSP Structural Designer Quarterly Time Sheet

Date	Time	Activity
4/6	2.25* hr	Discussion of layout and propulsion basics, mission scenario
4/7	0.50	Research on Viking, computer sketches
4/8	1.00	Preliminary MSP sketches
	1.50	Assessment of MSP I, sketches for MSP II
	2.25	Computer drawings of MSP I, nozzle detail
4/12	2.00*	Finalized layout; components, shield, chute, gear
4/23	1.00*	Discussion with Tim on component layout
	4.00	Layout of fuel, structure, fuel systems on computer
5/6	4.00	Research on landing gear
	1.50	Sketches of gear, calculations
5/13	2.50	Finalizing layout sketches
	1.00	Initial shock absorber calculations
5/16	1.50	More shock calc's
	3.00	Landing gear plan views, load calc's
5/20	2.00	Final general layout details
5/24	2.50*	Decisions made on tasks finalizations of tasks, synthesis
5/28	3.00	Stress calc's on bus, gear, platform
5/29	2.00	MSP final drawings started
5/30	1.00	First text for final report written
5/31	6.00	Final CAD work on MSP components
6/1	4.00	Text writing for final report
	2.00	FirstLaser printing of report
	1.00	Pasted report
	6.00	Finished text, drawings of report
6/2	2.00	Laser printed report
	2.00	Pasted, photocopied report
TOTAL	**61.50+**	**Hours for quarter**

*Involved group meetings (some not listed)

Section B:

Thermal Control and Guidance

Terrance Yee

SPACECRAFT THERMAL CONTROL

Thermal design for this craft is primarily driven by the need to keep the propellent tanks between +10 and +55 degrees celcius and the batteries between 0 and +25 degrees celcius.(ref D6) The most critical conditions are during nightime on the surface and during ascent in the atmosphere. To remain within the allowable temperature range a variety of suface coatings, insulation, and active cooling and heating units are employed.

Orbital Thermal Control

Thermal control before descent is accomplished though proper surface coatings and orientation of the spacecraft. After release from the MOV and a short burn to precess in its orbit the MSP assumes a slow "rotissary" mode of rotation about its axis of symmetry. The bottom of the hexagonal bus section is gold coated ; the top of the hexagonal bus is painted white and the sides are vertically striped with 50% gold and 50% white paint. This paint scheme together with the shadow of the heat shield allow the spacecraft to alter the effective absorbtivity vs. emmissivity ratio by changing the spacecraft angle with respect to the sun. The angle of the symmetry axis with respect to the incident radiation is chosen by the onboard computer to give a daylight (non-eclipse) equilibrium temperature of 20C. If the spacecraft begins to warm the computer will tilt the top of the craft towards the sun thereby shadowing some of the craft with the heat shield and exposing the white top of the hexagonal bus. This manuever will also be used prior to reentry to precool the craft to 15C which will lessen the impact of the aerodynamic heating on reentry. If during orbit the spacecraft is too cool the top can be tilted away from the sun exposing the gold bottom of the hexagonal bus which will tend to warm the craft.

This flexible effective surface was chosen due to the eccentricity of the martian solar orbit which alters the intensity of solar radiation depending on what time of year the mission is

performed during. It also allows us to be less precise in our calculation of the required mix of coatings. Those calculations were performed by analyzing the steady state radiation equilibrium setting the incident solar radiation and albedo radiation equal to the thermal radiation leaving the craft. Approximating the craft by a sphere of radius R the following results were obtained for the different mars-sun distances:

$Q_{emit} = Q_{abs.}$ $\quad \varepsilon 4\pi R^2 G T^4 = \alpha_s (I_s + I_{alb}) \pi R^2$ $\quad I_{alb} = \frac{a I_s}{g}\left[1 - \sqrt{1 - \frac{R_m}{R_m + 600 km}}\right]$

$T = 293.15°K$

minimum mars-sun distance $\rightarrow \frac{\alpha_s}{\varepsilon} = 2.356$

maximum mars-sun distance $\rightarrow \frac{\alpha_s}{\varepsilon} = 3.429$

selecting gold $(\frac{\alpha_s}{\varepsilon} = 6)$ and Titanium Oxide white paint with Methyl (.222)

$\Rightarrow$ minimum distance : 37% gold , 63% white paint

maximum distance : 56% gold , 44% white paint

For an eclipse the following relations were used to find the time of the eclipse:

for a 600 km altitude orbit above mars the angle that the penumbra makes with respect to the mars-sun radius is only 0.193° so we can approximate this angle as 0°.

therefore we can write

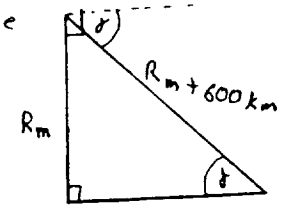

$\Rightarrow \gamma = 58.22°$

$\tau = 2\pi \mu^{-\frac{1}{2}} (R_m + 600 km)^{3/2}$

$t_{ecl.} = \frac{2\gamma}{360°} \tau$

$\rightarrow t_{ecl.} = 2486 s = 41 min \ 26 sec$

Using a lumped capacitance approximation for spheres of different radii the change in internal thermal energy is set equal to the energy radiated away during the eclipse. Specifying the allowable change in temperature as ten degrees celcius allows us to solve for the surface temperature. Once this is known a minimum ratio of insulation thickness to thermal conductivity can be derived from fourier's law of conduction. The actual thickness of insulation is seen to be greater than the minimum required so the craft will stay within the allowable temperature range. An analysis was also performed assuming no insulation and use of electric resistance heaters during eclipse as a comparison.

assuming $C_p \approx 1.0 \frac{kJ}{kg} K^{-1}$

$$mC_p \Delta T = t_{ecl} \varepsilon 4\pi R^2 G T_s^4 = 4\pi R^2 \frac{K}{L} (T - T_s) t_{ecl}$$

$$\rightarrow \frac{K}{L} = 0.334 \frac{W}{m^2 K} \quad \text{(for } R = 1m\text{)}$$

actual $\frac{K}{L}$ used $= \frac{2.9 \times 10^{-3}}{.01} = .29 \frac{W}{m^2 K}$

1cm Refrasil (see ref D1 pg 131)

if no insulation $P = 4\pi \varepsilon R^2 G T_s^4$

assuming $T_s = 293K$

R(m)	P required (W)
.5	612.1
.75	1377.2
1.0	2448.5
1.5	5509.03

Reentry Heating

The allowable temperature change on reentry is specified as 5 degrees Celcius which allows a factor of saftey of 2 before the batteries overheat. Originally an ablative heat shield was envisioned but after considerable research and a more accurate determination of the reentry heating it was found that a radiative heat shield using a high temperature multilayer insulation would function quite well in this environment.

The reentry heating of the shield was approximated by calculating the stagnation enthalpy and pressure at the stagnation point for numerous points during the descent then the heat transfer

rate was found using the chart provided. Setting the total heat transfer rate to the shield equal to the heat radiated away from the front surface allowed us to solve for the maximum temperature at this point on the front of the shield. This allowed us to choose the type and thickness of insulation to give the desired heat transfer and backface temperature. The beryllium honeycomb on the backface was not allowed to exceed 700 degrees Fahrenheit. It was also discovered that the thermal lag for a heat shield of about 45 seconds allowed for an additional factor of saftey in the backface support structure since it will be at a lower temperature than equilibrium when it experiences the maximum drag force.(ref)

Two computer programs were written for this section. The first helped coallate the atmospheric, trajectory, and heating rate tables and charts. The second calculated a few stagnation temperatures outside the boundary layer in front of the shield assuming no dissociation (not a very good assumption) in order to get a rough idea of how much error is induced by assuming a 300 degree Kelvin wall in using the given handout since a very high freestream temperature would make the differnce in heat shield temperature less important.(see appendix D1)

$\dot{q}_{max} = \varepsilon G T_{s_{max}}^4 \Rightarrow T_s = 991.3K$

$T_{back} = 644K$

assuming a veiw factor of $\frac{1}{4}$ between the craft and the back of the shield

$\Rightarrow \dot{q}_{allow}$ (heat shield) $= 11,111\ W$ for 180 seconds

$L_{req'd} = 0.112$ mm of Aluminum fiberglass multilayer blanket (max temp = 1033K)

minimum thickness manufactured = 5mm, $\rho = 18 lb/ft^3$

so our 5mm thick insulation weighs 2.55 kg and keeps the back face very cool with almost no heat transfer to the vehical

In the recirculation zone behind the heat shield the convective heat transfer is approximately one tenth of that experienced at the stagnation point.(ref D3) Approximating the temperature of the recirculation zone as 1400K and modeling the craft as a cylinder we get the following convective heat transfer relations for the bus during descent:

$h_{s\,tag.\,pt.} = \frac{\dot{q}}{\Delta T_{chart}} = \frac{46500\ \frac{W}{m^2}}{6000\ K} = 7.75\ \frac{W}{m^2 K}$ (ref D9)

$h_{sides} = 10\%\ h_{stag} = 0.775\ \frac{W}{m^2 K}$

[approximate $r = \frac{1}{\pi}$, $L = 1\,m$]

$mC_p \Delta T_{craft} = Q = 180sec \cdot \left[\frac{1}{.775\ \frac{W}{m^2 K} \cdot 2\,m^2} + \frac{\ln r_o/r_i}{2\pi K_{insl.} L}\right]^{-1} \Delta T_s$ ($\Delta T_s \sim 1100K$)

allowing ΔT_{craft} of 5k → $r_o - r_i = .7mm$ Refrasil which is well below the 1cm of Refrasil actually on the craft.

the actual $\Delta T_{craft} \cong 0.4\,^\circ K$ with 1cm Refrasil

In order to maintain stability during descent a reinforced carbon- carbon "drogue chute" is deployed when entering the atmosphere. This cone- shaped body is tethered to the rear of the craft on either side of the motor by high temperature titanium cables. The drag cone is stored as the lid to the main chute canister and when deployed by coil spring will trail 10 meters behind the craft. Since the heat shield stagnation point was at 991K we assumed this temperature as the worst case for the entire cable. To size the drag cone we assumed a 50 m/s gust which is approximately a 2% variation in drag force (about 100N). Letting this disturbance force act at 75cm from the center of the heatshield leads to a 75Nm disturbance torque. If we allow a maximum moment arm of the drag cone force of 1m then we require a minimum force of 75N which translates into an area of 220cm^2 if we assume that the drag force per area of the heatshield is equal to the drag force per area of the drag cone. With a right cone (45 degree half angle) this translates into a surface area of 707cm^2 and a base radius of 15 cm. Adding a factor of safety to this, we increase the base radius to 21cm and the surface area to 980cm^2. Making the cone out of 5mm reinforced carbon-carbon (RCC) leads to a cone weight of 784g. A simple stress analysis of the cable shows that a diameter

of 3.175mm is capable of supporting more than 1000N force and weighs 360g. Therefore a total weight estimate of the stability system is 1.3kg allowing 156g for fixtures such as bolts and a spring.

Thermal Control on the Surface

After reentry the MSP may be warmer than desired, therefore a method of rapid cooling is required. The method chosen to accomplish this is three small louvers which are placed 120 degrees apart on the ascent body above the ascent fuel tanks. The louvers are opened by thermally set springs and held shut by latches which the computer opens upon landing and locks at night. They are top hinged, opening outward to expose an 8cm high, 3cm wide opening for the martian atmosphere to flow through.

Some concern was originally felt for the cooling effect of the expanding helium in the propulsion system. The expansion is solved using the ideal gas law:

$$\frac{P_1 V_1}{P_2 V_2} = \frac{T_1}{T_2}$$

$T_1 = 293K$ $\quad V_1 = 4.905 \times 10^{-3} m^3$

$P_1 = 20 MPA$ $\quad V_2 = 2.9575 \times 10^{-2} m^3$

$P_2 = 3 MPA$

$\rightarrow T_2 = 220.8 K$

$m C_p \Delta T = 75 kJ$ for a .2 kg He tank

$\rightarrow \Delta T_{MSP} = -0.75 °C$ per He tank during descent

$\Delta T_{MSP} \cong -1.5 °C$ per He tank during ascent

This temperature decrease is certainly acceptable during the rocket firings while heat from the rocket motor and aerodynamic heating are offsetting the helium expansion effects.

This brings us to the next problem area, the rocket motor. While the thrust chamber is ablatively cooled and has negligible heat transfer to the rest of the ship, the nozzle and throat are radiatively cooled and must be isolated from the rest of the ship. This is done using a three layered system consisting of a highly reflective outer coating of silver with a protective coating of SiO (150 Angstroms), a layer of beryllium as a heat sink, and a final layer of refrasil, a multilayer high temperature insulation. The analysis of this system follows:

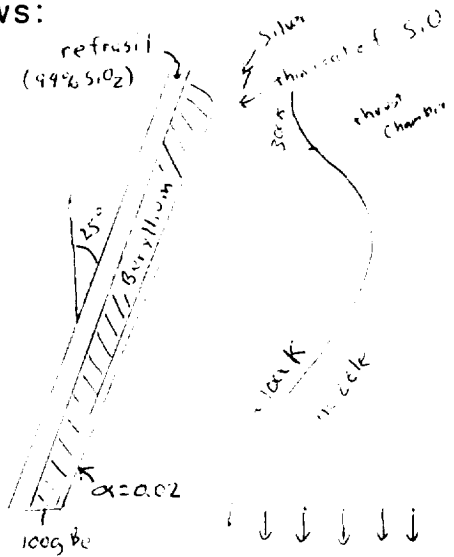

A worst case approximation of the radiation system would be as parallel plates

for which (ref. 89)

$$q_{12} = \frac{\varepsilon_1 \varepsilon_2 G (T_1^4 - T_2^4)}{\varepsilon_1 + \varepsilon_2 - \varepsilon_1 \varepsilon_2}$$

$(T_2 = 293)$ $.1 kg \times 1825 \frac{J}{kgK} = \dot{q}_{12} \tau_{burn}$ (τ 62 sec max)

$\rightarrow T_2 = 622 K$, $q_{12} \tau_{burn} = 61.1 KJ$

thermal resistance to conduction = $3.45 \frac{m^2 K}{W}$

thermal cooling due to radiation (end of burn) $= \frac{1}{4} G \varepsilon T^4$ (view factor)

$$q_{cond} = \frac{329}{3.45} = 95.4$$

$q_{rad} = 21.2 \frac{W}{m^2}$ @ 622 K

$\rightarrow \frac{4}{5}$ of energy transferred to spacecraft

$\rightarrow$ 48.9 KJ to craft

$\rightarrow$ 2.4 °C ΔT for ascent stage

$\rightarrow$ + .5 °C for deorbit burn

The last ground problem is cooling at night due to radiation loss and convection. It is this area which requires the most insulation and indeed sizes the insulation used. A small UDMH decomposition fuel cell is used to warm the ship at night.

since pressure stays the same at day & night $\rho_{night\ (180K)} = \rho_{day} \frac{T_{day}}{T_{night}} = 1.96 \times 10^{-5} \frac{g}{cm^3}$

$\mu = 91.5 \times 10^{-7} \frac{kg}{ms}$ $\rightarrow \nu = 4.67 \times 10^{-4}$, $k_{180K} = .00828 \frac{W}{mK}$

$C_{p\ 180K} = 770.4 \frac{m^2}{s^2 K}$ $\rightarrow \alpha = 5.484 \times 10^{-4} \frac{m^2}{s} = \frac{k}{C_p \rho}$

$$Pr = \frac{\nu}{\alpha} = 0.852 \qquad Re = \frac{V_\infty \ell_0}{\nu} = \frac{20 m/s \cdot .34 m}{4.67 \times 10^{-4} \frac{m^2}{s}} = 14561$$

using the relation

$$Nu = k\, Re^m\, Pr^{1/3}$$

w/ $k = .195$, $m = .618$ (ref 90)

for $Re = 14561$

$Nu = 69.1$

$h = Nu \frac{k}{\ell_0} = 1.68 \frac{W}{Km^2}$

$$\dot{q} = \frac{293 - 180}{\frac{1}{2\pi \cdot .17 m \cdot 1.68 \frac{W}{Km^2}} + \frac{\ln(\frac{.18}{.17})}{2\pi \cdot 2.9 \times 10^{-3} \frac{W}{mK}}} = 30.6 W$$

(1 cm retrasil)

over a uniform 180° night $Q = 1.327 \times 10^6$ J lost

given that the heat of combustion is 46×10^6 J/Kg for Kerosene

we estimate that hydrazine has at worst $\frac{1}{3}$ of this value

since the actual value is unavailable.

Th leads to 86 grams of Hydrazine required to maintain temperature levels.

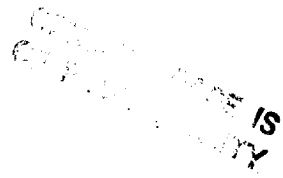

Ascent Heating

Using the same methods as the descent the ascent trajectory was analyzed but with a nose made of RCC and .96cm of refrasil protecting the skin. Again as in the descent, the craft was allowed to cool to 15C before launch in order to alleviate heating constraints.

Rendezvous Vehicle

The rendevous vehical has very little on board that is temperature sensitive; the electronics are very simple and can be built to withstand wide temperature variations, there are no batteries or fuel, only superstructure, dirt, solar cells and an omnidirectional radio beacon.
The surfaces not covered by solar cells are covered by gold to keep the temperature near 290K.

GUIDANCE AND POWER SUPPLY

Guidance is provided by inertial rate gyros and by sun and star sensors when outside the atmosphere. Final landing guidance is provided by a system which uses a prescanned map of the landing area which is stored in on board ROM computer memory.(see appendix D2) The map records safe landing sites and local landmarks for the entire probable region of landing. Just after the parachute is jettisoned and before the retro manuever a snapshot image is taken of the terrain and matched by landmarks and distinct features to the map stored in memory. Once the computer determines where it is, it can use the map to direct the craft to the closest known safe landing zone. A laser range finder is used to determine distances to the ground to allow the computer to make the decisions when to engage the main chute, when to jettison the chute, and when to engage and disengage the retro motor.

The sun and star sensors along with inertial rate gyros and an accurate timer allow the ascent computer to determine the correct timing of the firing of the apogee kick motor as well as its correct orientation. Also the ascent computer will set a timer on the apogee motor that will pyrotechnically pierce the combustion chamber to effectively kill the thrust when the correct orbit has been reached.

The on board computer actually consists of three parts. The first part is the descent computer which is the ROM board and the guidance for descent. This part is located in the hexagonal bus section and weighs about 1kg. The second part is the main or ascent computer. It is located in the ascent stage and weighs just under 2kg. Its functions include powered flight guidance, directing the sample collector, and orbital equations. The third part is a subpart of the main computer. Its function is to periodically check all systems, especially thermal, during the dormant periods while the MSP waits for a particular orbital conjunction. It has limited control over the attitude jets and thermal system and will activate the main computer if a serious problem is detected. It has negligible power usage and negligible mass.

Power is supplied to all but the rendevous stage by zinc-silver oxide batteries with a power density of 80 watt-hr/lb.(ref D2) There are two groups of batteries, one in the ascent stage and one in the hexagonal bus. The batteries for the sample collection motor are subdivided into many smaller cells in order to give a high voltage while the other batteries supply a lower voltage usable by the computers. The main computer system is assumed to operate at 30watts and the descent computer at 8 watts, the monitor subcomputer is estimated to have such a low power usage as to be negligible.

action	power(W)	time(min)	energy(watt-hr)
ascent	30	35	17.6
sample collection	330	10	55
final descent	38	5	3.17
deorbit and reentry	30	60	30
adjusting precession	30	40	20

burn to precession	30	10	5
unforseen/reserves			27.63
total			158.4

Total battery weight is 0.9kg, 0.8kg is stored in the hexagonal bus.

The beacon on the rendevous stage is an omnidirectional beacon broadcasting a narrow band 100W signal of 1millisecond duration five times every second. To provide this power 145cm^2 cross sectional area of solar cells must be used. On the 10cm diameter rendevous stage this translates into a 14.5cm strip around the cylinder of 11% efficient silicon cells at furthest distance from the sun. If 17% efficient GaAs cells are used the strip will be 9.4 cm wide. The remainder of the suface should be covered in gold to keep the craft warm. Silicon solar cells are currently available and their reliability is high so they were chosen for this mission, giving a weight of 0.15kg to the power system.

REFERENCES

D1. NASA SP-5027, "Thermal Insulation Systems" ,Technology Utilization Publication, Cambridge, Massachusetts,1967

D2. N63-11511,"Power for Spacecraft",NASA University Conference on the Science and Technology of Space Exploration, Washington D.C. 1962

D3. NASA SP-23,"Aerodynamics of Space Vehicles", NASA University Conference on the Science and Technology of Space Exploration, Washington D.C. 1962

D4. John D. Anderson Jr., "Fundamentals of Aerodynamics",MC Graw-Hill, 1984

D5. Frank Incropera and David De Witt, "Fundamentals of Heat and Mass Transfer",John Wiley and Sons, 1990

D6. Brij N. Agrawal, "Design of Geosynchronous Spacecraft",Prentice-Hall Inc., 1986

D7. AGARD-CP-411, "Advances in Guidance and Control Systems and Technology", NATO 1986

D8. Pruser,Faget,Smith, "Manned Spacecraft: Engineering Design and Operation", Fairchild Publications,1964

D9. Meyer, R. X. , various class handouts, Winter and Spring 1990, UCLA

MSP THERMAL/POWER/GUIDANCE/COORDINATOR TIME SHEET

WEEK	HOURS
1	3
2	5
3	3.5
4	5
5	8
6	10
7	6
8	15
9	20
10	25
total	100.5

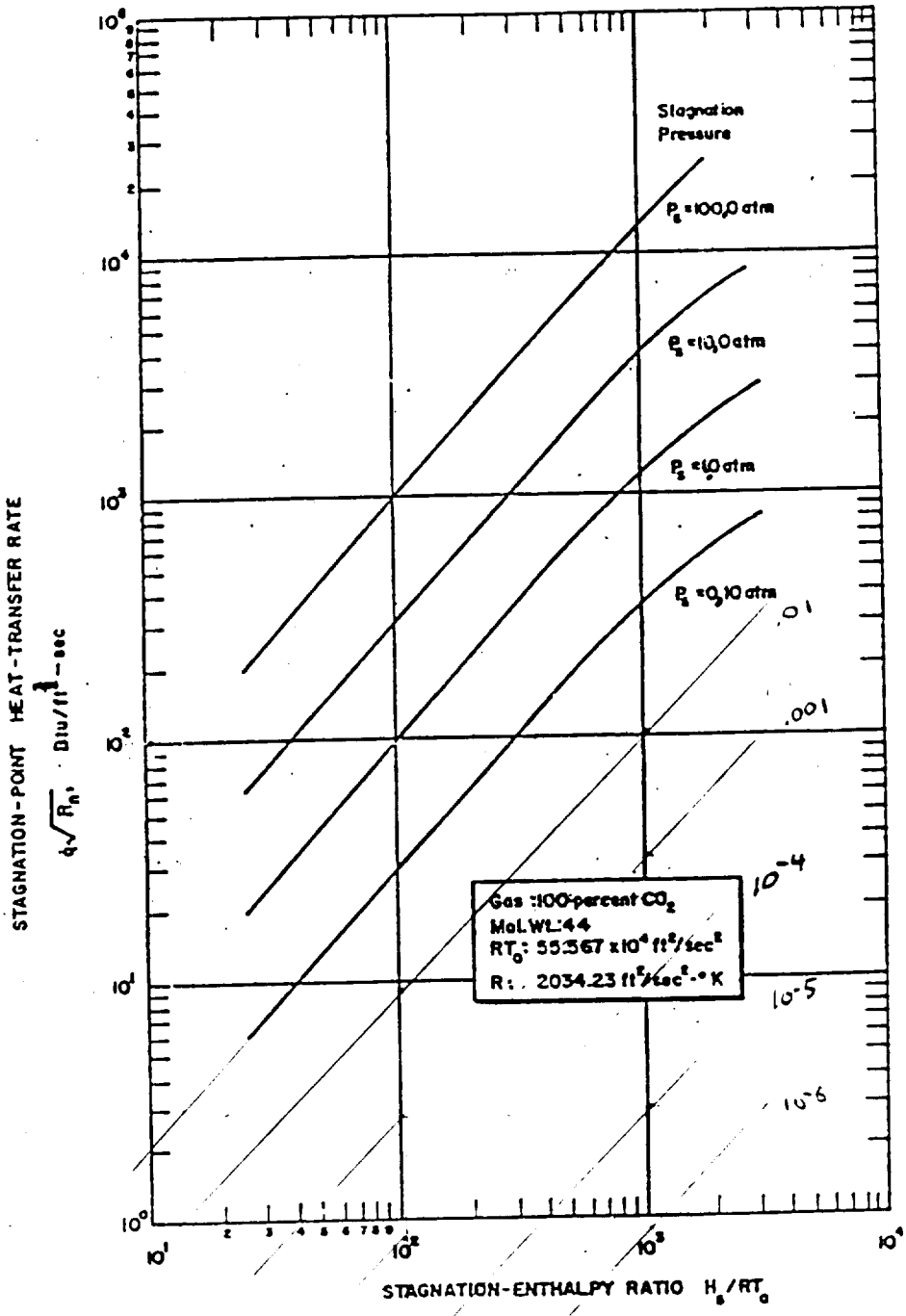

Figure 1 CONVECTIVE HEATING AT A STAGNATION POINT (100-PERCENT CO_2)
63-10199

For wall temperature = 300 °K.

chemical reactions are included (multi-component diffusion is neglected)

$\dot{q}$ = heat transferred to wall, per unit area and unit time.

R_n = nose radius

H_s = stagnation enthalpy

$H_\infty = h_\infty + \frac{v^2}{2} = c_p T_\infty$

III. BOUNDARY-LAYER SOLUTIONS

Heat-transfer rates and boundary-layer profiles have been found from a sin solution of the laminar boundary-layer equations. Local similarity assump are used to reduce the equations to a set of five first-order total differentia equations with variable coefficients. The solution is then found by an iterat technique using 400-point profiles. A detailed description of the solution is also given elsewhere.[2]

A number of assumptions are involved in this boundary-layer solution and v be mentioned for completeness: The atomic composition is assumed to be stant throughout the boundary layer. In essence, this means that multicom diffusion is neglected. The local similarity assumptions are exact for the studied in this report. All fluid properties are continuously variable throu out the boundary layer. The effects of chemical reactions are included by employing the reaction-conductivity concept.

All calculations in the report have assumed a wall temperature of 300°K. Similarly, only stagnation-point solutions are reported here. Other cases more realistic wall temperatures and other pressure gradients can be obta by application of this method.

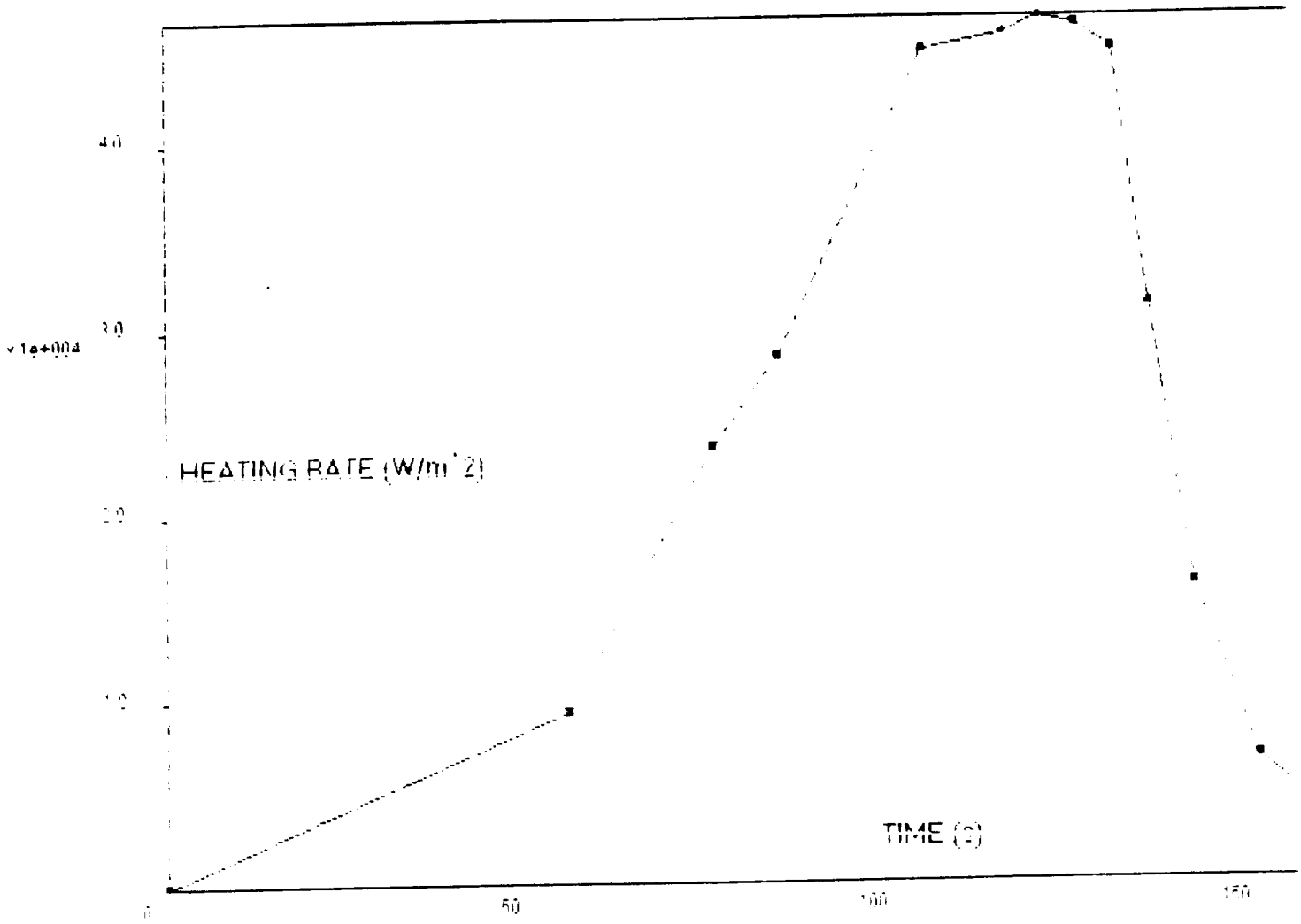
x 1e+004
HEATING RATE (W/m^2)
TIME (s)
0
50
100
150

capture of sample container

① MOV zeroes in on beacon, waits until closest approach, then manuevers to docking distance.

② MOV opens door to bay which housed MSP

③ MOV manuevers to capture sample container inside bay

④ MOV closes bay doors, sealing container inside

⑤ net system inside bay draws container tight against a corner read for return trip to earth. see diagrams:

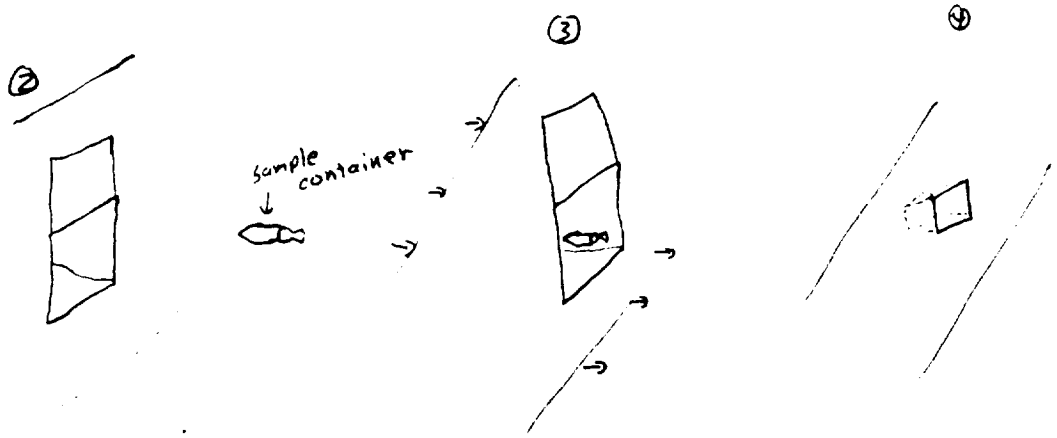

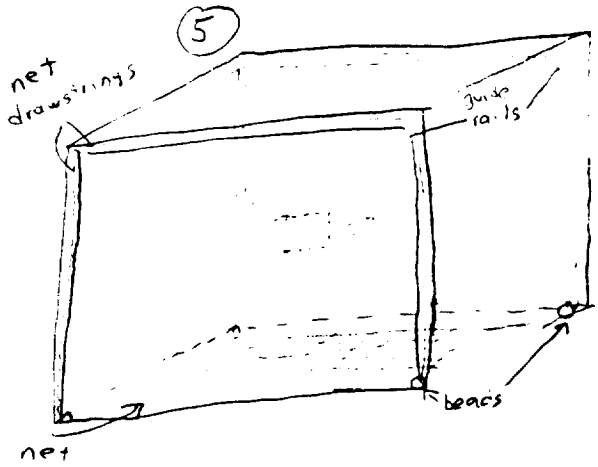

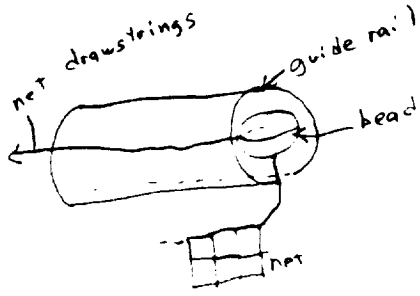

as drawstrings pull on beads the net rises pulling the sample toward the ceiling. When the net reaches the top the right side of the net is reeled along the ceiling while the left side is reeled through a gap at the top left edge. this process continues until the sample is held firmly against the upper left edge of the docking bay

STAGNATION PRESSURE ON SHIELD IS 9.324668E-07
X AXIS IS 112.718
VELOCITY(m/s)= 3520 HEATING RATE (W/m 2)= 88.66328
ALTITUDE(km)= 150

STAGNATION PRESSURE ON SHIELD IS 1.227144E-04
X AXIS IS 231.6017
VELOCITY(m/s)= 3562 HEATING RATE (W/m 2)= 9309.644
ALTITUDE(km)= 100

STAGNATION PRESSURE ON SHIELD IS 1.155286E-03
X AXIS IS 203.2755
VELOCITY(m/s)= 3552 HEATING RATE (W/m 2)= 23495.77
ALTITUDE(km)= 80

STAGNATION PRESSURE ON SHIELD IS 3.14366E-03
X AXIS IS 188.1773
VELOCITY(m/s)= 3520 HEATING RATE (W/m 2)= 28372.25
ALTITUDE(km)= 70

STAGNATION PRESSURE ON SHIELD IS 7.704226E-03
X AXIS IS 166.9835
VELOCITY(m/s)= 3425 HEATING RATE (W/m 2)= 44774.96
ALTITUDE(km)= 60

STAGNATION PRESSURE ON SHIELD IS 1.679816E-02
X AXIS IS 139.1813
VELOCITY(m/s)= 3220 HEATING RATE (W/m 2)= 45661.6
ALTITUDE(km)= 50

STAGNATION PRESSURE ON SHIELD IS 2.303351E-02
X AXIS IS 120.0036
VELOCITY(m/s)= 3020 HEATING RATE (W/m 2)= 46548.23
ALTITUDE(km)= 45

STAGNATION PRESSURE ON SHIELD IS 2.919942E-02
X AXIS IS 97.29362
VELOCITY(m/s)= 2750 HEATING RATE (W/m 2)= 46104.9
ALTITUDE(km)= 40

STAGNATION PRESSURE ON SHIELD IS 3.438264E-02
X AXIS IS 74.39153
VELOCITY(m/s)= 2400 HEATING RATE (W/m 2)= 44774.96
ALTITUDE(km)= 35

STAGNATION PRESSURE ON SHIELD IS 3.505111E-02

X AXIS IS 49.95343
VELOCITY(m/s)= 1950 HEATING RATE (W/m 2)= 31032.15
ALTITUDE(km)= 30

STAGNATION PRESSURE ON SHIELD IS 3.192682E-02
X AXIS IS 30.8775
VELOCITY(m/s)= 1500 HEATING RATE (W/m 2)= 15959.39
ALTITUDE(km)= 25

incorrect data

~~STAGNATION PRESSURE ON SHIELD IS 8.349418E-02~~
~~X AXIS IS 49.79182~~
~~VELOCITY(m/s)= 1990 HEATING RATE (W/m 2)= 0 ALTITUDE(km)= 20~~

STAGNATION PRESSURE ON SHIELD IS 2.101189E-02
X AXIS IS 15.34466
VELOCITY(m/s)= 990 HEATING RATE (W/m 2)= 6649.746
ALTITUDE(km)= 20

STAGNATION PRESSURE ON SHIELD IS 1.179943E-02
X AXIS IS 8.059934
VELOCITY(m/s)= 600 HEATING RATE (W/m 2)= 3103.215
ALTITUDE(km)= 15

```
10 CLS
20 REM**********PROGRAM TO DO HEAT SHIELD HEATING (MARS)**********
30 COLOR 7
40 INPUT "ALTITUDE (km)":ALT
50 INPUT "STATIC TEMP AT INFINITY(K)":T1
60 COLOR 9
70 INPUT "STATIC PRESS AT INFINITY(mb)":P1
80 COLOR 10
90 INPUT "SOUND SPEED AT INFINITY(m/s)":A
100 COLOR 11
110 MW=43.824
120 COLOR 12
130 INPUT "VELOCITY (m/s)":V
140 COLOR 14
150 PRINT
160 GAMMA=A^2*MW/(8314*T1)
170 CP=8314/MW*GAMMA/(GAMMA-1)
175 PRINT "CP":CP."830"
180 HS=CP*T1+V^2/2
190 X=HS/8314*MW/T1
200 M=V/A
202 PRINT "GAMMA=":GAMMA
204 PRINT "M=":M
210 P2=P1*((GAMMA+1)^2*M^2/(4*GAMMA*M^2-2*(GAMMA-1)))^(GAMMA/(GAMMA-1))
220 P2=P2*(1-GAMMA+2*GAMMA*M^2)/(GAMMA+1)/1013.25
230 PRINT"STAGNATION PRESSURE ON SHIELD IS":P2
235 LPRINT"STAGNATION PRESSURE ON SHIELD IS":P2
240 PRINT"X AXIS IS":X
245 LPRINT"X AXIS IS":X
250 COLOR 13
260 INPUT "INPUT Q*SQR(Rn) IN Btu/(Ft^(3/2)*sec)":Q1
270 COLOR 15
280 Q1=Q1/SQR(2*100/2.54/12)/9.4787E-04/144/2.54^2*10000
290 PRINT"HEATING RATE IN W/m^2 IS":Q1
300 PRINT
310 PRINT
320 LPRINT "VELOCITY(m/s)= ":V, "HEATING RATE (W/m^2)= ":Q1, "ALTITUDE(km)=":AL

330 LPRINT
340 GOTO 30
```

AMMA	VELOCITY	SOUND SPEED	STATIC TEMP OF STREAM	STAG. TEMP
1.206	3135	184	148	5006.855
1.24	3231	193	166	5994.24
1.3	3194	217	190	6364.406
1.345	3060	227	202	6546.186
1.34	2818	233	213.5	5022.552
1.33	2150	235	216	3603.902
1.324	1420	240	228	1521.016
1.322	522	245	241	417.1075
1.323	1000	244	236.2	876.9264
1.32	429	247	242.5	359.5449

Section C:

Propulsion Systems

Myles Baker

Propulsion:

1: Requirements:

The Mars Surface Probe places several demands on its propulsion system. From the Mission Scenario, at least five separate impulses are required:

Event:	Required Delta V:	Required Thrust:
Initial orbital maneuvering	<10 m/s	< 10000 N
Descent burn	<200 m/s	< 10000 N
Landing retro burn	<200 m/s	> 500 N
Ascent from Mars surface	~3920 m/s	> 1000 N
Apoapsis injection	~830 m/s	< 200 N

In addition, the propulsion system should be as small and light as possible, since mass is at a premium in such a mission. It should be as simple as possible to increase reliability, and it should be very stable due to the approximately two years it will spend in flight to Mars. An additional restriction placed on the propulsion system is that it never cause the vehicle to accelerate at more than 100 m/s^2, which is reflected in the maximum allowable thrusts.

With these criteria in mind, the decision was to use two separate engines; one for the low-thrust apoapsis injection burn and the other for all other, higher thrust burns. Due to the varying requirements of the first four impulses, it was decided to use a throttleable, re-startable liquid propellant engine. On the other hand, because of the decision to have no active guidance on the final payload capsule, the advantages of a solid motor far outweigh its slightly lower specific impulse. These

advantages include the lack of propellant control devices (valves, etc.), propellant tanks, and the fact that the pre-determined impulse delivered by a solid motor does not require any outside control mechanisms (other than a simple ignitor).

Liquid Propellant Engine:

The prime consideration in the design of this engine was its simplicity. There are several choices in the design of a rocket engine, each of which has a great impact on the final design of the vehicle. Some of the options, and selections for this mission, are listed below.

Thrust: The primary restrictions placed on the thrust of the engine are the imposed design restriction of less than 100 m/s^2 maximum acceleration and the need to overcome Mars' gravity with minimum gravity losses, which requires as high a thrust as possible. From Newton's second law of motion,

$$F_{t,max} = M_{min}a_{max}$$

With a burn-out ascent mass of 15 kg, a thrust of approximately 1500 Newtons is required.

Cooling: There are several methods of cooling a rocket engine, ranging from simple radiation cooling to regenerative cooling by pumping cool fuel through a cooling jacket around the engine. Since this engine is rather small, the extra hardware and complexity required for regenerative cooling eliminate it as a viable option, while radiation cooling is very well suited for such small engines. However, due to the fact that the actual combustion chamber is located inside the vehicle during much of

the mission, some additional cooling is required. Since there is a relatively short total burn time for the engine (approximately 120 seconds), an ablative combustion chamber liner will be used. Such materials are most reliable at chamber pressures of 1 MPa or lower, so 1 MPa is chosen as the maximum chamber pressure for the MSP liquid engine.

Fuels: There are many available fuels for liquid rockets, and various parameters for selecting a fuel for a particular mission. In this case, our requirements are a high specific impulse, high density, and easy storeability for up to two years without maintenance. The latter requirement eliminates several of the higher-energy propellants, such as the cryogenics (Liquid Hydrogen) and the fluoridated oxidizers. On this mission it was decided to use Nitrogen Tetroxide as an oxidizer and 50% Unsymmetrical Dimethyl Hydrazine, 50% Hydrazine (50-UDMH) as a fuel. This propellant combination has several advantages, including hypergolic ignition (no separate ignition system is required), extremely high storeability, a relatively high specific impulse, and a broad base of engineering experience with such propellant combinations.

Propellant feed: There are two types of propellant feed systems in use today: pump-fed and pressure-fed. The pump-fed system requires some additional machinery (a turbo pump, gas generator, and gas turbine), but it allows lower propellant tank pressures, and hence thinner tank walls, lowering the total mass of a large vehicle. Pressure-fed systems, on the other hand, maintain the entire propellant supply at a high pressure and thus

require heavier tanks, but virtually no machinery other than valves. For a vehicle as small as the Mars Surface Probe, the slight increase in tank mass is greatly compensated by the lack of supporting machinery, so a pressure-fed system is more appropriate.

Materials: Recent advances in high-temperature, relatively oxidation-resistant composite materials makes the choice of materials for the motor structure fairly straightforward. Multi-cycle burn times well over the required 100 seconds have been demonstrated with engines constructed almost entirely from a 3-Directional Novoltex(R) type carbon fiber reinforcement in a silicon-carbide matrix[C-1]. In the previously built engines, the fuels, flame temperatures, and motor sizes were similar to those in the Mars Surface Probe.

Solid Motor:

The solid rocket motor for re-insertion into the Mars Orbiting Vehicle's orbit is much simpler. It is only required to ignite, deliver a pre-determined impulse, and extinguish. The payload capsule will already be positioned in the correct attitude and spin-stabilized by the ascent stage, so no attitude control will be necessary. With spin-stabilization, if the spin rate is high enough, it is not necessary to adjust the thrust vector assuming a small uncertainty, so the engine mechanics can be extremely simple. The spin-stabilization of the uper stage will be provided by unwinding a pre-stressed "clockspring" mechanism, in effect spinning the ascent and final stages against

one another.

The fuel used in the solid motor is also well-tested, off the shelf technology. It consists of Aluminum and Ammonium Perchlorate powders in a polyurethane binder. This compound was chosen primarily for its slow burning rate of 6 mm/s, which makes it possible to remain within the 100 m/s^2 design acceleration limit. To minimize the motor case mass and surface area, a spherical case will be used, with a nozzle very similar in its proportions to that used in the liquid engine. The materials used are also very similar to those used in the liquid engine, with the addition of a 4-Directional Carbon-Carbon Sepcarb$^{(R)}$ throat insert to minimize erosion in this critical area.

Propellant Tanks:

There are two necessary sets of propellant tanks. The first set is used for the orbital maneuvering, de-orbit, and retro burns and is housed in the main bus of the vehicle, which is left behind on the planet surface. It contains approximately 5 liters each of N_2O_4 and 50-UDMH pressurized to 1.2 MPa, allowing for 5% ullage, and 2 liters of helium gas at 25 MPa to pressurize the tanks. These tanks will be split up into three identical sets of three tanks each, with similar tanks (e.g. N_2O_4, 50-UDMH, and He) arranged symmetrically about the axis of the vehicle. Due to the small size of the tanks, and the relatively low pressure, 2014-T6 Aluminum alloy (chosen for its good machining properties) will be used for the propellant tanks, and Ti 6Al-4V Titanium alloy (for its exceptionally high strength) for the Helium. Unfortunately,

Nitrogen Tetroxide is not compatible with aluminum tanks, so an interior protective coating will have to be used.

The second set of tanks, used only for the ascent burn, must contain about 19 liters of each of the propellants and 7 liters of helium, again allowing 5% ullage. The configuration for the ascent tanks is shown in figure C.7, with the materials similar to those in the descent tanks. The nested configuration was chosen in order to keep the ascent envelope as small as possible, and only weighs about fifty grams more than the optimum spherical tanks.

Propulsion System Analyses:

The design of a spacecraft is necessarily an iterative process, with the results from each part of the analysis affecting the parameters the remaining phases are based on. This necessitates a certain number of assumptions in the preliminary vehicle design, with succsessive refinements as the design progresses. The assumptions used in the analyses below have been through three such iterations, and so are fairly accurate.

Liquid Propellant Engine:

There are many parameters of interest in the design of a rocket engine, but perhaps the most important are the thrust (F_t), specific impulse (I_{sp}), mass (m), and dimensions, which will be developed here.

The combustion characteristics of Nitrogen Tetroxide and 50-UDMH are tabulated in several references, each with slightly

different values. The values below are taken from Sutton and Ross[C-2]:

Flame Temperature:	3100 K
Gas Constant (R) of Exhaust:	396 J/(kg-K)
Ratio of Specific Heats (Y):	1.24
Density: N_2O_4:	1450 kg/m^3
50-UDMH:	910 kg/m^3
Mixture Ratio (O:F)	
by Mass:	1.62
by Volume:	1.01

Table X.X:
Combustion Properties of Liquid Fuels

Nozzle: Assuming a ratio of ϵ=20 between the nozzle exit area (A_e) and throat area (A_t), the mach number (obtained through a computer iteration) at the exit plane is found to be M_e=3.93. Given the chamber pressure (P_c=1MPa), the pressure at the nozzle exit plane (P_e) can be obtained from the equations for isentropic flow:

$$P_e = P_c \times [1 + \frac{\gamma-1}{2} M_e^2]^{\gamma/(\gamma-1)}$$

$$P_e = 10^6 \times [1 + \frac{1.24-1}{2} (3.93)^2]^{1.24/(1.24-1)}$$

$$Pe = 4439 \text{ Pa}$$

Given the chamber pressure, the exit pressure, and the back pressure (P_b), the thrust coefficient, defined as

$$F_t = P_c A_t C_f$$

can be obtained from the relation

$$C_{f,ideal} = \sqrt{\frac{2\gamma^2}{\gamma-1}\left(\frac{2}{\gamma+1}\right)^{(\gamma+1)/(\gamma-1)}\left[1-\left(\frac{P_b}{P_c}\right)^{(\gamma-1)/\gamma}\right]} + \frac{P_e - P_a}{P_c}\epsilon$$

which, for this engine, at the mean surface pressure at the MSP landing site of 700 Pa, is

$$C_{f,ideal} = \sqrt{\frac{2(1.24)^2}{1.24-1}\left(\frac{2}{1.24+1}\right)^{\frac{1.24+1}{1.24-1}}\left[1-\left(\frac{4439}{1000000}\right)^{(1.24-1)/1.24}\right]} + \frac{4439-700}{1000000}(20)$$

$$C_{f,ideal} = 1.77$$

Assuming a bell nozzle profile of maximum efficiency (a perfect bell nozzle of expansion ratio 30:1 truncated to 20:1), the nozzle losses (due to friction and nozzle divergence) are approximately 2%[C-2], so the actual thrust coefficient is

$$C_f = C_{f,ideal} \times 0.98 = 1.73$$

Given a maximum thrust of 1500 N and a maximum P_c of 1 MPa, the required nozzle throat area is

$$A_t = F_t/(P_c C_f) = 1500/(1.73 \times 10^6)$$

$$A_t = 9 \text{ cm}^2$$

For a throat area of 9 cm^2, the inside diameter at the throat is 3.4 cm, the exit diameter is 15.1 cm, and from the bell nozzle optimization curves[C-3], the nozzle length is 18.6 cm.

The mass flow through the nozzle can be obtained by a mass balance at the throat, where flow is necessarily sonic, so

$$\dot{m} = A_t P_c \sqrt{\frac{\gamma}{R T_c}} \left(\frac{2}{\gamma+1}\right)^{\frac{\gamma+1}{2(\gamma-1)}}$$

$$\dot{m} = (10^6 \text{Pa})(10^{-4} \text{m}^2)\sqrt{\frac{1.24}{(386)(3100)}}\left(\frac{2}{1.24+1}\right)^{\frac{1.24+1}{2(1.24-1)}}$$

$$\dot{m} = 0.533 \text{ kg/s}$$

at a maximum thrust of

$$F_{t,max} = C_f A_t P_c = (1.73)(10^{-4})(10^6)$$

$$F_{t,max} = 1560 \text{ N (at surface)}$$
$$1575 \text{ N (in vacuum)}$$

This gives the liquid engine a specific impulse of

$$I_{sp} = \frac{F_t}{g_o \dot{m}}$$

$$Isp = 298 \text{ sec (at surface)}$$
$$301 \text{ sec (in vacuum)}$$

Combustion Chamber Geometry: In order to minimize pressure losses in the combustion chamber, the velocity just upstream of the throat should be very small, implying a large chamber to

throat area ratio (A_c/A_t). In this case, A_c/A_t will be set to 6.0. Thus the radius of the combustion chamber is

$$r_c = \sqrt{6A_c/\pi}$$

$$r_c = \sqrt{0.0054/\pi} = 4.45 \text{ cm}$$

A second parameter in the design of a liquid-fuel combustion chamber is the characteristic length (l^*), which is defined as the chamber volume divided by the throat area. This length is a useful measure of the amount of time a given element of the fuel-oxidizer mixture remains in the chamber, and must be high enough to ensure complete combustion. In the reaction control thrusters used on many early American launch vehicles, Monomethyl Hydrazine and N_2O_4 were used as propellants and the characteristic length was approximately 0.5 meters[C-2]. This thrust chamber was used as a model, thus requiring a combustion chamber length (approximating the chamber as a cylinder) for the MSP engine of

$$l_c = l^*(A_t/A_c)$$

$$l_c = 0.5/6 = 8.33 \text{ cm}$$

Allowing for 5 cm clearance at the injector for fuel lines and the thrust vector control (gimballing) mechanism, the total liquid engine dimensions are:

$$D_{max} = 16 \text{ cm}$$
$$l_{tot} = 30 \text{ cm}$$

Ablative Cooling Insert: Ablative materials are often used in cooling small, short duration thrust chambers. When exposed to the heat of combustion, the ablator, a fiber reinforcement in an organic matrix, decomposes, leaving a porous, insulating layer of char on the surface. The decomposition of the organic matrix

is an endothermic process, and the pyrolysis gases released tend to insulate the remaining material from the hottest of the combustion chamber gases.

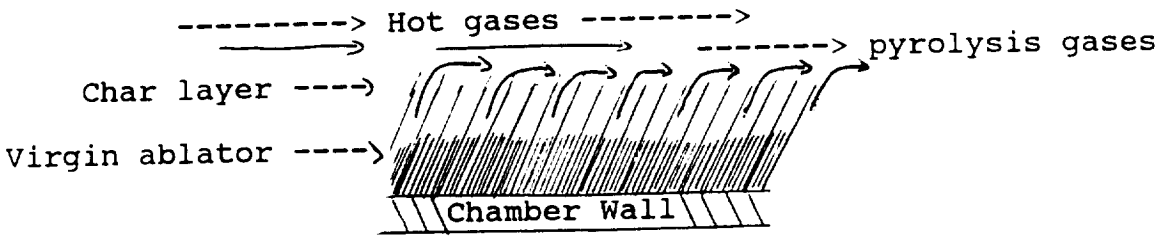

Figure C-1: Ablative Chamber Cooling

A silica fiber reinforcement in a phenolic matrix will be used as the ablative liner of the combustion chamber. The depth of the porous char layer, and hence the necessary thickness of the ablator, is given by the relation[C-3]

$$d_c = \sqrt{\text{burn time in seconds}} \quad \text{mm}$$

$$d_c = \sqrt{120} \text{ mm} = 11 \text{ mm}$$

This analysis does not consider the fact that the engine will reach ambient (spacecraft) temperature between firings, so the actual char depth should be significantly less. Nevertheless, adding a margin of safety, the thickness of the ablative material should be approximately 1.5 cm.

Propellant Injectors: Given the overall mass flow rate, the mixture mass ratio, and the propellant densities, it is easily seen that the necessary volumetric flows for maximum thrust are

$$Q_f = 0.225 \text{ l/s (50-UDMH)}$$

$$Q_o = 0.227 \text{ l/s } (N_2O_4)$$

and, given an orifice-type injector, the volumetric flow rate is

given by the equation[C-4]

$$Q = A_i C \sqrt{\frac{2\Delta P_i}{\rho}}$$

where C_i is an experimentally determined discharge coefficient, usually between 0.6 and 0.9 (assume 0.75), and P_i is the pressure drop across the injector. For a set of n injectors, the total area is

$$\sum_1^n A_i = \frac{Q}{C_i}\sqrt{\frac{\rho}{2\Delta P_i}}$$

which is, for a 200 kPa pressure drop,

$$A_{i,f} = 1.43 \text{ X } 10^{-5} \text{ m}^2$$

$$A_{i,o} = 1.82 \text{ X } 10^{-5} \text{ m}^2$$

For efficient combustion, it is desireable to have as many doublet-impinging pairs of injectors as possible in order to atomize the propellants effectively. This is limited, however, by the machining of the injector manifold and the injectors themselves. One possibility is a set of 19 injector pairs arranged as shown in figure C.2. The diameter of an individual injector is

$$D_i = \sqrt{\frac{A_i}{n\,\pi}}$$

so, for 19 injectors, the diameters for the fuel and oxidizer injectors, respectively, are

$$D_{i,f} = 0.979 \text{ mm}$$

$$D_{i,o} = 1.104 \text{ mm}$$

The injectors should be positioned at angles such that the net momentum of the fuel and oxidizer streams is parallel to the axis of the engine, so

$$\dot{m}_o v_o \sin(\varphi_o) = \dot{m}_f v_f \sin(\varphi_f)$$

$$\varphi_o = \sin^{-1}\left[\frac{\dot{m}_f^2 D_o A_{i,o}}{\dot{m}_o^2 \rho_f A_{i,f}} \sin\varphi_f\right]$$

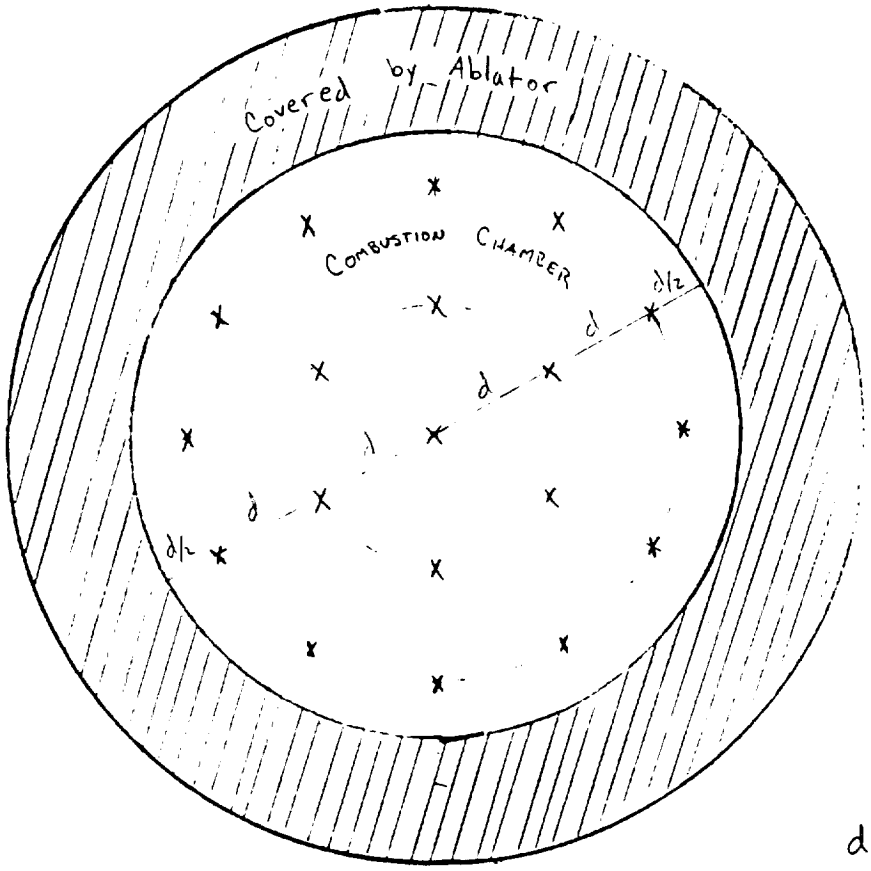

x - Injector Pair (F-O)

d = 1.66 cm

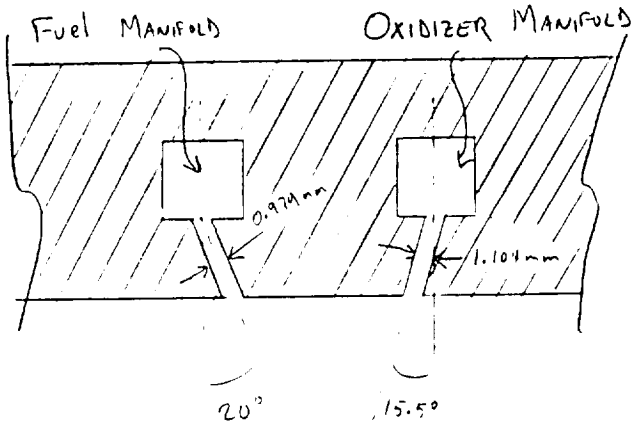

FIGURE C-1 LIQUID ENGINE INJECTOR

Assuming a fuel injector angle of 20° from the engine axis, the oxidizer injector angle should be

$$\varphi_o = \sin^{-1}\left[\left(\frac{0.203}{0.331}\right)^2\left(\frac{1450}{910}\right)\left(\frac{1.82}{1.43}\right)\sin 20^\circ\right]$$

$$\varphi_o = 15.5^\circ$$

Chamber Stress Analysis: The stress analysis of the combustion chamber is very straightforward, considering only the hoop stresses. For 3-Directional Carbon-Silicon Carbide Novoltex(R), ρ = 2300 kg/m^3, σ_y = 80MPa, and for hoop stresses,

$$t_w = r_c(P_c/\sigma_y) \text{ X S.F.}$$

where S.F. is the safety factor (1.5) and r_c contains the ablative chamber liner. Substituting in the values,

$$t_w = (0.0445 + 0.015)(10^6/(80 \text{ X } 10^6)) \text{ X } 1.5$$

$$t_w = 1.1 \text{ mm}$$

A combustion chamber with walls this thin would be extremely difficult to construct reliably, so an additional safety factor will be added to the wall thickness by increasing it to a uniform 2.0 mm.

Mass Estimates: Given the material properties and dimensions calculated above, it is very straightforward to compute the mass of the engine as the sum of the masses of the components. The volume of 3-D Novoltex(R) in the combustion chamber and nozzle shells is

$$V_{C/C} = (0.002 \text{ m})(2\pi(r_c + 0.015 \text{ m}) + A_n)$$

Where A_n, the nozzle surface area, is given by[C-2]

$$A_n = 70 \text{ X } A_t$$

$$V_{C/C} = (0.002)(2\pi(0.0445+0.015) + 70(0.0009)) \text{ m}^3$$

$$V_{C/C} = 8.74 \text{ X } 10^{-4} \text{ m}^3$$

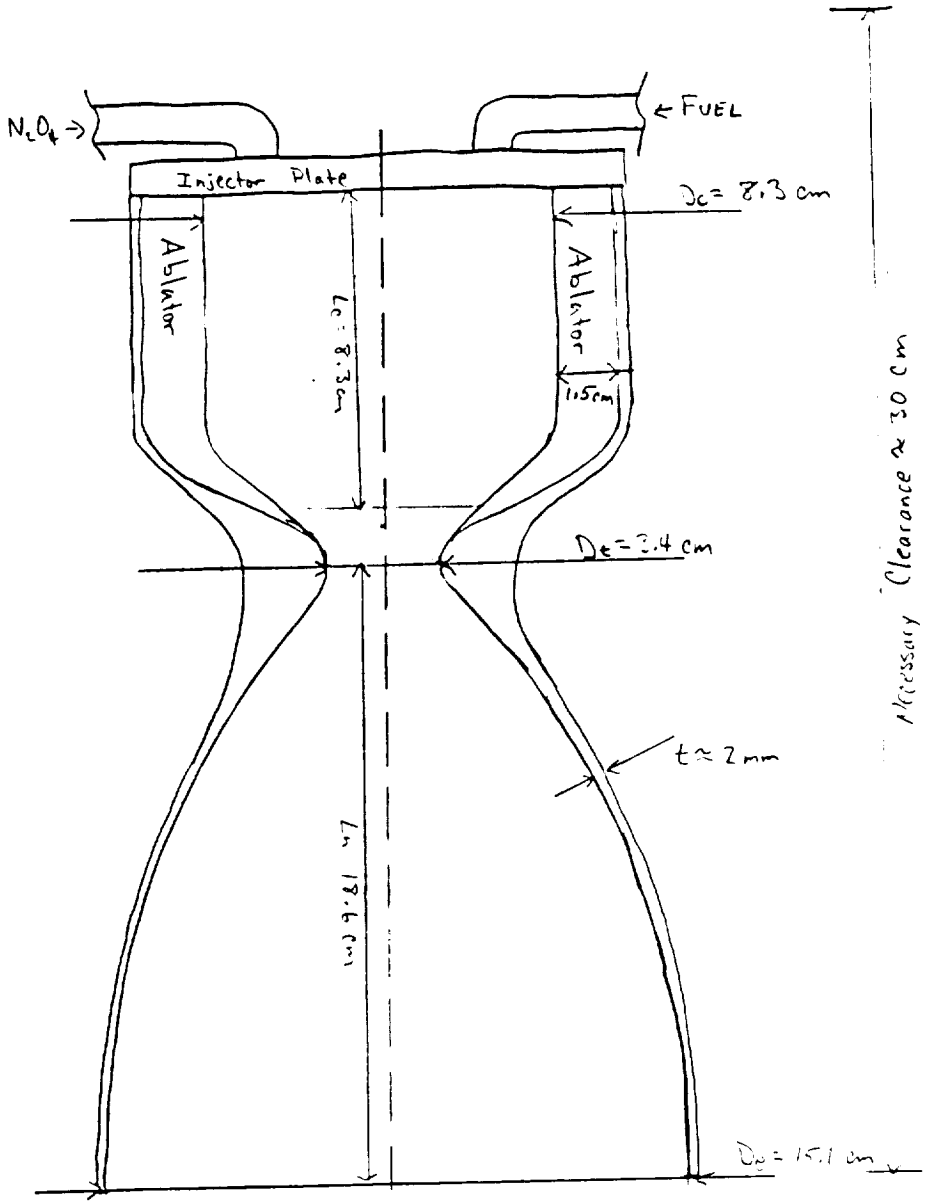

FIGURE C-3 MSP LIQUID ENGINE

So the mass of the chamber and nozzle shells is approximately

$$M_{shell} = 2300 \text{ kg/m}^3 \text{ X } 8.74 \text{ X}10^{-4} \text{ m}^3$$

$$Mshell = 0.20 \text{ kg}$$

The ablative insert mass, assuming a uniform density of 1740 kg/m^3 is

$$M_{abl} = 2\pi(r_c + 0.015/2) \text{ X } l_c \text{ X } _{abl} \text{ X } 0.015$$

$$Mabl = 2\pi(0.0445 + 0.0075) \text{ X } 0.0833 \text{ X } 1740 \text{ X } 0.015$$

$$M_{abl} = 0.71 \text{ kg}$$

And the mass of the injector plate, assumed stainless steel (ρ = 7600 kg/m^3), 1 cm thick, and 50% hollow for fuel manifolds,

$$M_{inj} = \pi(r_c + 0.015)^2 \text{ X } 0.01 \text{ X } 7600 \text{ X } 50\%$$

$$M_{inj} = 0.80 \text{ kg}$$

Thus the entire engine mass is approximately

$$M_{eng,liq} = 0.20 + 0.71 + 0.80 = 1.71 \text{ kg.}$$

Allowing some excess for throat reinforcement, plumbing, and the gimballing bearing,

$$M_{eng,liq} = 2.0 \text{ kg}$$

Solid Orbital Insertion Motor:

The analysis of the solid motor is very similar to that for the liquid motor. The properties of the solid Polyurethane/ Ammonium Perchlorate/Aluminum fuel, again from Sutton and Ross[C-2], are:

Flame Temperature:	3088°K
R of Exhaust Products:	284 J/(kg-K)
γ of Exhaust Products:	1.17
Burning Rate:	6 mm/s_3
Density:	1750 kg/m^3

Dimensions: Assuming a chamber pressure of 1 MPa and a

nozzle exit area ratio of 20:1, the Mach number at the exit plane is found (again by computer iteration) to be 3.65. At the exit,

$$P_e = (10^6)\left[1 + \frac{1.17-1}{2} 3.65^2\right]$$

$$P_e = 5452 \text{ Pa}$$

And the thrust coefficient is

$$C_{f,ideal} = \sqrt{\frac{2(1.17)^2}{1.17-1}\left(\frac{2}{1.17+1}\right)^{\frac{1.17+1}{1.17-1}}\left[1-\left(\frac{5452}{1000000}\right)^{\frac{1.17-1}{1.17}}\right]} + \frac{5452-0}{1000000}(20)$$

$$C_{f,ideal} = 1.849$$

Again applying the 98% nozzle efficiency (similar geometry to liquid engine):

$$C_f = 1.812$$

Assuming a maximum thrust of 200 N (2.0 kg final mass at 100 m/s^2),

$$A_t = \frac{F_t}{C_f P_c} = \frac{200 N}{1.812 (10^6 Pa)}$$

$$A_t = 1.103 \text{ X } 10^{-4} \text{ m}^2$$

$$A_t = 1 \text{ cm2}$$

So the actual maximum thrust is

$$F_{t,max} = (10^{-4})(10^6)(1.812) = 181.2 \text{ N}$$

The mass flow is again given by

$$m = a^* A^* \rho^* = P_c A_t \sqrt{\frac{\gamma}{RT_c}}\left(\frac{2}{\gamma+1}\right)^{\frac{\gamma+1}{2(\gamma-1)}}$$

$$m = (10^6)(10^{-4})\sqrt{\frac{1.17}{284.3688}}\left(\frac{2}{1.17+1}\right)^{\frac{1.17+1}{2(1.17-1)}}$$

$$m = 0.0687 \text{ kg/s}$$

And hence the specific impulse:

$$I_{sp} = 181.2/((0.0687)(9.81)) = 269 \text{ sec}$$

The specific impulse, from the ideal rocket equation, gives the propellant mass and volume:

$$M_p = 2.0 \text{ kg} \times \left[\exp\left(\frac{\Delta V}{g_o I_{sp}}\right) - 1\right]$$

$$M_p = 2\left[\exp\left(\frac{822}{(9.81)(264)}\right) - 1\right]$$

$$M_p = 0.734 \text{ kg}$$

$$V_p = M_p/\rho_p = 4.19 \times 10^{-4}$$

The burning area (A_b) for these conditions can be found from

$$A_{b,max} = \dot{m}/(\rho_p r_b)$$

$$A_{b,max} = (0.0687)/((1750)(0.0006))$$

$$A_{b,max} = 65.4 \text{ cm}^2$$

Grain Design: For a neutral-burning, cylinder-based grain configuration (such as the conventional star grain), the cylinder length and radius, in order to meet the criteria on area and volume, must be

$$r = 2V_p/A_b = 2(4.19 \times 10^{-4})/6.54 \times 10^{-3}$$

$$r = 17.1 \text{ cm}$$

$$l = V_p/(\pi r^2) = 6 \text{ mm}$$

Obviously this grain configuration is absurd, so another must be sought. Since this motor operates in free fall, a neutral burn is not required, and the options for grain configurations is almost endless. This motor will have a "sphere within a sphere" grain configuration as shown in figure C.4. The burning area as a function of time is

$$A_b = \frac{\pi(r_o + r_b t)}{r_c}\left[r_c^2 - (r_o + r_b t - r_c)^2\right]$$

and the remaining propellant mass is

$$M_p = \frac{\pi\rho_2}{3}\left[2r_c^3 + \frac{3}{2}r_c(r_o + r_b t)^2 - \frac{1}{8}(r_o + r_b t)^3\right]$$

Using the fact that the thrust in vacuum is directly proportional

to A_b and P_c, a computer spreadsheet was programmed to calculate the chamber pressure and acceleration as functions of time (figures x.x and x.x), and various dimensions were tested. The final propellant grain dimensions are a total grain radius of 4.65 cm and an initial bore radius of 1.0 cm. As can be seen from the graphs, the maximum acceleration is 90.0 m/s^2 and the maximum chamber pressure is 1.25 MPa. This pressure is slightly higher than initially assumed, but easily feasible.

Stress Analysis and Mass Estimate: The stress analysis is nearly a duplicate of that used for the liquid engine except for the fact that this case is spherical rather than cylindrical. Chamber wall thickness is given by

$$t_w = r_c/2 \text{ X } (P_c/\sigma_y) \text{ X S.F.}$$

With similar materials,

$$t_w = (0.0465/2)(1.25/80)(1.5)$$

$$t_w = 0.545 \text{ mm}$$

This chamber is also impossible to reliably construct, so again, a 2 mm uniform wall thickness is assumed. This gives the total mass of the case and nozzle:

$$M_{tot} = (0.002)(4\pi(0.0465)^2 + 70(0.0001))(2300)$$

$$M_{tot} = 0.157 \text{ kg}$$

Allowing 0.093 kg for throat inserts, internal insulation, and attachment hardware, the mass of the solid motor is

$$M_{fueled} = 0.984 \text{ kg}$$

$$M_{dry} = 0.250 \text{ kg}$$

Solid Motor Spin-up Mechanism (Clockspring): In order to have stability in a spin-stabilized spacecraft, the rotational

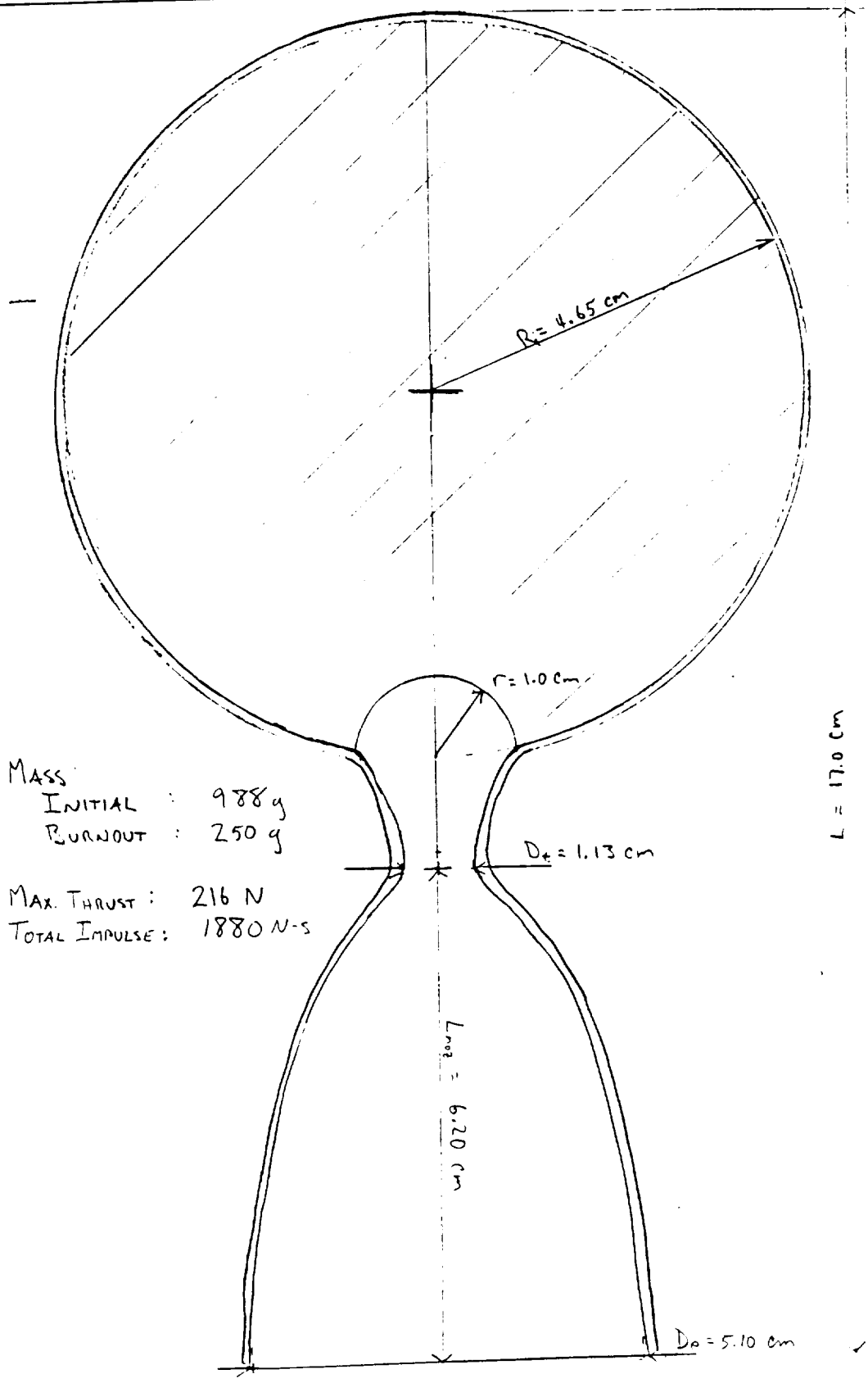

MASS
INITIAL : 988 g
BURNOUT : 250 g

MAX. THRUST : 216 N
TOTAL IMPULSE : 1880 N-s

FIGURE C.4
SOLID INSERTION MOTOR

Figure C.5: Final Stage Acceleration Profile

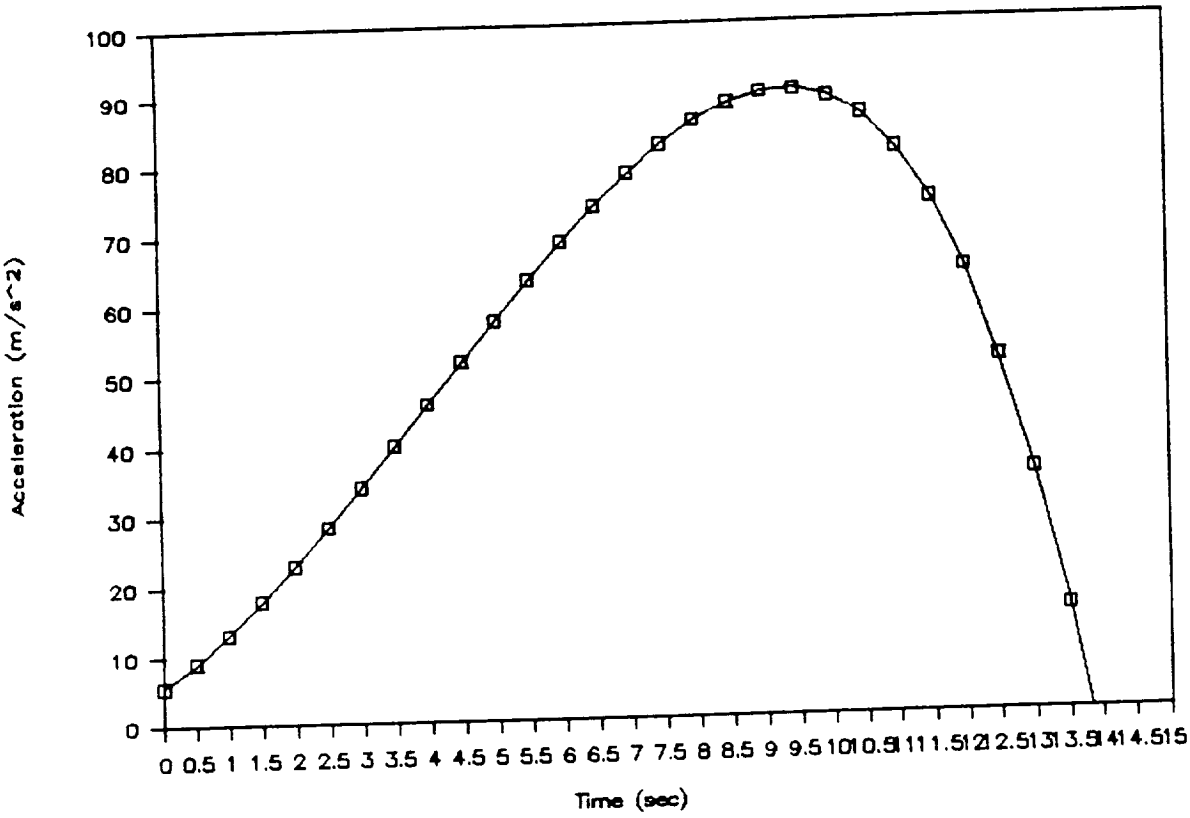

Figure C.6: Solid Motor Chamber Pressure Profile

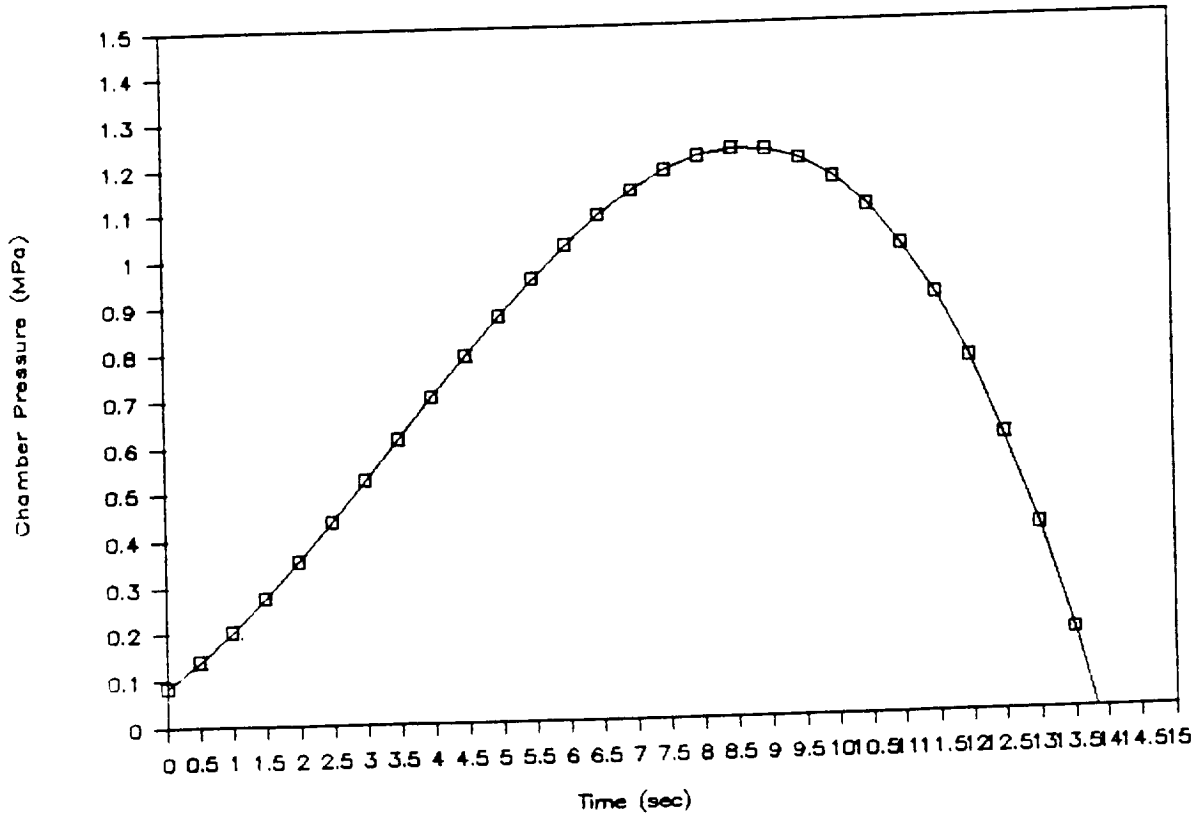

kinetic energy must be much greater than the maximum anticipated disturbing moment. Assuming a 1 mm misalignment of the thrust vector with the center of mass at 200 N thrust, the disturbance torque is

$$M_D = (0.001\ \text{m})(200\ \text{N}) = 0.2\ \text{N-m}$$

The rotational kinetic energy of a spinning body is given by

$$E_K = I\,\omega^2/2$$

where I is the moment of inertia about the spin axis and ω is the spin rate in radians per second. Assuming the rendezvous stage to be a uniform cylinder of r = 5 cm, m = 2.7 kg, then I is given by

$$I = mr^2/2 = (2.7\ \text{kg})(0.05\ \text{m})^2/2$$

$$I = 0.00375\ \text{kg-m}^2$$

Assuming a kinetic energy of five times the disturbance torque,

$$\omega = \sqrt{\frac{10(0.2\ \text{N-m})}{0.00375\ \text{kg-m}^2}}$$

$$\omega = 23.09\ \text{radians/sec}$$

With a safety factor of over 2 to include the depletion of propellant mass,

$$\omega = 50\ \text{radians/sec}$$

The angular acceleration of a rotational mass is

$$\alpha = \frac{T}{I} = \frac{d^2\theta}{dt^2}$$

and the torque exerted by a rotational spring is

$$T = -k\,\theta$$

which implies

$$\frac{d^2\theta}{dt^2} + \frac{k}{I}\theta = 0$$

$$\theta = -\theta_0 \cos\left(\sqrt{\frac{k}{I}}\,t\right)$$

$$\omega = \frac{d\theta}{dt} = \theta_0\sqrt{\frac{k}{I}}\sin\left(\sqrt{\frac{k}{I}}\,t\right)$$

At the maximum rotational velocity, this is

$$\omega_{max} = \theta_0 \sqrt{\frac{k}{I}}$$

$$k = \left(\frac{\omega_{max}}{\theta_0}\right)^2 I$$

Assuming a spin-up angle of 10 revolutions (62.8 radians),

$$k = \left(\frac{50}{62.8}\right)^2 (0.00375)$$

$$k = 0.00238 \text{ N-m/rad}$$

This is a very small torque, and a spring to provide it, along with a bearing and shaft, should weigh no more than 0.1 kg.

Liquid Propellant Tanks:

Descent: During the descent phase of the mission, there are three separate liquid motor firings: Orbital Maneuvering, De-Orbit, and Retro Landing. The mass of fuel required for each burn is calculated by applying the ideal rocket equation,

$$M_{fuel} = M_{veh}\left[\exp\left(\frac{\Delta V}{g_0 I_{sp}}\right) - 1\right]$$

using the ΔV's and M_{veh}'s at the given time. Applying the equation,

$$M_{f,om} = 0.802 \text{ kg}$$
$$M_{f,d\text{-}o} = 7.353 \text{ kg}$$
$$M_{f,ret} = 1.850 \text{ kg (max)}$$

$$M_{f,desc} = 10.105 \text{ kg}$$

Allowing almost 2 kg of fuel for ullage and contingencies such as an extended retro firing, the total descent fuel mass is 12 kg. Using the mixture ratio and densities of the propellants, the necessary tankage is 5.1 liters each of N_2O_4 and 50-UDMH. The volume of Helium necessary to keep these tanks pressurized to 1.2 MPa can be calculated by modelling the process as an adiabatic

expansion of an ideal gas where

$$pV^{\gamma} = \text{Constant}$$

For an adiabatic expansion from P_1, V_1 to P_2, V_2, the required V_1 is

$$V_1 = V_2 \times P_1^{1/\gamma} / (P_2^{1/\gamma} - P_1^{1/\gamma})$$

$$V_{He} = (2 \times 5.1) \times 1.2^{1/1.66} / (25^{1/1.66} - 1.2^{1/1.66})$$

$$V_{He} = 2.0 \text{ liters}$$

Taking three identical sets of tanks, the radii are

$$r_f = 7.4 \text{ cm}$$

$$r_o = 7.4 \text{ cm}$$

$$r_{He} = 5.4 \text{ cm}$$

Using 2014-T6 Aluminum ($\rho = 2800$ kg/m^3, $\sigma_y = 386$ MPa) for the propellant tanks and Ti-6Al-4V Titanium ($\rho = 4430$ kg/m^3, $\sigma_y = 999$MPa) for the Helium, the required wall thicknesses are, from an analysis identical to that used in the spherical solid rocket case:

$$t_f = 0.17 \text{ mm}$$

$$t_o = 0.17 \text{ mm}$$

$$t_{He} = 1.01 \text{ mm}$$

The thicknesses of the fuel and oxidizer tanks are thinner than can be practically manufactured, so assuming a minimum machineability of aluminum to be 0.3 mm, the total tank mass is

$$M_t = 12\pi (r_f^2 t_f \rho_{Al} + r_o^2 t_o \rho_{Al} + r_{He}^2 t_{He} \rho_{Ti})$$

$$M_t = 12\pi ((2)(2800)(0.074^2)(0.0003) + (4430)(0.054)^2(0.00101))$$

$$M_t = 0.84 \text{ kg}$$

Adding over 50% for valves and plumbing, the total fuel system mass for the descent stage is M = 1.50 kg.

Ascent: The fuel requirements for the ascent burn cannot be calculated from the ideal rocket equation due to the effects of aerodynamic drag, but since the burn time and thrust are known, the mass of fuel expended can be calculated using the specific impulse:

$$M_p = \frac{F_t\, t}{g_o I_{sp}}$$

Where t_b is the burn time in seconds. For the ascent stage, with a 1500 Newton constant thrust for 82 seconds,

$$M_p = (1500)(82)/((9.81)(298))$$

$$M_p = 42.0 \text{ kg}$$

Adding 5% for ullage,

$$M_p = 44.1 \text{ kg}$$

Using a breakdown similar to the descent tanks, this requires volumes of

$$V_f = 18.5 \text{ liters}$$

$$V_o = 18.9 \text{ liters}$$

$$V_{He} = 7.3 \text{ liters}$$

In order to minimize the envelope of the ascent vehicle, the tank configuration shown in figure C.7 was selected. The spherical caps and the cylindrical section have a radius of

$$R = \sqrt[3]{\frac{3V_f}{4\pi}}$$

$$R = 18.5 \text{ cm}$$

and the cylindrical section (containing N_2O_4) has a length of

$$L = V_o/(\pi R^2)$$

$$L = 18.0 \text{ cm}$$

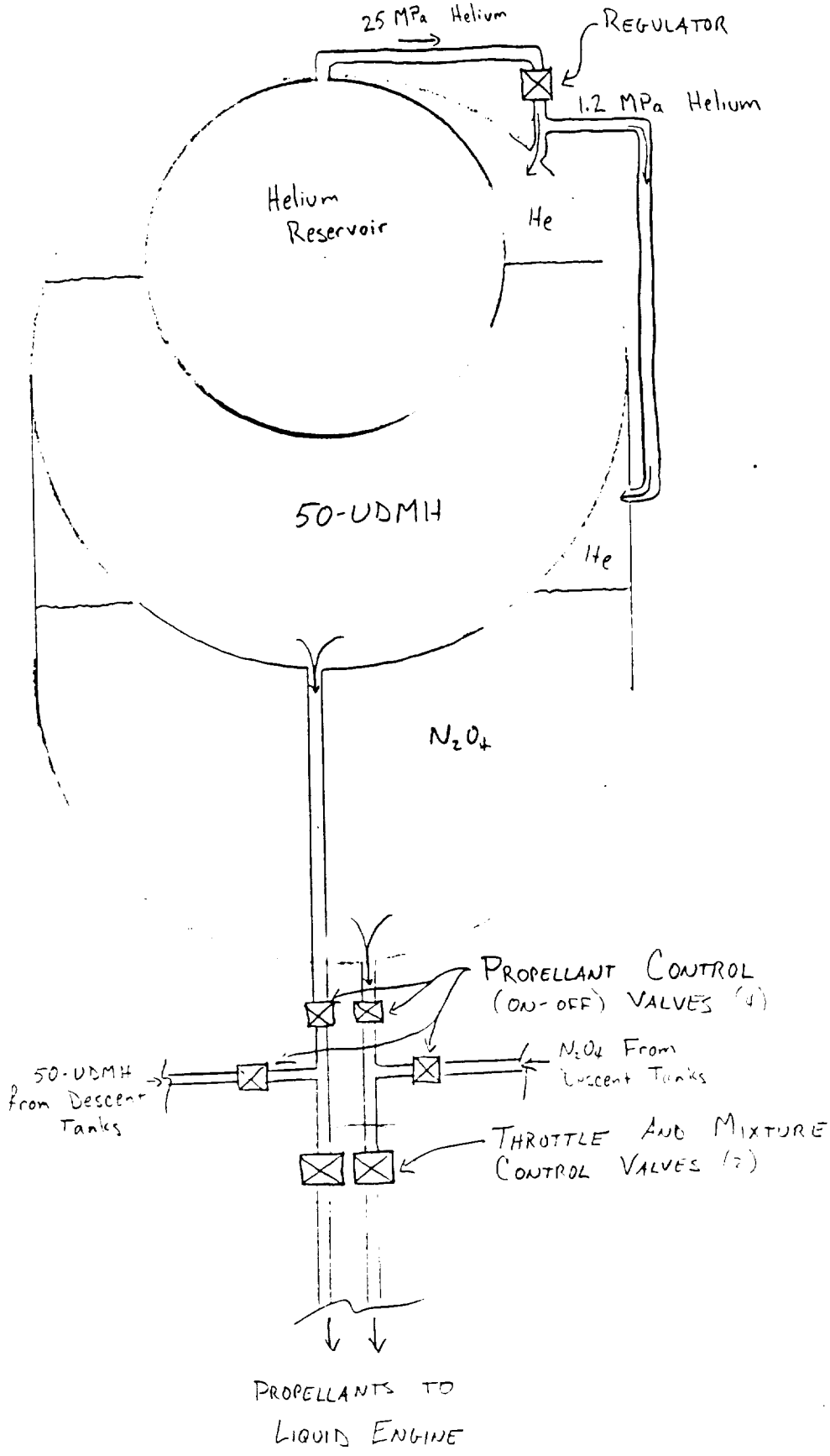

FIGURE 4-7.
ASCENT PROPELLANT TANKS AND PLUMBING

The Helium tank has radius

$$R_{He} = \sqrt[3]{\frac{3(0.0073)}{4\pi}}$$

$$R_{He} = 12.0 \text{ cm}$$

Again using 2014-T6 Aluminum for propellant tanks and Ti-6Al-4V Titanium for the Helium, the required thicknesses are:

$$t_{sphere} = 0.43 \text{ mm}$$

$$t_{cyl} = 0.86 \text{ mm}$$

$$t_{He} = 2.26 \text{ mm}$$

The total mass of the ascent tank structure is

$$M = \pi((6R^2 t_{sphere} + 2RLt_{cyl})(\rho_{Al}) + 4R_{He}^2 t_{He}(\rho_{Ti})$$

$$M = \pi(6(0.185)^2(0.00043)+2(0.185)(0.180)(0.00086)) \times (2800) + \pi(4)(.120)^2(0.00226)(4430)$$

$$M = 3.07 \text{ kg}$$

Adding 0.43 kg for plumbing and valves, the final tank mass is

$$M = 3.50 \text{ kg}$$

References:

C-1: Paul Donguy and Jacques Broca, "High Temperature Composite Materials for Rocket Propulsion," AGARD Conference Proceedings #449, 1988.

C-2: George P. Sutton and Donald M. Ross, Rocket Propulsion Elements: An Introduction to the Engineering of Rockets, John Wiley and Sons, N.Y., 1976.

C-3: J. L. Tuttle and D. H. Blount, Perfect Bell Nozzle Parametric and Optimization Curves, NASA Reference Publication 1104, 1983.

C-4: Liquid Rocket Engine Self-Cooled Combustion Chambers, NASA Technical Report N78-21211, 1978.

C-5: Elliot Ring, Rocket Propellant and Pressurization Systems, Prentice-Hall, N.J., 1964

C-6: F. A. Williams, M. Barrere, and N. C. Huang, Fundamental Aspects of Solid Propellant Rockets, AGARD, 1969.

C-7: Pressurization Systems for Liquid Rockets, NASA Technical Report N76-22300, 1976.

Section D:

Orbital Mechanics

Bob Langberg

Orbital Transfer and Ascent/Descent Trajectories

Planetary Characteristics Pertinent to Orbital Calculations

Mass	$6.4182\ 10^{23}$ (kg)
Universal Gravitational Constant	$6.6732\ 10^{-11}$ (m3/kg s2)
μ Gravitational Constant for Mars	$4.2830\ 10^{13}$ (m3/s2)
	42830.(km3/s2)
Equatorial Gravitational Acceleration	3.73 (m/s2)
Mean Radius	3402 (km)
Sidereal Day	24 hours 37 minutes 23 seconds
	24.623 (hours)
	1477.4 (minutes)
	88643. (seconds)
Angular Velocity	0.24367 (deg/min)
	$4.2529\ 10^{-3}$ (rad/min)
Rotational Speed (Equatorial)	14.468 (m/min)
	0.24113 (m/s)
(28.5° Latitude)	12.715 (m/min)
	0.21191 (m/s)

Mars Orbiting Vehicle (MOV) Orbital Parameters

Circular
Ascending Node at 250° Longitude
Inclination 30°
Altitude 600 (km) above mean radius
Orbital Radius 4002 (km)
Orbital Velocity 3.2715 (km/s)
Orbital Period 2 hours 8 minutes 6 seconds
2.1351 (hours)
128.11 (minutes)
7686.4 (seconds)

Landing Site

Depression Hellas, near Crater 29

Altitude	4.2 (km) Below Mean Radius
Radius of Site	3397.8 (km)
Longitude	283 (Deg)
Latitude	-28.5 (Deg)

Descent Analysis

Ideal Descent Analysis, Neglecting Atmospheric Drag

Initially the descent trajectory was modeled without taking the atmosphere into account, using ideal equations for elliptical orbital motion (Kepler Motion). In this analysis there was an orbital plane change, calculated with spherical trigonometry, at the same time as the deorbit burn. This combined burn put the Mars Surface Probe (MSP) on an elliptical orbit that intersects the Martian Surface at the landing site. It was optimized with the constraint that the flight angle at landing could not be less (not shallower) than 15°. Orbits of eccentricity varying from 0.08 (nearly circular) to 0.93 (an extremely narrow ellipse) were examined. The delta v required was least at the more circular ellipses, with an absolute minimum occurring at the ellipse with eccentricity of 0.14, which had the minimum plane change angle (10.1°), unfortunately its angle with the horizon upon landing was 7.83° which was too shallow.

The best case which did meet the 15° requirement was the transfer ellipse with eccentricity of 0.270 . It had a velocity at apoapse (4002 km) of 2.795 km/sec, which is 0.476 km/sec less than the MOV's circular orbital velocity of 3.271 km/sec. This orbit takes the MSP through a 58.7° change in true anomaly, to land with an impact velocity of 3.409 km/sec. The entire deorbit takes 21.8 minutes, during which time Mars rotates 5.31° on its axis. The plane change angle for this case was 11.7°, which when combined with its velocity change for deorbit (0.476 km/sec) required a total delta v of 0.781 km/sec. This was the best that could be done with the plane change while neglecting the atmosphere.

Detailed Descent Analysis, With Atmospheric Drag

Avoiding the Plane Change Maneuver

After the ideal analysis was completed it was decided that a significant fuel savings (305 m/sec) could be attained by avoiding the 11.7° plane change. By leaving the MOV orbit with a small delta v of 8.1 m/s (0.2% of the circular velocity) the MSP would advance or recede by a rate of 2.5° per orbit. After 72 orbits, the MSP may move up to ±180°, allowing it to be positioned anywhere on the orbit. With precise positioning it may then deorbit as Mars rotates and the target point passes below, without the necessity of a plane change. This positioning would take up to 6.2432 Mars sidereal days (6 sidereal days and 9 hours) and would allow the MSP to position itself at any point in orbit to successfully deorbit and land at the specified sampling site. The extended time in orbit presents no apparent thermal problems.

Limits of Atmospheric Effects

To accurately model the effects of the atmosphere, the deorbit trajectory was assumed to be a Kepler ellipse until an altitude of 250 km was attained. The drag force on the MSP at an altitude of 250 km is $1.04\ 10^{-4}$ N. The maximum drag is $6.92\ 10^{+3}$N which occurs at an altitude of 30.1 km. This difference, in excess of seven orders of magnitude, shows that not only is it a very reasonable assumption to ignore atmospheric effects above 250 km, but that atmospheric drag probably could have been ignored until about 150 km altitude where the drag is approximately 0.6 N.

Incremental Time Step Analysis

At 250 km, the velocity and flight path angle was computed for the ideal transfer orbit. These were used as initial conditions for a time stepping analysis. In this analysis, the aerodynamic force on the MSP, which was assumed to be drag only, with no lift is computed. The drag

force was computed based on a Cd of 1.0 which is referenced to the projected area of the MSP. The gravitational acceleration was computed as a position of radius using the standard inverse square law at each position during the descent. These two forces were used to compute the acceleration in the radial and tangential directions and the resultant changes in velocity and position. Time increments ranged from one second to ten seconds, with five second increments used during the period of maximum aerodynamic forces. The MSP mass was changed as the heat shield is dropped as the parachute is deployed. The Cd reference area was changed at the time of parachute deployment, but the Cd is kept at 1.0. Both of these changes take place approximately 1.2 km above the landing site.

Terminal Velocity of Heat Shield and Parachute

Terminal velocity design charts were generated for the heat shield and parachute design analysis. These charts were used in the sizing process only and were not directly part of the incremental time/dynamic analysis. The final dimensions for the heat shield and parachute diameters are 1.5 and 4.0 m respectively.

Atmospheric Model

The atmospheric model used to calculate the variation of density with altitude, used for drag calculations is based on: *The Mars Reference Atmosphere, 1982, published by The Committee on Space Research, Chapter 1: "Post-Viking Models for the Structure of the Summer Atmosphere of Mars", written by A. Seiff.* Data from this source concerning the atmosphere in the southern hemisphere, during summer, at low altitudes was used to construct an exponentially decaying atmosphere model. The model is based on the density at the mean surface, 1.78 10^{-2} kg/m3, and an exponential scale height, 11.75 km, where the density has fallen off by 1/e.

$$\text{density(alt)} = \text{density(0)} * \exp[-\text{alt/scale ht.}]$$

This model is most accurate where it has the greatest influence on the MSP, at low altitudes where the density is greatest, and the resulting aerodynamic forces are largest. See graphs for the shape of the atmospheric models. It is significant to note that the density has fallen off the linear scale at 70 km altitude. (0.26% of the density at the surface.

Optimizing Deorbit Delta V with respect to Eccentricity

The transfer ellipse that sets the initial conditions for the descent analysis was originally assumed to be the transfer ellipse from the ideal case with an eccentricity 0.27 . Due to the drag on the heat shield and parachute, the landing trajectory is nearly vertical near the surface. Thus the 15° restriction on landing angle is no longer a constraint for the real descent case.

By doing a computation comparing the deorbit fuel required vs. the eccentricity of the exoatmospheric transfer ellipse, a simple relationship was developed. It shows that the delta v only depends on the original circular velocity and the transfer ellipse eccentricity, e:

$$\text{Delta V} = \text{V Circular} * [\ 1 - \text{Sqrt}(1-e)\ ]$$

This function is tabulated and graphed. It was found that another significant fuel savings could be realized by making an even shallower approach to the Martian surface, and the shallower the approach, the more fuel saved.

The problem with making the approach more shallow is that the distance traversed becomes greater, and the accuracy of the reentry is reduced. For this reason the transfer ellipse was made only slightly more circular. The original eccentricity was 0.27, requiring a delta v of 0.476 km/sec, and the new eccentricity is 0.10, requiring a delta v of only 0.169 km/sec. This causes the true anomaly traversed in descent to increase from 53.42° to 98.10°, and

the time of descent to increase from 22.37 to 36.04 minutes. However, most of this increased travel is exoatmospheric. The atmospheric true anomaly traversed (250 km to surface) increases from 11.23° to 16.00°, and the time in the atmosphere (250 km to surface) goes from 5.85 to 7.19 minutes.

These two trajectories are essentially the same near the surface where the velocities and flight path angles are: 161.7 vs. 159.9 m/sec and 66.8° vs. 68.8°, for the old and new cases respectively. These values are for an altitude 5 km above the surface. Thus, for this analysis they are essentially compatible, and since the e = 0.10 case is more fuel efficient, (0.169 vs. 0.476 km/sec, a 64% savings) it was chosen as the final descent trajectory. The fuel savings was approximately 10 kg.

Range Error Due to Uncertainty in Deorbit Delta V

Because we enter the atmosphere at a rather shallow angle, (17.6° at 100 km altitude), the accuracy of the trajectory was questionable. Since the vehicle is in free flight with only small attitude control thrusters for orbital corrections, it is of importance to know how sensitive the trajectory is to the only parameter we can effectively control, the deorbit delta v. The same time stepping analysis was run for a 2% decrease in delta v. The new case placed the MSP 13.64 km short of its original target, but this is a small change considering the fact that the deorbit trajectory traverses over 5800 km.

The final descent trajectory has the following characteristics:

Eccentricity	0.10
True Anomaly Traversed (exoatmospheric/atmospheric)	82.1°/16.0°
Radius at Apoapse	4002 km
V Apoapse	3.102 km/sec
V Terminal (300 m above surface)	< 45 m/sec
Delta V (deorbit)	168 m/sec
Delta V (combined deorbit & retrofire)	211 m/sec
Max. Mach (100 km alt.)	19.3
Max. Dyn. Press. (30.1 km alt.)	1968. N/m2
Max. Deceleration (30.1 km)	8.2 earth g's
Time during max deceleration (3000/250 m/s)	75 sec

Ascent Analysis

The ascent was modeled the same way as the descent. The assumed Cd was again 1.0 . The gravitational acceleration and the atmospheric density varied with radial position. Because the 82 second 1500 N ascent burn cannot be assumed to be impulsive for a ten minute flight, the thrust was considered to act in a constant manner and was just considered to be another force on the body for the duration of the burn. It was assumed that the mass decreased linearly during this period. The resulting acceleration was computed each second during the burn and every five or ten seconds after burn out. These accelerations were used to calculate the new velocity and position in polar coordinates, just as they were in the descent analysis. The basic parameters that were varied were the length of the 1500 N burn and the launch angle. From these initial conditions, the delta v required at 600 km to circularize the orbit at the same velocity as the MOV was computed.

Optimum Ascent Angle and Minimum Insertion Delta V

The required delta v was quite sensitive to launch angle, as measured from the horizon. The optimum angle varied between 60° and 62° in a nonlinear fashion, depending on the duration of the ascent burn. At each burn duration, the optimum angle was determined to within 0.5°. By launching at 0.5° too low an angle, the ascent stage fell approximately 25 km short of its 600 km target altitude. If launched at 0.5° too great an angle, it would reach 600 km with a flight path angle of about 10°, which must be corrected for with a larger delta v for circularization. The optimum launch angle allows the ascent stage to just reach the 600 km mark with a flight path angle as close to zero as possible to minimize the delta v required.

It was also found that with longer launch burns the velocity at 600 km was greater (at the optimum launch angle), requiring less and less insertion/circularization delta v. The penalty here is the increased launch mass for fuel and tanks. There is obviously an optimum distribution of the increased mass between the boost stage and the apoapse stage, but we had a driving design condition other that total mass to consider.

The driving criteria for the launch trajectory turned out to be the apoapse kick solid rocket motor. With its burn characteristics determined by the spherical grain configuration, the maximum delta v it could provide without exceeding 10 g's was between 800 and 850 m/s. With our original launch mass of 46.4 kg the minimum possible delta v at the optimum launch angle was 1481. m/s, which could not safely be considered. A number of alternate cases were investigated.

The final optimum launch profile increased the launch mass to 56.8 kg (a 10.4 kg increase), neglecting the increase in fuel tank mass. This profile required a launch angle of 61.0° and a burn for 82 sec of 1500 N. The ascent stage reaches 600 km altitude after 10.8 minutes, with a flight path angle of only 2.92°. The required delta v is 828.0 m/sec.

If the flight path angle had been 61.5° the required delta v would have been 930.4 m/sec (a 102.4 m/s increase), and if launched at 60.5° the ascent stage would have fallen about 40 km short of its 600 km target.

Rendezvous Strategy

For rendezvous purposes the ascent stage could be placed into an orbit with a slightly different period than that of the MOV, thus letting the sample return vehicle catch up to the MOV without the MOV having the burn any additional fuel (passive recovery). As discussed for the deorbit positioning, a ±8.1 m/sec delta v would let the

ascent stage advance/recede by a rate of 2.5°/orbit. This allows for rendezvous in less than seven days. The ascent stage is not thermally sensitive at this point in the mission, therefore the rendezvous passage presents no thermal problems.

The final ascent trajectory has the following characteristics:

Ascent Thrust (82 seconds)	1500 N
Delta V Launch	4020.3 m/sec
Maximum Acceleration at Launch	10 g's
Launch Angle	61.0°
Max. Mach (75 km alt.)	16.8
Max. Dyn. Press. (10 km alt.)	2732. N/m2
True Anomaly Traversed (exoatmospheric/atmospheric)	1.64°/2.37°
Time in Atmosphere (up to 250 km altitude)	196 sec
Flight Path Angle at Insertion	2.92°
V (600.9 km Altitude)	2456.1 m/sec
V Circular (MOV)	3271.4 m/sec
Delta V insertion	828.0 m/sec
Delta V (combined launch & insertion)	4848.3 m/sec
Maximum Acceleration at Insertion	< 10 g's

Total Delta V: (m/s)	
Positioning	8.1
Deorbit	167.9
Retrofire	42.9
Ascent	4020.3
Insertion	828.0
Rendezvous	8.1
	5075.3

Orbit and Trajectory Supplemental Information

- Mission Overview Diagram
- Mission Profile
- Ideal Descent
  - Equations
  - Plane Change Calculation
  - Time Elapsed During Orbital Motion Calculation
- Detailed Analysis
  - Force Balance Diagram
  - Pertinent Equations
  - Iterative Time Stepped Procedure
    - Used in Spread Sheet Calculations
  - Selected Results From Descent Trajectory, Including:
    - Parachute Deployment
    - Retro Fire Requirements
- Mars Atmosphere Model
  - Linear Plot
  - Logarithmic Plot
- Terminal Velocity Design Charts
  - Heat Shield
  - Parachute
- Deorbit Delta V vs.Eccentricity
  - Graph
  - Table
- Final Descent Profile (e = 0.10) Spreadsheet
  - Graphs
    - Descent Altitude vs. Time
    - Descent Velocity vs. Time (e = 0.10)
    - Descent Velocity Vs. Time (e = 0.27)
- Ascent Analysis
  - Minimum Insertion Delta V vs. Lift-Off Mass
  - At Optimum Launch Angle
    - Graph
    - Chart
  - Final Ascent Profile Spreadsheet
  - Launch Delta V Due To Constant 1500 N Thrust
  - Calculation
- Mach Number vs. Altitude for Ascent and Descent
  - Graph
  - Chart (Includes Dynamic Pressure)

MISSION OVERVIEW

0→1	DE-ORBIT BURN (LIQUID)
2	IMMEDIATELY BEFORE PARACHUTE DEPLOYMENT (VERY NEAR SURFACE)
3	IMMEDIATELY PRECEDING IMPACT
4	GROUND CONDITION
5→6	ASCENT BURN (LIQUID)
7→8	APOGEE KICK BURN (SOLID) AND RENDEZVOUS
9	RENDEZVOUS

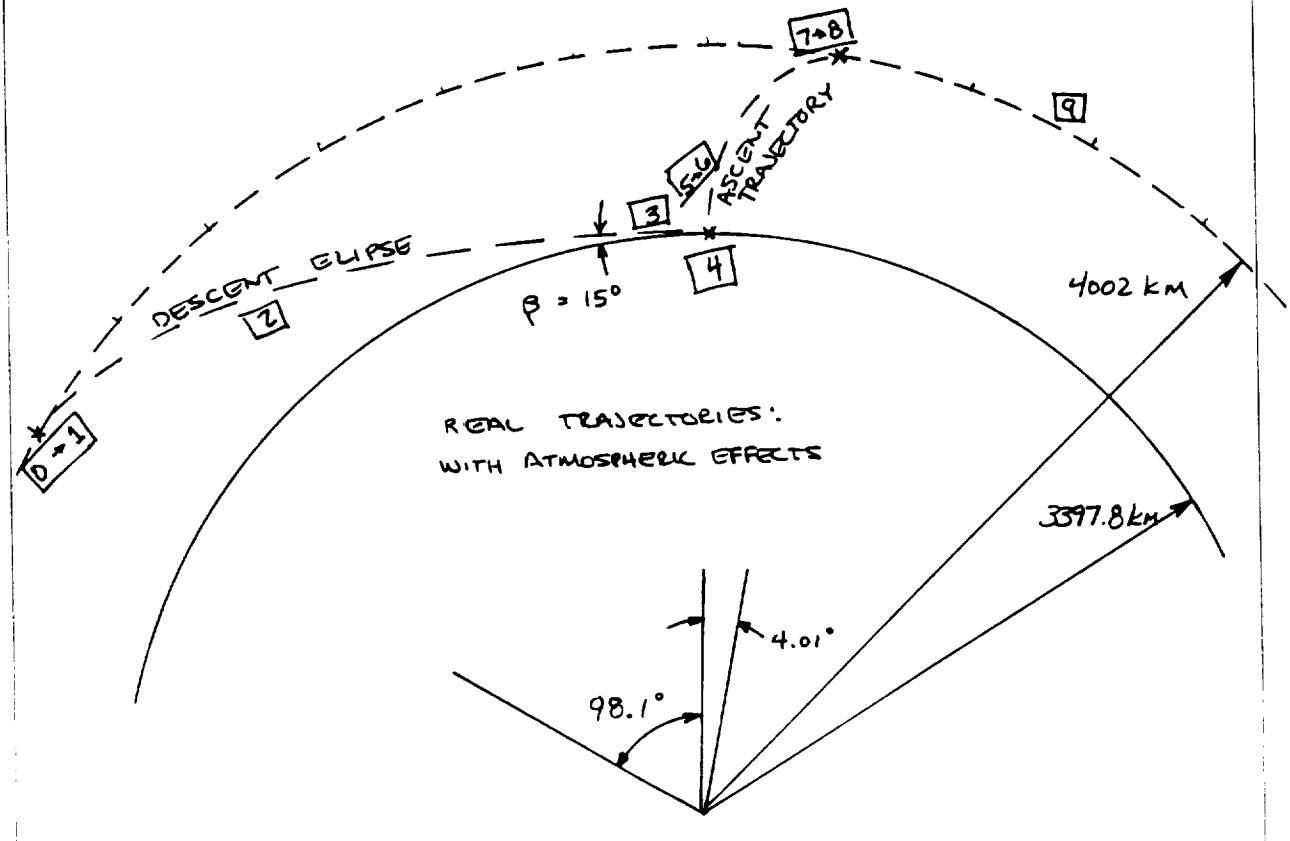

DISTANCES & ANGLES NOT TO SCALE.

MISSION PROFILE

- DETACH FROM M.O.V. AND GIVE SMALL BURN FOR POSITIONING. ~ 8.0 M/S
- SPEND UP TO SEVEN DAYS POSITIONING (COASTING), M.S.P. FOR DE-ORBIT BURN (LIQUID ENGINES) - MODIFY POSITION UP TO 180° TO AVOID PLANE CHANGE
- DESCENT AND LANDING (PARACHUTE AND LIQUID ENGINE RETRO-FIRE)
  - MUST BE ON SURFACE AT LEAST ~12 HOURS UNTIL ORBITAL PLANE PASSES OVERHEAD.
  - COMPLETE SAMPLING MISSION DURING THIS TIME
- ASCENT WITH LIQUID ENGINE. (SAME AS USED FOR DE-ORBIT AND DESCENT RETRO-FIRE) LEAVE BEHIND SIGNIFICANT FRACTION OF VEHICLE MASS.
- APOGEE KICK WITH SOLID TO SEPARATE FROM ASCENT MOTORS AND TANKS, AND REACH ORBIT NEAR THE CIRCULAR ORBIT OF M.O.V. (AT VELOCITY SLIGHTLY GREATER OR SLIGHTLY BELOW THAT OF M.O.V., FOR SUBSEQUENT RENDEVOUS.)

IDEAL ORBIT CALCULATIONS

1. ECCENTRICITY e TABULATED

2. SEMI MAJOR AXIS a (km)

$$a = \frac{r_{apogee}}{(1+e)}$$

$r_{apogee} = 4002$ km

3. APOGEE VELOCITY FOR DEORBIT TRAJECTORY (km/sec)

$$V_a = \sqrt{\mu\left[\frac{2}{r_a} - \frac{1}{a}\right]}$$

$r_a = r_{apogee}$ $\quad \mu = 4.283 \cdot 10^4 \frac{km^3}{sec^2}$

4. ANGULAR MOMENTUM OF DESCENT ORBIT (km^2/sec)

$$h = r_{apogee} V_{apogee}$$

5. PARAMETER FOR POLAR EQN. p OF DESCENT ORBIT (km)

$$p = \frac{h^2}{\mu}$$

6. THETA (θ) TRUE ANOMALY (degrees)

$$\theta = \cos^{-1}\left[\frac{p - r}{re}\right]$$

FROM: $r = \dfrac{p}{1 + e\cos\theta}$

7. "IMPACT" VELOCITY (km/sec)

$$V_i = \sqrt{\mu\left[\frac{2}{r_i} - \frac{1}{a}\right]}$$

WHERE $r_i = 3397.8$ km

8. LANDING (FLIGHT PATH) ANGLE (degrees)

$h = rV\cos\beta$

$$\beta = \cos^{-1}\left[\frac{h}{r_{impact} V_{impact}}\right]$$

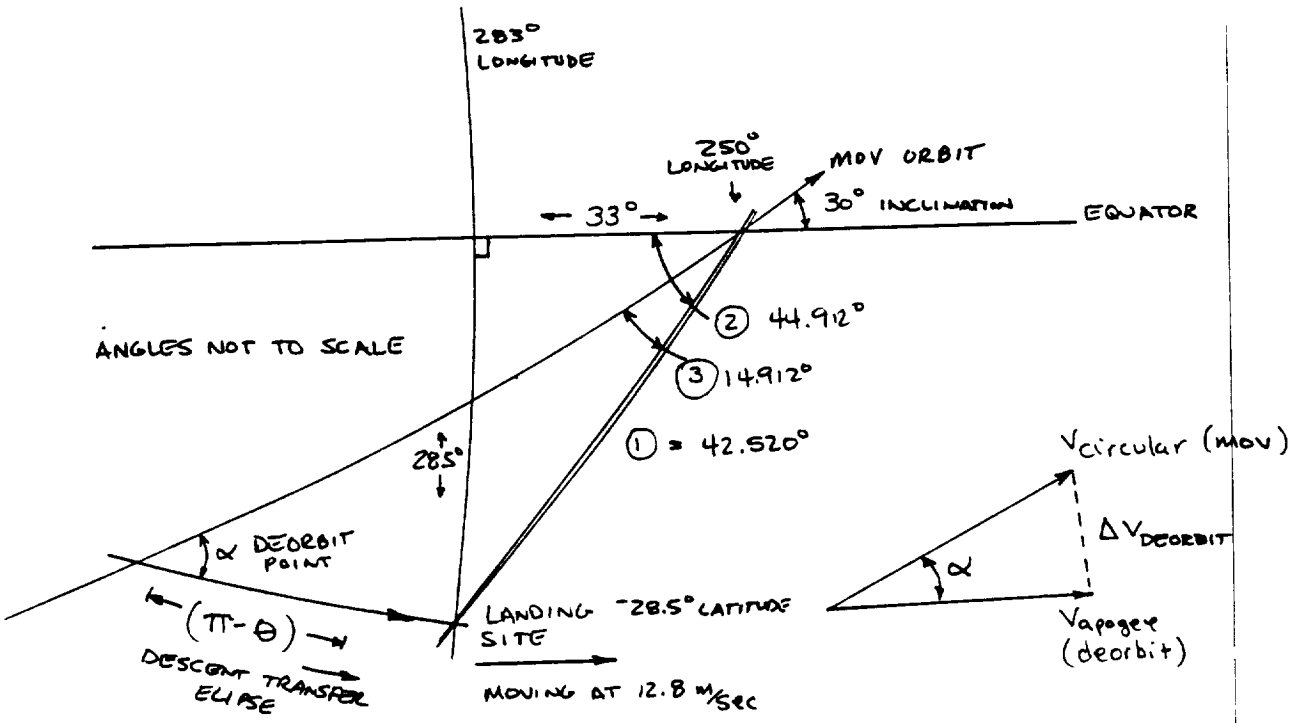

* $\cos ① = \cos(28.5°)\cos(33°) \Rightarrow ① = 42.520°$

* $\dfrac{\sin ②}{\sin(28.5°)} = \dfrac{\sin(90°)}{\sin(42.520°)} \Rightarrow ② = 44.912°$

* $③ = ② - 30° = 44.912° - 30° \Rightarrow ③ = 14.912°$

SOLVE FOR PLANE CHANGE ANGLE α

* $\dfrac{\sin\alpha}{\sin(42.520°)} = \dfrac{\sin ③}{\sin(\pi-\theta)}$ BUT $\sin(\pi-\theta) = \sin\theta$

$$\sin\alpha = \frac{\sin(14.912°)\sin(42.520°)}{\sin\theta} = \frac{0.17391}{\sin\theta}$$

9. PLANE CHANGE ANGLE (deg)

$$\boxed{\alpha = \sin^{-1}\left[\frac{0.17391}{\sin\theta}\right]}$$

10. DE-ORBIT DELTA V. (km/sec)

$$\boxed{\Delta V = \left[V_{circular}^2 + V_{apogee}^2 - 2V_{circular}V_{apogee}\cos\alpha\right]^{1/2}}$$

$$V_{circular} = \sqrt{\frac{\mu}{r}} = 3.2714 \text{ km/sec}$$

TIME ELAPSED IN DEORBIT.

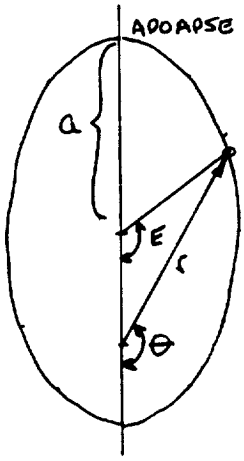

E = ECCENTRIC ANOMALY, ANGLE MEASURED FROM CENTER OF ELIPSE FROM PERIAPSE.

θ = TRUE ANOMALY, MEASURED FROM PERIAPSE AT MASS/FORCE CENTER

GIVEN θ FIND TIME FROM DEORBIT AT APOAPSE:

$$E = \cos^{-1}\left[e + \frac{r}{a}\cos\theta\right]$$

WHERE a IS THE SEMI-MAJOR AXIS AND r IS THE DISTANCE FROM THE MASS CENTER

$$t_r = \frac{E - e\sin E}{\sqrt{\mu/a^3}}$$

WHERE e IS ECCENTRICITY AND μ IS THE GRAVITATIONAL PARAMETER FOR MARS.

$$t_{apoapse} = \pi\sqrt{\frac{a^3}{\mu}}$$

$$\Delta t = t_{apoapse} - t_r$$

DESCENT FORCE BALANCE

TAKE r, V, β FROM IDEAL ORBIT INITIALLY

CALCULATE INITIAL r, θ, V_r, V_θ

FROM THESE CALCULATE L, D

} USE THESE TO GENERATE NEXT r, θ, V_r, V_θ, L, D, etc.

L & D DEPEND ON BODY (HEATSHIELD) AND/OR PARACHUTE

POLAR COORDINATES

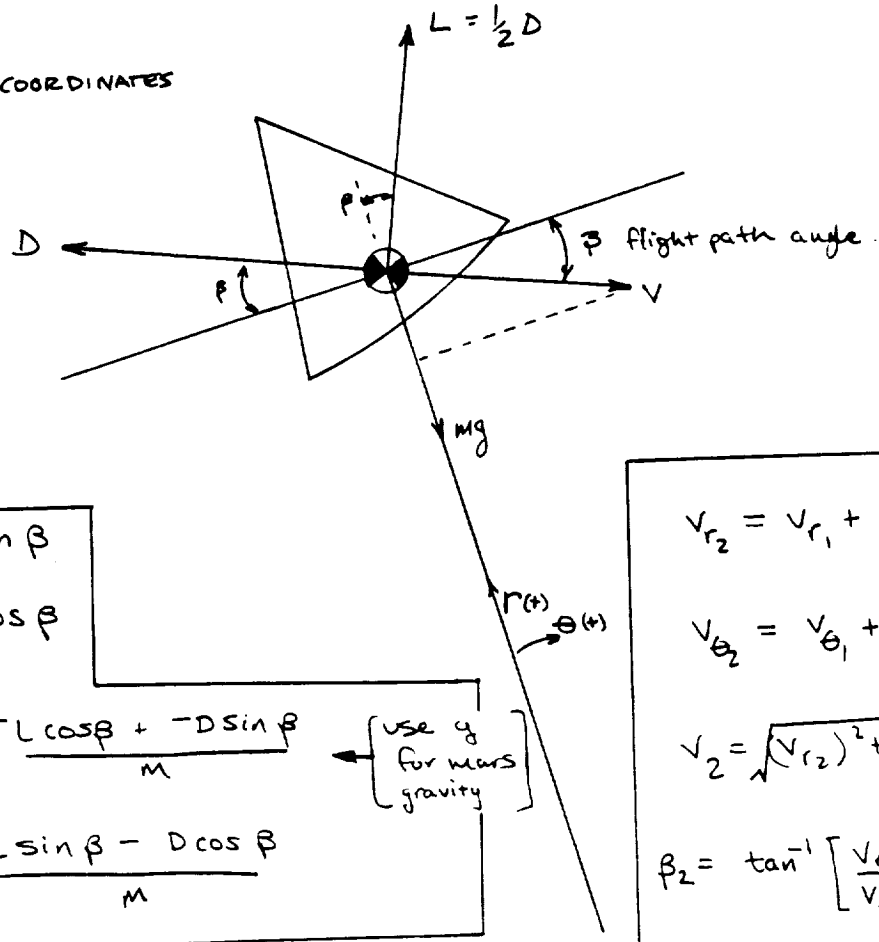

$$V_r = V \sin\beta$$

$$V_\theta = V \cos\beta$$

$$a_r = g + \frac{-L\cos\beta + -D\sin\beta}{M}$$

[use g for mars gravity]

$$a_\theta = \frac{L\sin\beta - D\cos\beta}{M}$$

$$V_{r_2} = V_{r_1} + a_r \Delta t$$

$$V_{\theta_2} = V_{\theta_1} + a_\theta \Delta t$$

$$V_2 = \sqrt{(V_{r_2})^2 + (V_{\theta_2})^2}$$

$$\beta_2 = \tan^{-1}\left[\frac{V_r}{V_\theta}\right]$$

$$r_2 = r_1 + \frac{(V_{r_2} + V_{r_1})}{2}\Delta t$$

$$\theta_2 = \theta_1 + \frac{(V_{\theta_2} + V_{\theta_1})}{2\left(\frac{r_2 + r_1}{2}\right)}\Delta t$$

1.	r_1	θ_1	V_{r_1}	V_{θ_1}	V_1	β_1	L_1	D_1	a_{r_1}	a_{θ_1}
2.	r_2	θ_2	V_{r_2}	V_{θ_2}	V	β_2	L_2	D_2	a_{r_2}	a_{θ_2}

3. CONTINUE TO "STEP DOWN" UNTIL $r = r_{surface}$

ORBITAL PARAMETERS:

GIVEN ε — ECCENTRICITY

1. $a = \dfrac{r_{apogee}}{[1+e]}$ — SEMI-MAJOR AXIS

2. $p = a(1-e^2)$ — ORBITAL PARAMETER

3. $h = \sqrt{p\mu}$ — ANGULAR MOMENTUM

POSITION DEPENDENT BASIC VALUES

1. $\theta = \cos^{-1}\left[\dfrac{p-r}{re}\right]$ — TRUE ANOMALY AS FUNCT OF RADIUS

2. $v = \sqrt{\mu\left[\dfrac{2}{r} - \dfrac{1}{a}\right]}$ — VELOCITY AS FUNCT OF RADIUS

3. $\beta = \cos^{-1}\left[\dfrac{h}{rv}\right]$ — FLIGHT PATH ANGLE AS FUNCT OF RADIUS (AND VELOCITY WHICH IS A FUNCT. OF RADIUS)

DERIVED QUANTITIES NEEDED FOR ITERATION

1. $V_\theta = V\cos\beta$ — TANGENTIAL VELOCITY AS FUNCT. OF β AND VELOCITY

2. $V_r = V\sin\beta$ — RADIAL VELOCITY AS FUNCT. OF β AND VELOCITY

1. $\rho = \rho_0 e^{-\text{alt.}/\lambda}$ — DENSITY FUNCT. (ρ_0 = SURF. DENSITY, λ = SCALE HT. 14.5 km)

2. $g = \dfrac{\mu}{r^2}$ — GRAVITATIONAL ACCEL AT GIVEN RADIUS

IDEAL ORBITAL EQUATIONS DURING KEPLERIAN PHASE OF DESCENT

ITERATIVE PROCEDURE

TAKE INITIAL VALUES FROM IDEAL ORBIT

RADIUS	r	GIVEN m	MASS
ANGLE	θ	GIVEN μ	GRAV. CONST.
VELOCITY	V	GIVEN r	MARS MEAN
COMPONENTS	V_θ, V_r	VARIABLE	m, A, C_D, K, Δt
ANGLE	β		

CALCULATE FORCES, ACCELERATIONS, VELOCITIES, POSITIONS

1. FORCES:

$$g = \frac{\mu}{r^2}$$

$$\rho = \rho_0 \exp\left[-\frac{r - r_{mars}}{\lambda}\right]$$

$$D = \left[\tfrac{1}{2}\rho V^2\right]\left[A C_D\right]$$

$$L = K D$$

2. ACCELERATION

$$a_r = g - \left[\frac{L\cos\beta + D\sin\beta}{m}\right]$$

$$a_\theta = \left[\frac{L\sin\beta - D\cos\beta}{m}\right]$$

3. VELOCITIES

$$V_{r_{new}} = V_{r_{old}} + a_r \Delta t$$

$$V_{\theta_{new}} = V_{\theta_{old}} + a_\theta \Delta t$$

$$V_{new} = \sqrt{V_{\theta_{new}}^2 + V_{r_{new}}^2}$$

4. POSITIONS

$$\beta = \tan^{-1}\left[\frac{V_{r_{new}}}{V_{\theta_{new}}}\right]$$

$$r_{new} = r_{old} + \tfrac{1}{2}\left[V_{r_{new}} + V_{r_{old}}\right]\Delta t$$

$$\theta_{new} = \theta_{old} + \left[\frac{V_{\theta_{old}} + V_{\theta_{new}}}{r_{old} + r_{new}}\right]\Delta t$$

RETURN TO CALCULATE FORCES FOR NEXT STEP AND REPEAT CYCLE UNTIL LANDING.

FINAL DESCENT PROFILE

* SEPARATION FROM MOV $V = 3.272$ km/sec ALT = 600 KM

* $\Delta V \sim 8.0$ m/s FOR POSITIONING (ALT ± 20 km, 180° IN 6 DAYS, 9.73 HOURS)

  2.5°/ORBIT ADVANCE/RECEDE MASS BEFORE DEORBIT ≈ 80 kg

  0.758 kg FUEL REQ'D.

* DE ORBIT $\Delta V = 167.9$ m/s TRANSFER ECCENTRICITY $e = 0.10$

$a_r = 0.33$ g's ↓	$\beta_{250} = 6.3°$	$V = 3421.$ m/s	ALT. 250 km	time (min) 29.02
$a_r = 0.34$ g's ↓	$\beta_{100} = 17.6°$	$V = 3562.$ m/s	ALT. 100 km	32.52
$a_r = 2.61$ g's ↑	$\beta_{30} = 21.6°$	$V = 1975.$ m/s	ALT. 30 km	33.60
$a_r = 0.25$ ↑	$\beta_{10} = 36.5°$	$V = 330$ m/s	ALT. 10 km	34.35

BASED ON DESCENT MASS OF 84.7 kg $C_D = 1.0$ ↑110 secs

DIA = 1.5 m

✓ $\Delta V_{DEORBIT} = V_{circular}\left[1 - \sqrt{1-e}\right]$ ✓ REDUCTION OF ΔV BY 300 m/s SAVES 10 kg

* DEPLOY PARACHUTE AT -3.0 km ALT. / DROP HEAT SHIELD
  1.2 km ABOVE SURFACE 21 SECONDS BEFORE IMPACT

$V = 108.8$ m/s M =

$a_r = 27.5$ m/s² ↑ ~3 g's DURING FIRST SECOND

$\beta = 78.9°$

PERIOD 10 sec

AT ALT -3.5 km 20 sec TO IMPACT

$V = 56.5$ m/s

$a_r = 3.35$ m/s² ↑ ~ 1/3 g. $C_D = 1.0$, DIA = 4.0 m

$\beta = 82.1°$ BASED ON MASS = 75.7 kg

* RETRO FIRE AT < 100 m ABOVE SURFACE
  THRUST ~ 21 m/s² RESULT < 2 g's

  REQUIRES 53.5 m TRAVEL TO BRING V TO ZERO.
  FIRES FOR ~ 2.5 SEC.
  IMPACT 36.1 MINUTES AFTER DEORBIT

* REMAIN ON SURFACE ~ 12 HOURS TO PERFORM SAMPLING MISSION
  (12 HRS, 19 MIN)

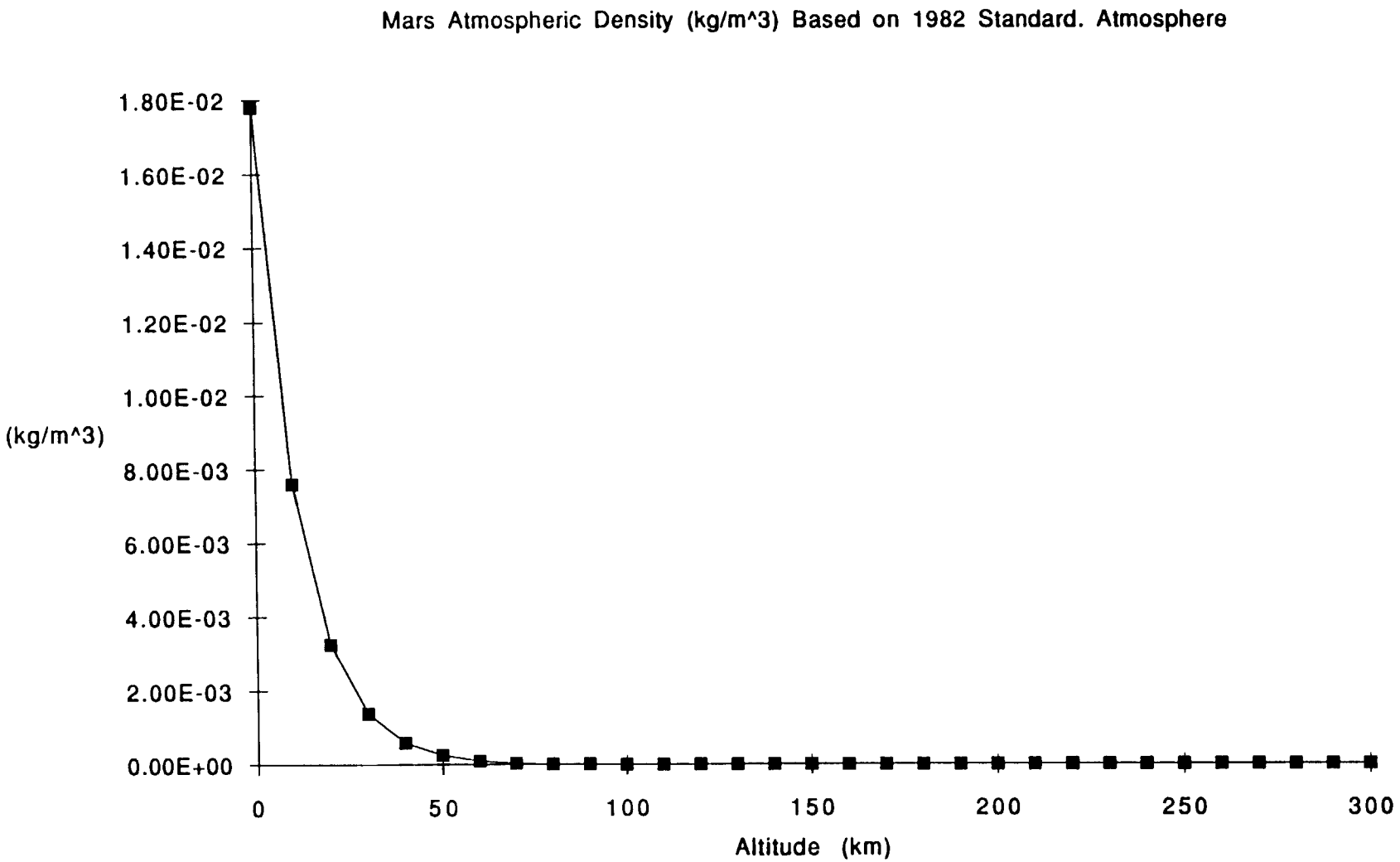
Mars Atmospheric Density (kg/m^3) Based on 1982 Standard. Atmosphere
1.80E-02
1.60E-02
1.40E-02
1.20E-02
1.00E-02
(kg/m^3)
8.00E-03
6.00E-03
4.00E-03
2.00E-03
0.00E+00
0
50
100
150
200
250
300
Altitude (km)

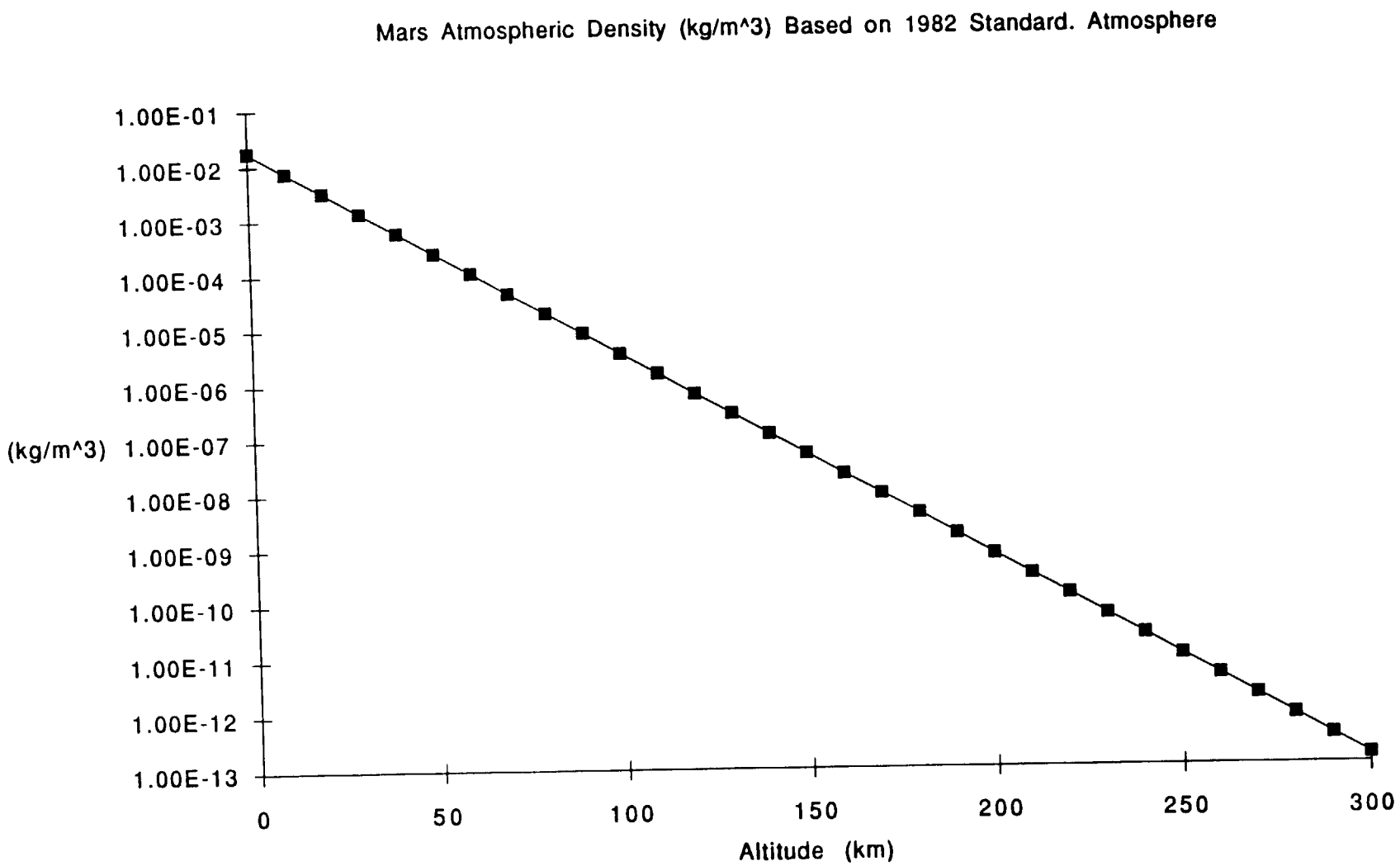
Mars Atmospheric Density (kg/m^3) Based on 1982 Standard. Atmosphere
1.00E-01
1.00E-02
1.00E-03
1.00E-04
1.00E-05
1.00E-06
(kg/m^3) 1.00E-07
1.00E-08
1.00E-09
1.00E-10
1.00E-11
1.00E-12
1.00E-13
0
50
100
150
200
250
300
Altitude (km)

HEAT SHIELD TERMINAL VELOCITY DESIGN CHART

VTERM_HS.XLS Terminal Velocity

	Weight (N)	315.93	Terminal Velocity for Descent with Heat Shield								
	Cd	1.00									
	Mass (kg)	84.70	Terminal Velocity (meters/second)								
			R(m)	1.250	1.125	1.000	0.875	0.750	0.625	0.500	0.375
Alt	Density	Speed of	A(m2)	4.909	3.976	3.142	2.405	1.767	1.227	0.785	0.442
(km)	(kg/m^3)	Sound(m/s)	D(m)	2.500	2.250	2.000	1.750	1.500	1.250	1.000	0.750
			D (ft)	8.202	7.382	6.562	5.741	4.921	4.101	3.281	2.461
-4	1.35E-02	255		97.65	108.50	122.06	139.50	162.75	195.29	244.12	325.49
-2	1.18E-02	253		104.44	116.05	130.56	149.21	174.07	208.89	261.11	348.15
0	1.02E-02	252		112.34	124.82	140.42	160.48	187.23	224.68	280.84	374.46
2	8.89E-03	251		120.33	133.70	150.41	171.90	200.55	240.66	300.83	401.10
4	7.72E-03	249		129.13	143.47	161.41	184.47	215.21	258.25	322.82	430.42
6	6.67E-03	248		138.92	154.36	173.65	198.46	231.53	277.84	347.30	463.07
8	5.74E-03	247		149.75	166.39	187.19	213.93	249.59	299.50	374.38	499.17
10	4.91E-03	246		161.91	179.90	202.39	231.31	269.86	323.83	404.79	539.71
15	3.34E-03	244		196.31	218.13	245.39	280.45	327.19	392.63	490.79	654.38
20	2.28E-03	240		237.61	264.01	297.01	339.44	396.01	475.21	594.02	792.02
25	1.53E-03	236		290.06	322.28	362.57	414.36	483.43	580.11	725.14	966.85
30	9.99E-04	235		358.96	398.84	448.70	512.80	598.26	717.92	897.39	1196.53
35	6.49E-04	234		445.35	494.84	556.69	636.22	742.25	890.70	1113.38	1484.51
40	4.19E-04	233		554.27	615.85	692.83	791.81	923.78	1108.53	1385.67	1847.56
45	2.74E-04	230		685.41	761.57	856.76	979.16	1142.35	1370.82	1713.53	2284.70
50	1.76E-04	227		855.20	950.23	1069.01	1221.72	1425.34	1710.41	2138.01	2850.68
55	1.13E-04	222		1067.30	1185.89	1334.13	1524.72	1778.84	2134.60	2668.25	3557.67
60	7.12E-05	217		1344.58	1493.98	1680.72	1920.83	2240.96	2689.16	3361.45	4481.93
65	4.43E-05	212		1704.61	1894.01	2130.76	2435.15	2841.01	3409.21	4261.52	5682.02
70	2.72E-05	207		2175.41	2417.13	2719.27	3107.73	3625.69	4350.83	5438.53	7251.38
75	1.64E-05	203		2801.59	3112.88	3501.98	4002.27	4669.31	5603.18	7003.97	9338.63
80	9.75E-06	199		3633.49	4037.21	4541.86	5190.70	6055.82	7266.98	9083.72	12111.63
85	5.74E-06	195		4735.55	5261.72	5919.43	6765.07	7892.58	9471.10	11838.87	15785.16
90	3.32E-06	190		6226.69	6918.54	7783.36	8895.27	10377.81	12453.38	15566.72	20755.63
95	1.88E-06	186		8274.60	9194.00	10343.26	11820.86	13791.01	16549.21	20686.51	27582.01
100	1.02E-06	184		11233.78	12481.98	14042.23	16048.26	18722.97	22467.57	28084.46	37445.95
110	2.75E-07	206		21635.15	24039.05	27043.93	30907.35	36058.58	43270.29	54087.86	72117.15
120	8.72E-08	236		38420.93	42689.93	48026.17	54887.05	64034.89	76841.87	96052.34	128069.78
130	3.52E-08	252		60472.07	67191.19	75590.09	86388.67	100786.78	120944.14	151180.18	201573.57
140	1.61E-08	264		89415.59	99350.65	111769.48	127736.55	149025.98	178831.17	223538.97	298051.96
150	8.11E-09	272		125984.10	139982.33	157480.13	179977.29	209973.50	251968.20	314960.25	419947.00
160	4.34E-09	277		172219.10	191354.55	215273.87	246027.28	287031.83	344438.19	430547.74	574063.65
170	2.41E-09	281		231109.42	256788.24	288886.78	330156.31	385182.37	462218.84	577773.55	770364.73
180	1.34E-09	288		309937.25	344374.72	387421.56	442767.49	516562.08	619874.49	774843.12	1033124.15
190	7.86E-10	291		404682.94	449647.71	505853.68	578118.49	674471.57	809365.88	1011707.35	1348943.13
200	4.66E-10	294		525573.20	583970.22	656966.50	750818.86	875955.33	1051146.40	1313933.00	1751910.67
210	2.81E-10	297		676819.73	752021.92	846024.66	966885.33	1128032.88	1353639.46	1692049.32	2256065.76
220	1.71E-10	301		867617.12	964019.03	1084521.40	1239453.03	1446028.54	1735234.25	2169042.81	2892057.08
230	1.06E-10	305		1101978.79	1224420.88	1377473.49	1574255.42	1836631.32	2203957.59	2754946.98	3673262.64
240	6.60E-11	310		1396542.64	1551714.05	1745678.31	1995060.92	2327571.07	2793085.29	3491356.61	4655142.15
250	4.17E-11	315		1756944.90	1952161.00	2196181.13	2509921.29	2928241.50	3513889.80	4392362.25	5856483.01
260	2.66E-11	324		2199810.91	2444234.34	2749763.64	3142587.01	3666351.51	4399621.82	5499527.27	7332703.03
270	1.73E-11	332		2727740.91	3030823.24	3409676.14	3896772.74	4546234.86	5455481.83	6819352.29	9092469.72
280	1.14E-11	343		3360266.67	3733629.63	4200333.33	4800380.95	5600444.44	6720533.33	8400666.67	11200888.89
290	7.63E-12	354		4107370.70	4563745.22	5134213.37	5867672.43	6845617.83	8214741.40	10268426.75	13691235.66
300	5.22E-12	367		4965819.37	5517577.08	6207274.21	7094027.67	8276365.61	9931638.74	12414548.42	16552731.23
310	3.65E-12	380		5938540.70	6598378.56	7423175.88	8483629.57	9897567.83	11877081.40	14846351.75	19795135.67
320	2.61E-12	394		7022729.10	7803032.33	8778411.37	10032470.14	11704548.50	14045458.20	17556822.75	23409097.00
330	1.91E-12	407		8209363.50	9121515.00	10261704.37	11727662.14	13682272.49	16418726.99	20523408.74	27364544.99
340	1.43E-12	419		9487638.98	10541821.09	11859548.73	13553769.97	15812731.64	18975277.96	23719097.45	31625463.27
350	1.09E-12	430		10867081.41	12074534.90	13583851.76	15524402.01	18111802.35	21734162.82	27167703.53	36223604.70
360	8.52E-13	439		12291542.08	13657268.97	15364427.60	17559345.82	20485903.46	24583084.15	30728855.19	40971806.92
370	6.74E-13	448		13819623.82	15355137.57	17274529.77	19742319.74	23032706.36	27639247.63	34549059.54	46065412.72
380	5.42E-13	454		15410847.62	17123164.02	19263559.53	22015496.60	25684746.04	30821695.24	38527119.05	51369492.07
390	4.40E-13	460		17104084.42	19004538.24	21380105.52	24434406.31	28506807.36	34208168.83	42760211.04	57013614.72
400	3.61E-13	465		18883068.50	20981187.22	23603835.63	26975812.14	31471780.83	37766137.00	47207671.25	62943561.67
410	2.99E-13	468		20748684.90	23054094.34	25935856.13	29640978.43	34581141.50	41497369.81	51871712.26	69162283.01
420	2.49E-13	471		22736651.02	25262945.58	28420813.78	32480930.03	37894418.37	45473302.05	56841627.56	75788836.74
430	2.08E-13	473		24876799.28	27640888.09	31095999.10	35538284.69	41461332.14	49753598.56	62191998.20	82922664.27
440	1.75E-13	475		27121090.33	30134544.81	33901362.91	38744414.76	45201817.22	54242180.66	67802725.83	90403634.44
450	1.48E-13	477		29491394.72	32768216.35	36864243.40	42130563.88	49152324.53	58982789.44	73728486.79	98304649.06
460	1.25E-13	478		32090106.84	35655674.27	40112633.55	45843009.77	53483511.40	64180213.68	80225267.10	###########
470	1.06E-13	479		34847629.20	38719588.00	43559536.50	49782327.43	58079382.00	69695258.40	87119072.99	###########
480	9.03E-14	480		37755679.81	41950755.35	47194599.77	53936685.45	62926133.02	75511359.62	94389199.53	###########

PARACHUTE TERMINAL VELOCITY DESIGN CHART

VTERM_PA.XLS Terminal Velocity

	Weight (N)	282.36	Terminal Velocity for Descent with Parachute								
	Cd	1.00									
	Mass (kg)	75.70		Terminal Velocity (meters/second)							
			R(m)	4.500	4.000	3.500	3.000	2.500	2.000	1.500	1.000
Alt	Density	Speed of	A(m2)	63.617	50.265	38.485	28.274	19.635	12.566	7.069	3.142
(km)	(kg/m^3)	Sound(m/s)	D(m)	9.000	8.000	7.000	6.000	5.000	4.000	3.000	2.000
			D (ft)	29.528	26.247	22.966	19.685	16.404	13.123	9.843	6.562
-4	1.35E-02	255		25.64	28.85	32.97	38.46	46.16	57.70	76.93	115.39
-2	1.18E-02	253		27.43	30.86	35.26	41.14	49.37	61.71	82.28	123.42
0	1.02E-02	252		29.50	33.19	37.93	44.25	53.10	66.38	88.50	132.75
2	8.89E-03	251		31.60	35.55	40.63	47.40	56.88	71.10	94.80	142.20
4	7.72E-03	249		33.91	38.15	43.60	50.86	61.04	76.30	101.73	152.59
6	6.67E-03	248		36.48	41.04	46.90	54.72	65.67	82.08	109.44	164.16
8	5.74E-03	247		39.33	44.24	50.56	58.99	70.79	88.48	117.98	176.96
10	4.91E-03	246		42.52	47.83	54.67	63.78	76.54	95.67	127.56	191.34
15	3.34E-03	244		51.55	58.00	66.28	77.33	92.80	115.99	154.66	231.99
20	2.28E-03	240		62.40	70.20	80.22	93.60	112.31	140.39	187.19	280.79
25	1.53E-03	236		76.17	85.69	97.93	114.26	137.11	171.38	228.51	342.77
30	9.99E-04	235		94.26	106.05	121.20	141.40	169.68	212.09	282.79	424.19
35	6.49E-04	234		116.95	131.57	150.37	175.43	210.51	263.14	350.86	526.28
40	4.19E-04	233		145.55	163.75	187.14	218.33	262.00	327.50	436.66	654.99
45	2.74E-04	230		179.99	202.49	231.42	269.99	323.99	404.98	539.98	809.97
50	1.76E-04	227		224.58	252.65	288.75	336.87	404.25	505.31	673.74	1010.62
55	1.13E-04	222		280.28	315.31	360.36	420.42	504.50	630.63	840.84	1261.26
60	7.12E-05	217		353.09	397.23	453.98	529.64	635.57	794.46	1059.28	1588.92
65	4.43E-05	212		447.64	503.59	575.54	671.46	805.75	1007.19	1342.92	2014.38
70	2.72E-05	207		571.28	642.68	734.50	856.91	1028.30	1285.37	1713.83	2570.74
75	1.64E-05	203		735.71	827.68	945.92	1103.57	1324.28	1655.35	2207.14	3310.71
80	9.75E-06	199		954.17	1073.45	1226.80	1431.26	1717.51	2146.89	2862.52	4293.78
85	5.74E-06	195		1243.58	1399.03	1598.89	1865.37	2238.45	2798.06	3730.74	5596.11
90	3.32E-06	190		1635.16	1839.56	2102.35	2452.74	2943.29	3679.12	4905.49	7358.23
95	1.88E-06	186		2172.96	2444.58	2793.80	3259.43	3911.32	4889.15	6518.87	9778.30
100	1.02E-06	184		2950.05	3318.81	3792.93	4425.08	5310.10	6637.62	8850.16	13275.24
110	2.75E-07	206		5681.51	6391.70	7304.79	8522.26	10226.71	12783.39	17044.52	25566.78
120	8.72E-08	236		10089.55	11350.74	12972.27	15134.32	18161.18	22701.48	30268.64	45402.96
130	3.52E-08	252		15880.30	17865.33	20417.52	23820.44	28584.53	35730.66	47640.89	71461.33
140	1.61E-08	264		23481.02	26416.15	30189.88	35221.53	42265.84	52832.30	70443.06	105664.59
150	8.11E-09	272		33084.11	37219.63	42536.71	49626.17	59551.40	74439.25	99252.33	148878.50
160	4.34E-09	277		45225.67	50878.88	58147.29	67838.51	81406.21	101757.76	135677.02	203515.53
170	2.41E-09	281		60690.59	68276.92	78030.76	91035.89	109243.07	136553.83	182071.78	273107.67
180	1.34E-09	288		81391.21	91565.11	104645.84	122086.81	146504.18	183130.22	244173.63	366260.44
190	7.86E-10	291		106271.95	119555.94	136635.36	159407.92	191289.50	239111.88	318815.84	478223.75
200	4.66E-10	294		138018.39	155270.68	177452.21	207027.58	248433.10	310541.37	414055.16	621082.74
210	2.81E-10	297		177736.55	199953.62	228518.42	266604.82	319925.79	399907.24	533209.65	799814.47
220	1.71E-10	301		227840.98	256321.11	292938.41	341761.48	410113.77	512642.21	683522.95	1025284.43
230	1.06E-10	305		289385.64	325558.84	372067.25	434078.45	520894.14	651117.68	868156.91	1302235.36
240	6.60E-11	310		366739.71	412582.17	471522.48	550109.56	660131.48	825164.34	1100219.13	1650328.69
250	4.17E-11	315		461383.31	519056.22	593207.11	692074.96	830489.95	1038112.44	1384149.92	2076224.87
260	2.66E-11	324		577682.33	649892.62	742734.43	866523.50	1039828.20	1299785.25	1733047.00	2599570.49
270	1.73E-11	332		716319.63	805859.58	920982.38	1074479.44	1289375.33	1611719.16	2148958.89	3223438.33
280	1.14E-11	343		882424.34	992727.38	1134545.58	1323636.51	1588363.81	1985454.76	2647273.01	3970909.52
290	7.63E-12	354		1078617.93	1213445.17	1386794.48	1617926.89	1941512.27	2426890.34	3235853.78	4853780.67
300	5.22E-12	367		1304051.23	1467057.63	1676637.29	1956076.84	2347292.21	2934115.26	3912153.68	5868230.52
310	3.65E-12	380		1559493.15	1754429.79	2005062.62	2339239.72	2807087.67	3508859.58	4678479.45	7017719.17
320	2.61E-12	394		1844206.93	2074732.80	2371123.20	2766310.40	3319572.47	4149465.59	5532620.79	8298931.19
330	1.91E-12	407		2155823.59	2425301.54	2771773.19	3233735.38	3880482.46	4850603.08	6467470.77	9701206.15
340	1.43E-12	419		2491505.70	2802943.91	3203364.47	3737258.55	4484710.26	5605887.82	7474517.09	11211775.64
350	1.09E-12	430		2853754.80	3210474.15	3669113.31	4280632.19	5136758.63	6420948.29	8561264.39	12841896.58
360	8.52E-13	439		3227825.93	3631304.17	4150061.91	4841738.89	5810086.67	7262608.34	9683477.79	14525216.68
370	6.74E-13	448		3629108.52	4082747.09	4665996.67	5443662.78	6532395.34	8165494.17	10887325.56	16330988.35
380	5.42E-13	454		4046972.56	4552844.13	5203250.44	6070458.85	7284550.61	9105688.27	12140917.69	18211376.54
390	4.40E-13	460		4491625.77	5053078.99	5774947.42	6737438.66	8084926.39	10106157.99	13474877.32	20212315.98
400	3.61E-13	465		4958796.69	5578646.27	6375595.74	7438195.03	8925834.04	11157292.55	14876390.06	22314585.09
410	2.99E-13	468		5448717.72	6129807.44	7005494.21	8173076.58	9807691.90	12259614.87	16346153.16	24519229.74
420	2.49E-13	471		5970768.46	6717114.51	7676702.30	8956152.69	10747383.22	13434229.03	17912305.37	26868458.06
430	2.08E-13	473		6532783.05	7349380.93	8399292.50	9799174.58	11759009.49	14698761.87	19598349.16	29397523.73
440	1.75E-13	475		7122146.11	8012414.38	9157045.00	10683219.17	12819863.00	16024828.75	21366438.33	32049657.50
450	1.48E-13	477		7744600.96	8712676.08	9957344.09	11616901.44	13940281.73	17425352.16	23233802.88	34850704.32
460	1.25E-13	478		8427036.92	9480416.54	10834761.76	12640555.39	15168666.46	18960833.08	25281110.77	37921666.16
470	1.06E-13	479		9151177.32	10295074.49	11765799.41	13726765.98	16472119.18	20590148.97	27453531.97	41180297.95
480	9.03E-14	480		9914847.26	11154203.17	12747660.76	14872270.89	17846725.07	22308406.33	29744541.78	44616812.67

Deorbit Velocity Change for Mars Descent

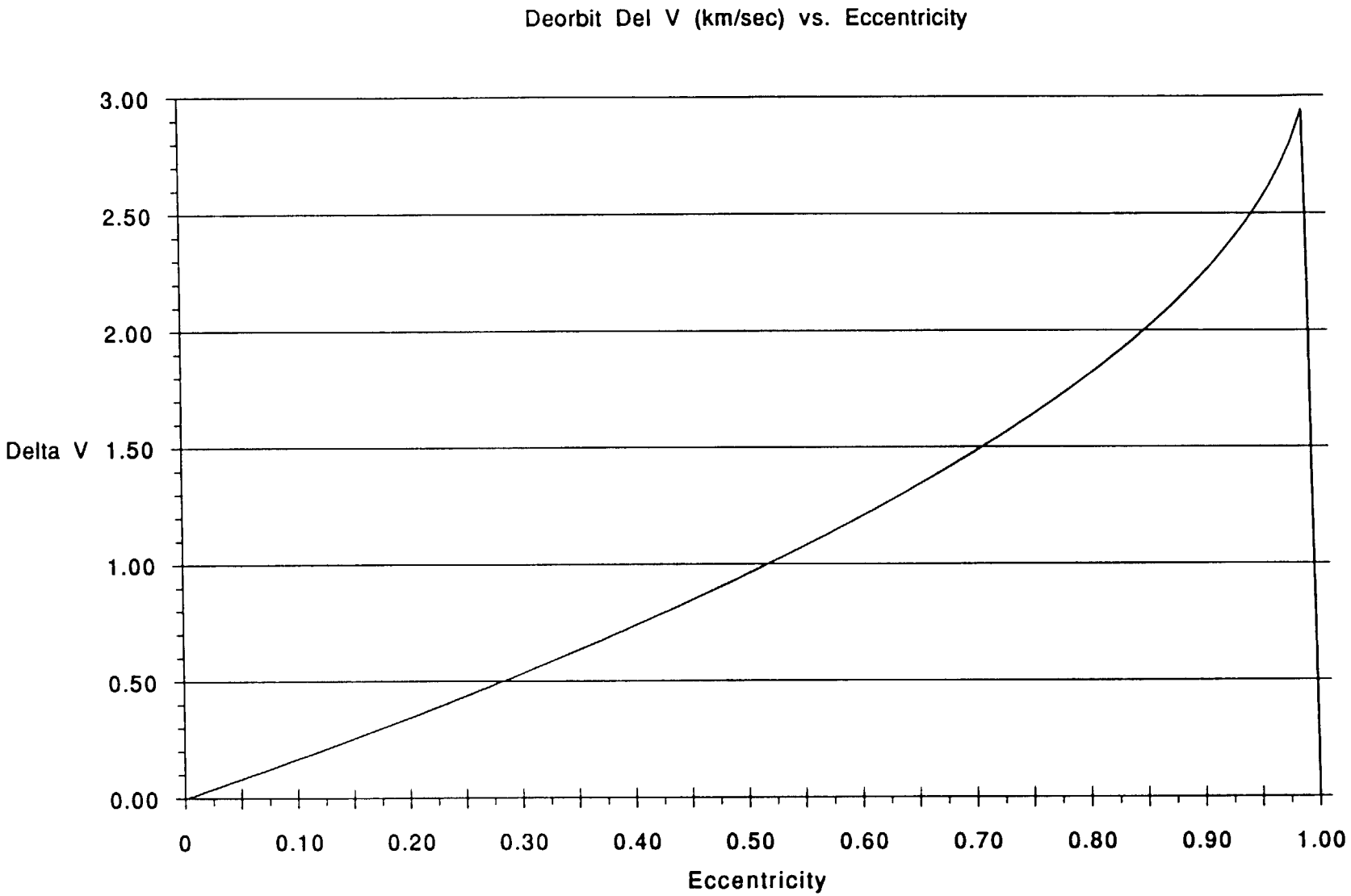

5/29/90 5:40 PM

DELTA V DEORBIT VS ECCENTRICITY

u Mars:	42830.00	km3/sec2	Delta V = V circular * [1 - Sqrt(1 - e)]
Rapogee	4002.00	km	
V circular	3.27	km/sec	

e	Del V (km/sec)	e	Del V (km/sec)	e	Del V (km/sec)	e	Del V (km/sec)	e	Del V (km/sec)
0.01	0.02	0.21	0.36	0.41	0.76	0.61	1.23	0.81	1.85
0.02	0.03	0.22	0.38	0.42	0.78	0.62	1.25	0.82	1.88
0.03	0.05	0.23	0.40	0.43	0.80	0.63	1.28	0.83	1.92
0.04	0.07	0.24	0.42	0.44	0.82	0.64	1.31	0.84	1.96
0.05	0.08	0.25	0.44	0.45	0.85	0.65	1.34	0.85	2.00
0.06	0.10	0.26	0.46	0.46	0.87	0.66	1.36	0.86	2.05
0.07	0.12	0.27	0.48	0.47	0.89	0.67	1.39	0.87	2.09
0.08	0.13	0.28	0.50	0.48	0.91	0.68	1.42	0.88	2.14
0.09	0.15	0.29	0.51	0.49	0.94	0.69	1.45	0.89	2.19
0.10	0.17	0.30	0.53	0.50	0.96	0.70	1.48	0.90	2.24
0.11	0.19	0.31	0.55	0.51	0.98	0.71	1.51	0.91	2.29
0.12	0.20	0.32	0.57	0.52	1.00	0.72	1.54	0.92	2.35
0.13	0.22	0.33	0.59	0.53	1.03	0.73	1.57	0.93	2.41
0.14	0.24	0.34	0.61	0.54	1.05	0.74	1.60	0.94	2.47
0.15	0.26	0.35	0.63	0.55	1.08	0.75	1.64	0.95	2.54
0.16	0.27	0.36	0.65	0.56	1.10	0.76	1.67	0.96	2.62
0.17	0.29	0.37	0.67	0.57	1.13	0.77	1.70	0.97	2.70
0.18	0.31	0.38	0.70	0.58	1.15	0.78	1.74	0.98	2.81
0.19	0.33	0.39	0.72	0.59	1.18	0.79	1.77	0.99	2.94
0.20	0.35	0.40	0.74	0.60	1.20	0.80	1.81	1.00	#NUM!

FINAL DESCENT PROFILE

DESCO10.XLS Incremental Descent in Actual Atmosphere (Eccentricity 0.10)

	A	B	C	D	E
1	u Mars:	42830	km3/sec2	4.283E+13	m3/sec2
2	Rapogee	4002	km	4002000	m
3	R scan	3402	km	3402000	m
4	R site	3397.8	km	3397800	m
5	V circular	3.27214	km/sec	3272.1414	m/sec
6	Rho B	0.0170	kg/m3		
7	Lambda	11.75	km		
8	Cd	1.0			

	F	G	H	I	J	K	L	M
	GIVEN							
	e	a	p	h	Vri	Vti	Vi	Beta i
	(-)	(km)	(km)	(km2/sec)	(m/sec)	(m/sec)	(m/sec)	(rad)
	0.10	3636.181818	3601.8	12420.35	341.5639243	3400.9731	3418.0809	0.1000956

9														
10	Altitude	m	A	Del T	q	Rho	Drag	ar	at	vr new	vt new	v new	Beta new
11	(km)	(kg)	(m2)	(sec)	(m/sec2)	(kg/m3)	(N)	(m/sec2)	(m/sec2)	(m/sec)	(m/sec)	(m/sec)	(rad)
12	250.0	84.7	1.767	10.0	3.21	1.02E-11	1.06E-04	3.21E+00	-1.24E-06	373.68	3400.97	3421.44	0.109
13	246.4	84.7	1.767	10.0	3.22	1.39E-11	1.44E-04	3.22E+00	-1.68E-06	405.85	3400.97	3425.10	0.119
14	242.5	84.7	1.767	10.0	3.23	1.93E-11	2.00E-04	3.22E+00	-2.35E-06	438.10	3400.97	3429.07	0.128
15	238.3	84.7	1.767	10.0	3.23	2.77E-11	2.88E-04	3.23E+00	-3.37E-06	470.42	3400.97	3433.38	0.137
16	233.8	84.7	1.767	10.0	3.24	4.08E-11	4.25E-04	3.24E+00	-4.96E-06	502.82	3400.97	3437.94	0.147
17	228.9	84.7	1.767	10.0	3.25	6.17E-11	6.44E-04	3.25E+00	-7.52E-06	535.31	3400.97	3442.84	0.156
18	223.7	84.7	1.767	10.0	3.26	9.59E-11	1.00E-03	3.26E+00	-1.17E-05	567.89	3400.97	3448.06	0.165
19	218.2	84.7	1.767	10.0	3.27	1.53E-10	1.61E-03	3.27E+00	-1.88E-05	600.57	3400.97	3453.59	0.175
20	212.3	84.7	1.767	10.0	3.28	2.52E-10	2.66E-03	3.28E+00	-3.09E-05	633.35	3400.97	3459.44	0.184
21	206.2	84.7	1.767	10.0	3.29	4.26E-10	4.51E-03	3.29E+00	-5.23E-05	666.25	3400.97	3465.62	0.193
22	199.7	84.7	1.767	10.0	3.30	7.41E-10	7.87E-03	3.30E+00	-9.11E-05	699.27	3400.97	3472.11	0.203
23	192.9	84.7	1.767	10.0	3.31	1.33E-09	1.41E-02	3.31E+00	-1.63E-04	732.41	3400.97	3478.94	0.212
24	185.7	84.7	1.767	10.0	3.33	2.44E-09	2.61E-02	3.33E+00	-3.01E-04	765.69	3400.97	3486.09	0.221
25	178.2	84.7	1.767	10.0	3.34	4.61E-09	4.95E-02	3.34E+00	-5.70E-04	799.10	3400.96	3493.58	0.231
26	170.4	84.7	1.767	10.0	3.36	8.97E-09	9.68E-02	3.36E+00	-1.11E-03	832.66	3400.95	3501.40	0.240
27	162.2	84.7	1.767	10.0	3.37	1.80E-08	1.95E-01	3.37E+00	-2.23E-03	866.37	3400.93	3509.54	0.249
28	153.7	84.7	1.767	10.0	3.39	3.70E-08	4.03E-01	3.39E+00	-4.61E-03	900.23	3400.88	3518.01	0.259
29	144.9	84.7	1.767	10.0	3.40	7.85E-08	8.59E-01	3.40E+00	-9.80E-03	934.25	3400.78	3526.77	0.268
30	135.7	84.7	1.767	10.0	3.42	1.71E-07	1.88E+00	3.42E+00	-2.14E-02	968.41	3400.57	3535.77	0.277
31	126.2	84.7	1.767	10.0	3.44	3.85E-07	4.25E+00	3.43E+00	-4.83E-02	1002.68	3400.08	3544.85	0.287
32	116.4	84.7	1.767	10.0	3.46	8.91E-07	9.89E+00	3.43E+00	-1.12E-01	1036.95	3398.96	3553.82	0.296
33	106.2	84.7	1.767	10.0	3.48	2.12E-06	2.37E+01	3.40E+00	-2.67E-01	1070.94	3396.29	3561.14	0.305
34	95.6	84.7	1.767	5.0	3.50	5.20E-06	5.83E+01	3.39E+00	-6.57E-01	1087.41	3393.01	3563.00	0.310
35	90.2	84.7	1.767	5.0	3.51	8.24E-06	9.24E+01	3.18E+00	-1.04E+00	1103.30	3387.81	3562.94	0.315
36	84.7	84.7	1.767	5.0	3.52	1.31E-05	1.47E+02	2.98E+00	-1.65E+00	1118.22	3379.55	3559.74	0.320
37	79.2	84.7	1.767	5.0	3.53	2.11E-05	2.36E+02	2.66E+00	-2.64E+00	1131.52	3366.33	3551.41	0.324
38	73.6	84.7	1.767	5.0	3.55	3.40E-05	3.79E+02	2.12E+00	-4.24E+00	1142.13	3345.13	3534.74	0.329
39	67.9	84.7	1.767	5.0	3.56	5.91E-05	6.09E+02	1.23E+00	-6.80E+00	1148.30	3311.12	3504.89	0.334
40	62.2	84.7	1.767	5.0	3.57	8.98E-05	9.74E+02	-2.00E-01	-1.09E+01	1147.30	3256.79	3452.97	0.339
41	56.4	84.7	1.767	5.0	3.58	1.46E-04	1.54E+03	-2.47E+00	-1.72E+01	1134.98	3170.97	3367.97	0.344
42	50.7	84.7	1.767	5.0	3.59	2.38E-04	2.36E+03	-5.89E+00	-2.65E+01	1109.53	3038.83	3233.40	0.349
43	45.1	84.7	1.767	5.0	3.60	3.83E-04	3.54E+03	-1.07E+01	-3.93E+01	1052.15	2842.27	3030.77	0.355
44	39.7	84.7	1.767	5.0	3.62	6.06E-04	4.92E+03	-1.65E+01	-5.45E+01	969.42	2569.94	2746.70	0.361
45	34.7	84.7	1.767	5.0	3.63	9.32E-04	6.21E+03	-2.23E+01	-6.86E+01	858.13	2226.89	2386.47	0.368
46	30.1	84.7	1.767	5.0	3.64	1.37E-03	6.92E+03	-2.57E+01	-7.62E+01	729.47	1848.79	1984.71	0.376
47	26.1	84.7	1.767	5.0	3.64	1.93E-03	6.71E+03	-2.55E+01	-7.36E+01	602.16	1477.55	1595.94	0.387
48	22.8	84.7	1.767	5.0	3.65	2.56E-03	5.75E+03	-2.20E+01	-6.29E+01	492.31	1162.96	1263.84	0.400
49	20.1	84.7	1.767	5.0	3.66	3.23E-03	4.55E+03	-1.73E+01	-4.95E+01	405.81	915.60	1001.80	0.417
50	17.8	84.7	1.767	5.0	3.66	3.91E-03	3.46E+03	-1.29E+01	-3.74E+01	341.25	728.64	804.89	0.438
51	15.9	84.7	1.767	5.0	3.67	4.58E-03	2.62E+03	-9.66E+00	-2.80E+01	293.96	588.82	657.85	0.463
52	14.4	84.7	1.767	5.0	3.67	5.25E-03	2.01E+03	-6.91E+00	-2.12E+01	259.40	482.89	547.89	0.493
53	13.0	84.7	1.767	5.0	3.67	5.80E-03	1.57E+03	-5.08E+00	-1.63E+01	234.03	401.31	464.47	0.528
54	11.7	84.7	1.767	5.0	3.68	6.55E-03	1.25E+03	-3.76E+00	-1.27E+01	215.23	337.50	400.29	0.568
55	10.6	84.7	1.767	5.0	3.68	7.21E-03	1.02E+03	-2.80E+00	-1.02E+01	201.22	286.69	350.25	0.613
56	9.6	84.7	1.767	5.0	3.68	7.88E-03	8.54E+02	-2.11E+00	-8.25E+00	190.65	245.43	310.77	0.660
57	8.6	84.7	1.767	5.0	3.68	8.56E-03	7.31E+02	-1.61E+00	-6.81E+00	182.59	211.35	279.30	0.713
58	7.7	84.7	1.767	5.0	3.68	9.27E-03	6.39E+02	-1.25E+00	-5.71E+00	176.35	183.80	253.95	0.767
59	6.8	84.7	1.767	5.0	3.69	1.00E-02	5.71E+02	-9.91E-01	-4.85E+00	171.39	158.56	233.49	0.824
60	5.9	84.7	1.767	5.0	3.69	1.08E-02	5.19E+02	-8.11E-01	-4.16E+00	167.34	137.75	216.74	0.882
61	5.0	84.7	1.767	5.0	3.69	1.16E-02	4.81E+02	-6.93E-01	-3.61E+00	163.87	119.71	202.94	0.940
62	4.2	84.7	1.767	5.0	3.69	1.24E-02	4.52E+02	-6.20E-01	-3.15E+00	160.77	103.96	191.46	0.997
63	3.4	84.7	1.767	5.0	3.69	1.33E-02	4.31E+02	-5.83E-01	-2.77E+00	157.86	90.14	181.78	1.052
64	2.6	84.7	1.767	5.0	3.69	1.43E-02	4.16E+02	-5.71E-01	-2.44E+00	155.00	77.96	173.50	1.105
65	1.8	84.7	1.767	5.0	3.70	1.52E-02	4.05E+02	-5.77E-01	-2.15E+00	152.12	67.21	166.31	1.155
66	1.1	84.7	1.767	5.0	3.70	1.63E-02	3.97E+02	-5.93E-01	-1.90E+00	149.15	57.73	159.94	1.202
67	0.3	84.7	1.767	5.0	3.70	1.73E-02	3.92E+02	-6.14E-01	-1.67E+00	146.08	49.38	154.20	1.245
68	-0.4	84.7	1.767	5.0	3.70	1.85E-02	3.88E+02	-6.37E-01	-1.47E+00	142.90	42.05	148.96	1.285
69	-1.2	84.7	1.767	5.0	3.70	1.96E-02	3.85E+02	-6.56E-01	-1.28E+00	139.62	35.63	144.09	1.321
70	-1.9	84.7	1.767	5.0	3.70	2.08E-02	3.82E+02	-6.71E-01	-1.12E+00	136.27	30.05	139.54	1.354
71	-2.5	84.7	1.767	1.0	3.71	2.22E-02	3.80E+02	-6.79E-01	-9.67E-01	135.59	29.08	138.67	1.359
72	-2.7	84.7	1.767	1.0	3.71	2.24E-02	3.80E+02	-6.80E-01	-9.41E-01	134.91	28.14	137.81	1.365
73	-2.8	84.7	1.767	1.0	3.71	2.26E-02	3.80E+02	-6.81E-01	-9.15E-01	134.22	27.23	136.96	1.371
74	-3.0	84.7	12.566	1.0	3.71	2.28E-02	2.70E+03	-2.75E+01	-6.33E+00	106.72	20.90	108.75	1.377
75	-3.1	84.7	12.566	1.0	3.71	2.31E-02	1.72E+03	-1.62E+01	-3.90E+00	90.52	17.00	92.11	1.385
76	-3.2	75.7	12.566	1.0	3.71	2.33E-02	1.24E+03	-1.24E+01	-3.03E+00	78.10	13.97	79.34	1.394
77	-3.3	75.7	12.566	1.0	3.71	2.35E-02	9.29E+02	-8.37E+00	-2.16E+00	69.73	11.81	70.72	1.403
78	-3.3	75.7	12.566	1.0	3.71	2.36E-02	7.43E+02	-5.96E+00	-1.64E+00	63.76	10.17	64.57	1.413
79	-3.4	75.7	12.566	1.0	3.71	2.38E-02	6.23E+02	-4.41E+00	-1.30E+00	59.35	8.88	60.01	1.422
80	-3.5	75.7	12.566	1.0	3.71	2.39E-02	5.41E+02	-3.35E+00	-1.06E+00	55.99	7.82	56.54	1.432
81	-3.5	75.7	12.566	1.0	3.71	2.40E-02	4.82E+02	-2.60E+00	-8.81E-01	53.39	6.94	53.84	1.442
82	-3.6	75.7	12.566	1.0	3.71	2.41E-02	4.39E+02	-2.05E+00	-7.48E-01	51.35	6.19	51.72	1.451
83	-3.6	75.7	12.566	1.0	3.71	2.42E-02	4.07E+02	-1.63E+00	-6.44E-01	49.71	5.55	50.02	1.460
84	-3.7	75.7	12.566	1.0	3.71	2.43E-02	3.83E+02	-1.31E+00	-5.60E-01	48.40	4.99	48.66	1.468
85	-3.7	75.7	12.566	1.0	3.71	2.44E-02	3.63E+02	-1.07E+00	-4.92E-01	47.33	4.49	47.55	1.476
86	-3.8	75.7	12.566	1.0	3.71	2.45E-02	3.48E+02	-8.74E-01	-4.35E-01	46.46	4.06	46.64	1.484
87	-3.8	75.7	12.566	1.0	3.71	2.46E-02	3.37E+02	-7.21E-01	-3.87E-01	45.74	3.67	45.89	1.491
88	-3.9	75.7	12.566	1.0	3.71	2.47E-02	3.27E+02	-5.99E-01	-3.46E-01	45.14	3.33	45.26	1.497

DESCD1C.XLS Incremental Descent in Actual Atmosphere (Eccentricity 0.10)

	N	O	P	Q	R	S	T	U	V	W	X	Y	Z
1													
2													
3													
4			GIVEN										
5	Beta 1	R 1	R 1	Alt 1	Alt 1	Theta(r)	DEL Theta	E	n	t apogee	Time(r)	Del T1	Del T1
6	(deg.)	(m)	(km)	(m)	(km)	(Rad)	(Deg.)	(Rad)	(Rad/sec)	(sec)	(sec)	(sec)	(min)
7	5.7350871	3652000	3652	250000	250	1.708691856	82.09916816	1.608786	0.00094308	3331.21324	1599.93	1731.283	28.85471
8													
9													
10	Beta new	r new	r new	new alt	new alt	del theta new	t new	t new					
11	(deg.)	(m)	(km)	(m)	(km)	(Deg.)	(sec)	(min)					
12	6.27	3648424	3648.4	246424	246.42	82.63	1741.3	29.02					
13	6.81	3644826	3644.8	242826	242.83	83.17	1751.3	29.19					
14	7.34	3640306	3640.3	238306	238.31	83.70	1761.3	29.35					
15	7.88	3638764	3638.8	233764	233.76	84.24	1771.3	29.52					
16	8.41	3630898	3630.9	226898	226.90	84.77	1781.3	29.69					
17	8.94	3628707	3628.7	223707	223.71	85.31	1791.3	29.85					
18	9.48	3620191	3620.2	218191	218.19	85.85	1801.3	30.02					
19	10.01	3614349	3614.3	212349	212.35	86.39	1811.3	30.19					
20	10.55	3608179	3608.2	206179	206.18	86.93	1821.3	30.35					
21	11.08	3601681	3601.7	199681	199.68	87.47	1831.3	30.52					
22	11.62	3594853	3594.9	192853	192.85	88.01	1841.3	30.69					
23	12.15	3587698	3587.7	185698	185.70	88.55	1851.3	30.85					
24	12.69	3580208	3580.2	178208	178.20	89.10	1861.3	31.02					
25	13.22	3572381	3572.4	170381	170.38	89.64	1871.3	31.19					
26	13.76	3564232	3564.2	162232	162.23	90.19	1881.3	31.35					
27	14.29	3555737	3555.7	153737	153.73	90.73	1891.3	31.52					
28	14.83	3546894	3546.9	144894	144.89	91.28	1901.3	31.69					
29	15.36	3537721	3537.7	135721	135.72	91.83	1911.3	31.85					
30	15.90	3528208	3528.2	126208	126.21	92.38	1921.3	32.02					
31	16.43	3518383	3518.4	116383	116.38	92.94	1931.3	32.19					
32	16.97	3508184	3508.2	106184	106.18	93.49	1941.3	32.35					
33	17.50	3497615	3497.6	95615	95.61	94.05	1951.3	32.52					
34	17.77	3492319	3492.3	90319	90.32	94.33	1956.3	32.60					
35	18.04	3486742	3486.7	84742	84.74	94.60	1961.3	32.69					
36	18.31	3481189	3481.2	79189	79.19	94.88	1966.3	32.77					
37	18.58	3475564	3475.6	73564	73.56	95.16	1971.3	32.85					
38	18.85	3469860	3469.9	67860	67.86	95.44	1976.3	32.94					
39	19.13	3464194	3464.2	62194	62.15	95.72	1981.3	33.02					
40	19.41	3458415	3458.4	56415	56.41	95.98	1986.3	33.10					
41	19.69	3452709	3452.7	50709	50.71	96.25	1991.3	33.19					
42	19.99	3447108	3447.1	45108	45.11	96.51	1996.3	33.27					
43	20.31	3441714	3441.7	39714	39.71	96.79	2001.3	33.35					
44	20.67	3436660	3436.7	34660	34.66	96.98	2006.3	33.44					
45	21.07	3432091	3432.1	30091	30.09	97.18	2011.3	33.52					
46	21.56	3428122	3428.1	26122	26.12	97.35	2016.3	33.60					
47	22.17	3426793	3426.8	23793	23.79	97.49	2021.3	33.69					
48	22.94	3423057	3423.1	20057	20.06	97.60	2026.3	33.77					
49	23.90	3419812	3419.8	17812	17.81	97.68	2031.3	33.85					
50	25.10	3417944	3417.9	15944	15.94	97.75	2036.3	33.94					
51	26.54	3416356	3416.4	14356	14.36	97.81	2041.3	34.02					
52	28.26	3414973	3415.0	12973	12.97	97.85	2046.3	34.10					
53	30.25	3413739	3413.7	11739	11.74	97.89	2051.3	34.19					
54	32.53	3412616	3412.6	10616	10.62	97.92	2056.3	34.27					
55	35.06	3411575	3411.6	9575	9.58	97.95	2061.3	34.35					
56	37.84	3410595	3410.6	8595	8.60	97.97	2066.3	34.44					
57	40.83	3409663	3409.7	7663	7.66	97.99	2071.3	34.52					
58	43.97	3408765	3408.8	6765	6.77	98.01	2076.3	34.60					
59	47.23	3407896	3407.9	5896	5.90	98.02	2081.3	34.69					
60	50.54	3407049	3407.0	5049	5.05	98.03	2086.3	34.77					
61	53.85	3406221	3406.2	4221	4.22	98.04	2091.3	34.85					
62	57.11	3405409	3405.4	3409	3.41	98.05	2096.3	34.94					
63	60.27	3404613	3404.6	2613	2.61	98.06	2101.3	35.02					
64	63.30	3403830	3403.8	1830	1.83	98.07	2106.3	35.10					
65	66.16	3403063	3403.1	1063	1.06	98.07	2111.3	35.19					
66	68.84	3402309	3402.3	309	0.31	98.08	2116.3	35.27					
67	71.32	3401571	3401.6	-429	-0.43	98.08	2121.3	35.35					
68	73.60	3400849	3400.8	-1151	-1.15	98.09	2126.3	35.44					
69	75.68	3400143	3400.1	-1857	-1.86	98.09	2131.3	35.52					
70	77.56	3399453	3399.5	-2547	-2.55	98.09	2136.3	35.60					
71	77.89	3399317	3399.3	-2683	-2.68	98.09	2137.3	35.62					
72	78.22	3399182	3399.2	-2818	-2.82	98.10	2138.3	35.64					
73	78.53	3399047	3399.0	-2953	-2.95	98.10	2139.3	35.65					
74	78.92	3398927	3398.9	-3073	-3.07	98.10	2140.3	35.67					
75	79.36	3398828	3398.8	-3172	-3.17	98.10	2141.3	35.69					
76	79.86	3398744	3398.7	-3256	-3.26	98.10	2142.3	35.70					
77	80.39	3398670	3398.7	-3330	-3.33	98.10	2143.3	35.72					
78	80.94	3398603	3398.6	-3397	-3.40	98.10	2144.3	35.74					
79	81.49	3398542	3398.5	-3458	-3.46	98.10	2145.3	35.75					
80	82.05	3398484	3398.5	-3516	-3.52	98.10	2146.3	35.77					
81	82.60	3398429	3398.4	-3571	-3.57	98.10	2147.3	35.79					
82	83.13	3398377	3398.4	-3623	-3.62	98.10	2148.3	35.80					
83	83.63	3398326	3398.3	-3674	-3.67	98.10	2149.3	35.82					

ALT_TIME.XLC

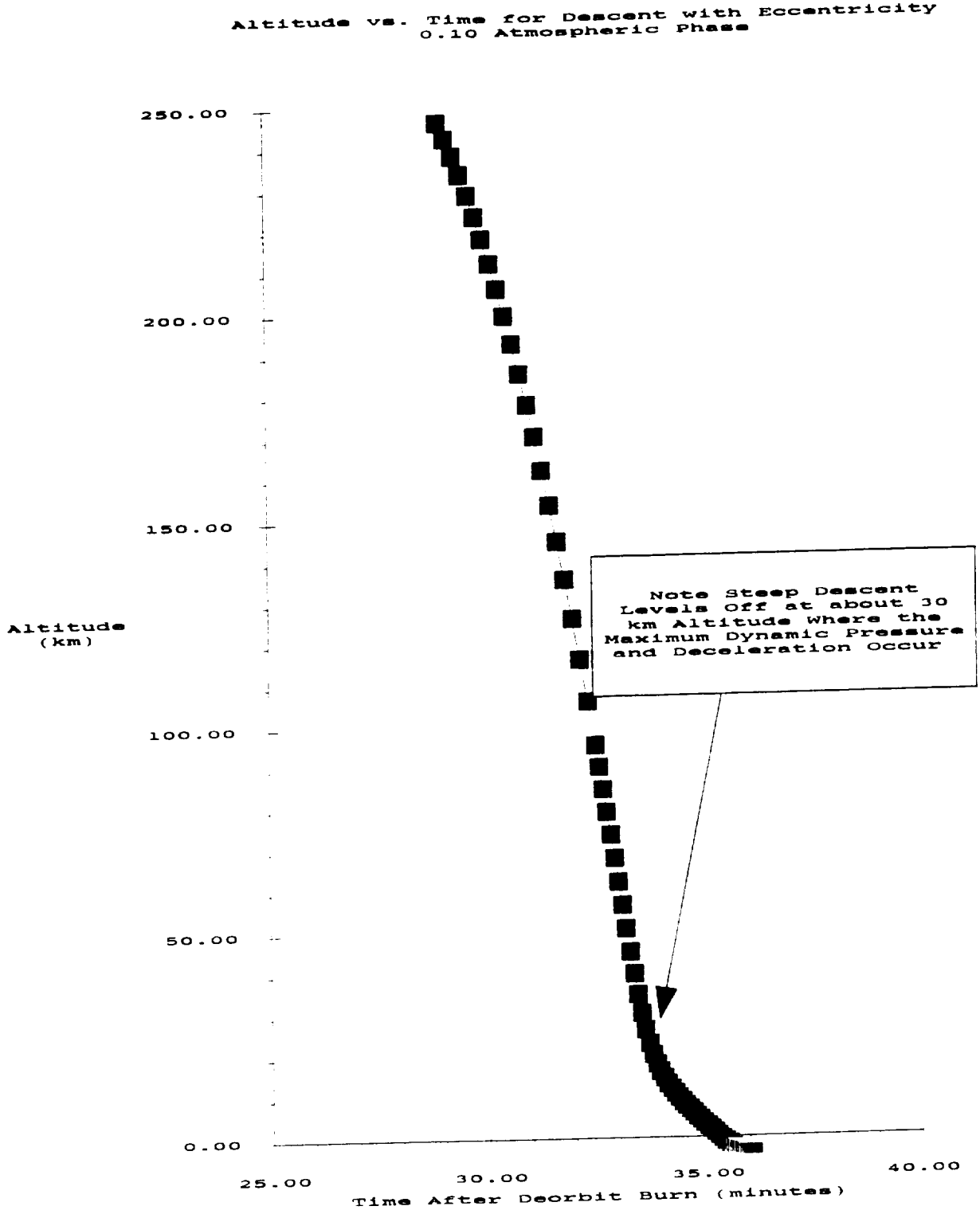

Velocity vs. Altitude Graphed with Transfer Ellipse of Eccentricity 0.10

DESCENT W/ ECCENTRICITY = 0.10

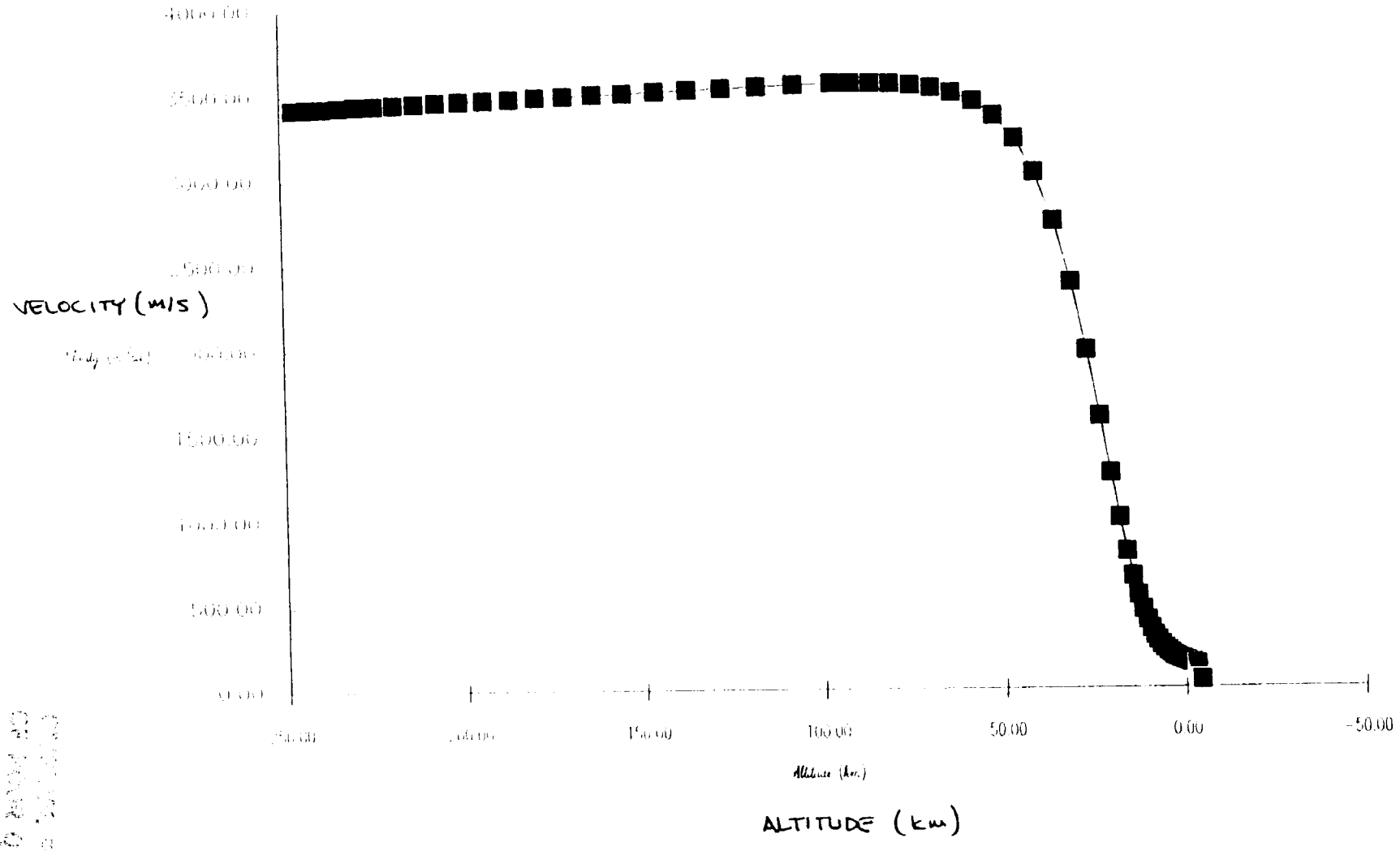

ALTITUDE (km)

Velocity vs. Altitude Braided with Transfer Ellipse with Eccentricity 0.27

DESCENT w/ ECCENTRICITY = 0.27

INTERMEDIATE SIMILAR TO FINAL CASE

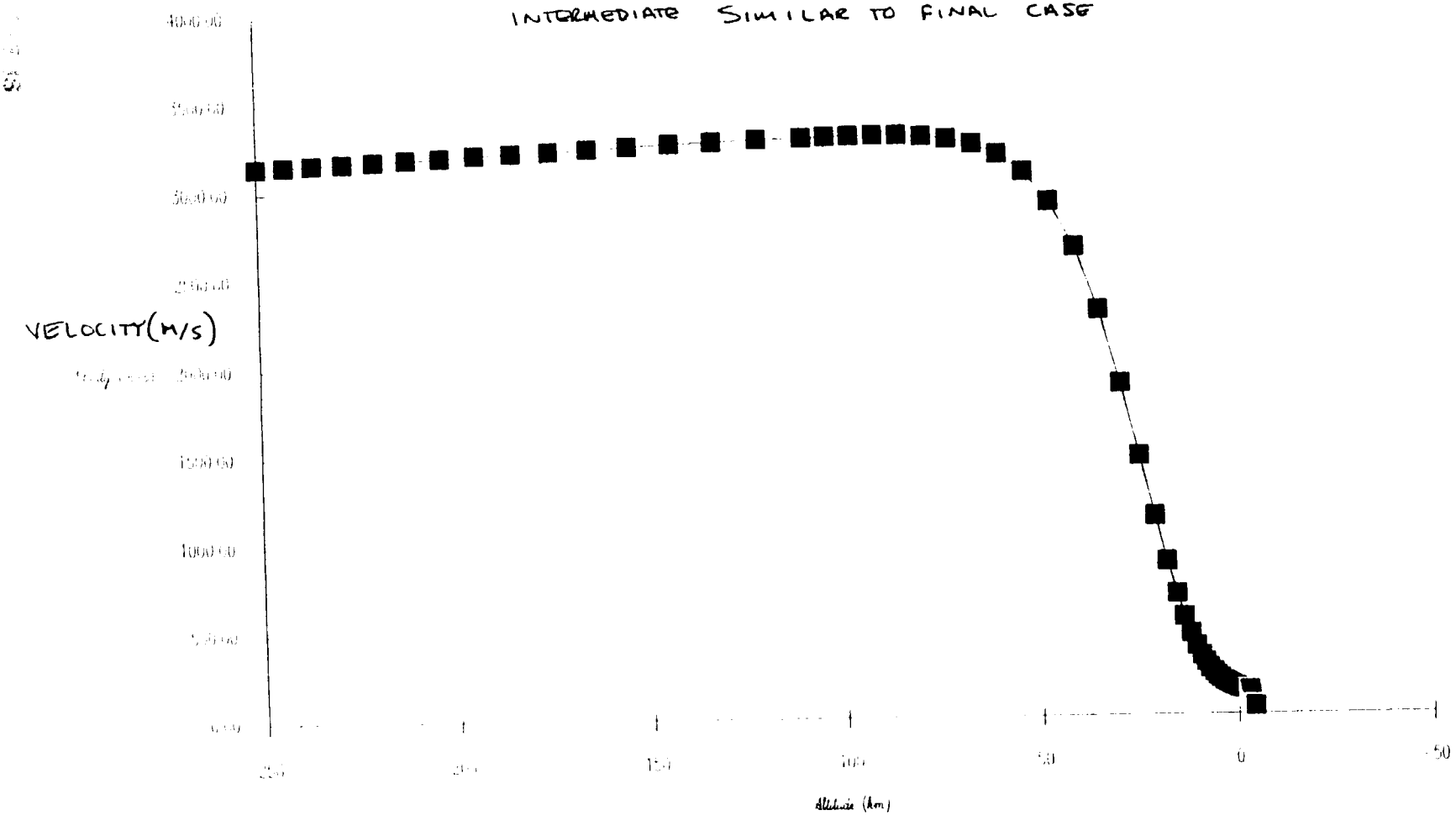

ALTITUDE (KM)

Minimum Insertion Delta V vs. Lift-Off Mass at Optimum Launch Angle

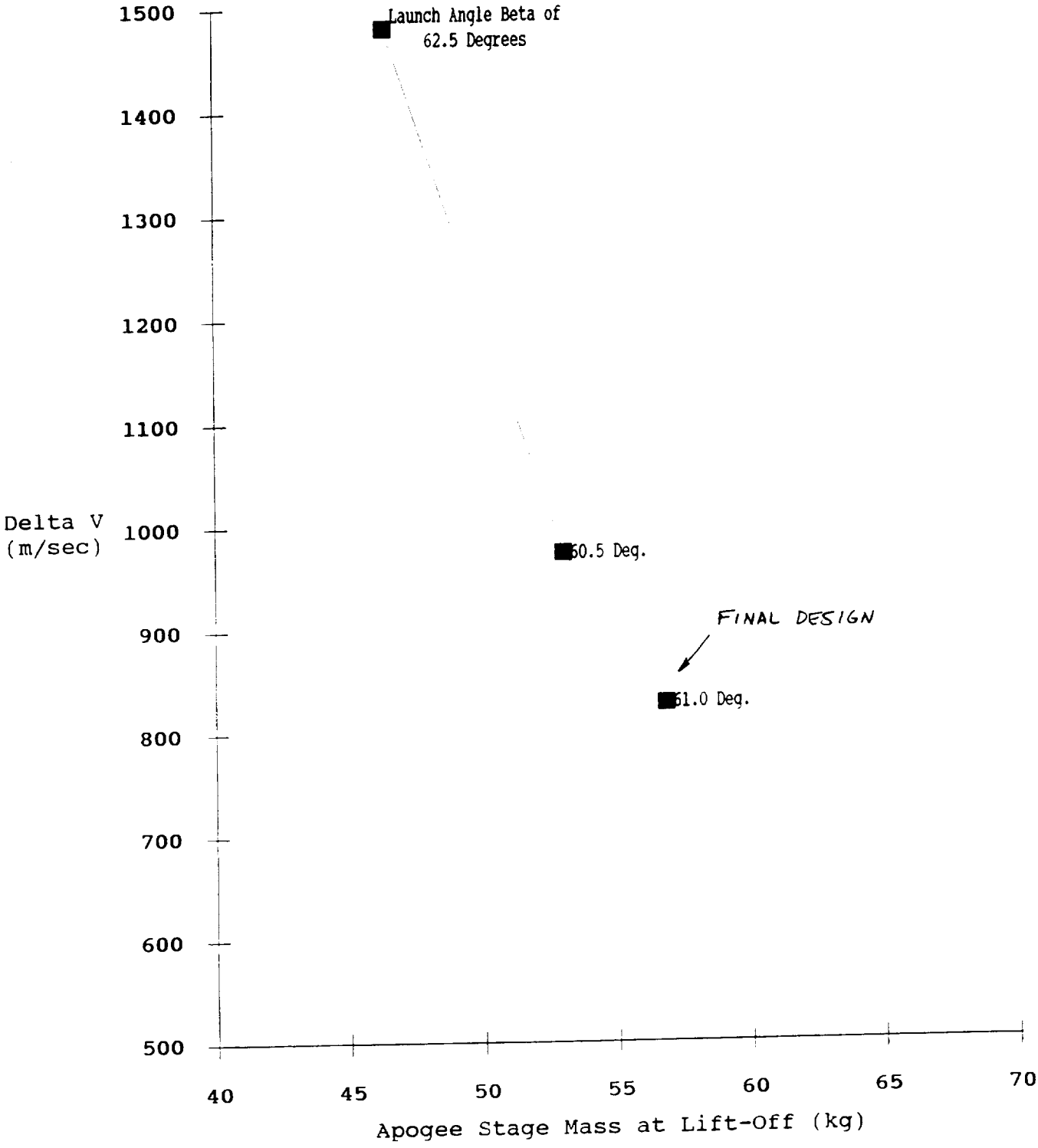

56.8 Mass at Lift Off (kg) 14.9 Mass at Burn Out (kg)
133% Of Original Fuel Mass (31.5 kg)
3271.414 V Circular

Beta LO (deg)	Max Alt (km)		Alt (km)	Beta (deg)	Velocity (m/sec)	Delta V (m/sec)
55	280					
60	541		600.91	2.92	2456.09	828.02
61	604		602.33	9.56	2470.65	930.44
61.5	636.21		601	19.37	2529.4	1219.57
63						

53 Mass at Lift Off (kg) 14.9 Mass at Burn Out (kg)
121% Of Original Fuel Mass (31.5 kg)
3271.414 V Circular

Beta LO (deg)	Max Alt (km)		Alt (km)	Beta (deg)	Velocity (m/sec)	Delta V (m/sec)
59	517					
60	579		601.18	4.96	2326.45	974.66
60.5	609.82		602.25	10.8	2345.89	1062.29
61	641.02					

46.4 Mass at Lift Off (kg) 14.9 Mass at Burn Out (kg)
100% Of Original Fuel Mass (31.5 kg)
3271.414 V Circular

Beta LO (deg)	Max Alt (km)		Alt (km)	Beta (deg)	Velocity (m/sec)	Delta V (m/sec)
61	530.31					
62	575.46		575.46	0.5	1805.89	1465.68
62.5	598.51		598.51	0	1790.72	1480.69
63	621.96		602.57	9.84	1801.06	1528.17

ASCENT61.XLS Ascent in Actual Atmosphere (Launch Angle 61 Degrees)

	A	B	C	D	E	F	G	H	I	J	K	L	M
1	u Mars:	42830	km3/sec2	4.283E+13	m3/sec2								
2	Rapogee	4002	km	4002000	m								
3	R mean	3402	km	3402000	m								
4	R site	3397.8	km	3397800	m								
5	V circular	3.2721414	km/sec	3272.1414	m/sec								
6	Rho m	0.0178	kg/m3										
7	Lambda	11.75	km										
8	Cd	1.0											
9													
10	Delta T	m	g	Rho	Drag	ar	at	vr new	vt new	v new	Beta	Beta	r
11	(sec)	(kg)	(m/sec2)	(kg/m3)	(N)	(m/sec2)	(m/sec2)	(m/sec)	(m/sec)	(m/sec)	(rad)	(deg.)	(m)
12	10.0	14.9	2.7	0.0	0.0	-2.7	0.0	125.1	2452.9	2456.1	0.1	2.9	4002906.5
13	Delta V Required for apogee:			828.74	Delta V at Launch (Thrust Only):			4020.32	Combined:	4849.06			
14													
15	Launch V	0		Area	0.101787602		Thrust	1500	(N)				
16	Beta Launch	61		Cd	1								
17				Mass T.O.	56.8		46.4	Mass depletion rate					
18				Mass B.O.	14.9			0.508064516					
19													
20	Delta T	m	g	Rho	Drag	ar	at	vr new	vt new	v new	Beta	Beta	r
21	(sec)	(kg)	(m/sec2)	(kg/m3)	(N)	(m/sec2)	(m/sec2)	(m/sec)	(m/sec)	(m/sec)	(rad)	(deg.)	(m)
22	1.0	56.8	3.71	2.54E-02	0.00E+00	1.94E+01	1.28E+01	19.39	12.80	23.23	1.065	61.00	3397800
23	1.0	56.3	3.71	2.54E-02	6.98E-01	1.96E+01	1.29E+01	38.97	25.72	46.69	0.988	56.58	3397819
24	1.0	55.8	3.71	2.53E-02	2.81E+00	1.87E+01	1.48E+01	57.66	40.50	70.46	0.959	54.92	3397858
25	1.0	55.3	3.71	2.52E-02	6.37E+00	1.84E+01	1.55E+01	76.07	56.03	94.47	0.936	53.63	3397916
26	1.0	54.8	3.71	2.50E-02	1.14E+01	1.82E+01	1.61E+01	94.24	72.15	118.69	0.917	52.57	3397992
27	1.0	54.3	3.71	2.48E-02	1.78E+01	1.80E+01	1.66E+01	112.23	88.75	143.08	0.902	51.66	3398086
28	1.0	53.8	3.71	2.46E-02	2.56E+01	1.78E+01	1.70E+01	130.03	105.77	167.61	0.888	50.88	3398199
29	1.0	53.2	3.71	2.43E-02	3.48E+01	1.76E+01	1.74E+01	147.67	123.13	192.27	0.876	50.18	3398329
30	1.0	52.7	3.71	2.40E-02	4.52E+01	1.75E+01	1.77E+01	165.15	140.80	217.02	0.865	49.55	3398476
31	1.0	52.2	3.71	2.37E-02	5.68E+01	1.73E+01	1.79E+01	182.47	158.72	241.85	0.855	48.98	3398641
32	1.0	51.7	3.71	2.33E-02	6.94E+01	1.72E+01	1.82E+01	199.63	176.88	266.72	0.846	48.46	3398824
33	1.0	51.2	3.71	2.29E-02	8.30E+01	1.70E+01	1.83E+01	216.64	195.23	291.62	0.837	47.98	3399024
34	1.0	50.7	3.71	2.25E-02	9.74E+01	1.68E+01	1.85E+01	233.48	213.74	316.54	0.829	47.53	3399240
35	1.0	50.2	3.71	2.21E-02	1.13E+02	1.67E+01	1.87E+01	250.16	232.41	341.46	0.822	47.11	3399474
36	1.0	49.7	3.71	2.16E-02	1.28E+02	1.65E+01	1.88E+01	266.68	251.20	366.36	0.815	46.71	3399724
37	1.0	49.2	3.71	2.11E-02	1.44E+02	1.64E+01	1.89E+01	283.04	270.10	391.24	0.809	46.34	3399990
38	1.0	48.7	3.70	2.06E-02	1.61E+02	1.62E+01	1.90E+01	299.25	289.10	416.09	0.803	45.99	3400274
39	1.0	48.2	3.70	2.01E-02	1.77E+02	1.61E+01	1.91E+01	315.30	308.19	440.90	0.797	45.65	3400573
40	1.0	47.7	3.70	1.96E-02	1.94E+02	1.59E+01	1.92E+01	331.20	327.35	465.67	0.791	45.34	3400888
41	1.0	47.1	3.70	1.90E-02	2.10E+02	1.58E+01	1.92E+01	346.96	346.58	490.41	0.786	45.03	3401219
42	1.0	46.6	3.70	1.85E-02	2.26E+02	1.56E+01	1.93E+01	362.58	365.89	515.11	0.781	44.74	3401566
43	1.0	46.1	3.70	1.79E-02	2.42E+02	1.55E+01	1.94E+01	378.08	385.26	539.79	0.776	44.46	3401929
44	1.0	45.6	3.70	1.73E-02	2.57E+02	1.54E+01	1.94E+01	393.46	404.70	564.44	0.771	44.19	3402307
45	1.0	45.1	3.70	1.68E-02	2.72E+02	1.53E+01	1.95E+01	408.74	424.22	589.09	0.767	43.93	3402700
46	1.0	44.6	3.70	1.62E-02	2.86E+02	1.52E+01	1.96E+01	423.92	443.82	613.75	0.762	43.69	3403109
47	1.0	44.1	3.70	1.56E-02	3.00E+02	1.51E+01	1.97E+01	439.03	463.51	638.42	0.758	43.45	3403533
48	1.0	43.6	3.70	1.50E-02	3.12E+02	1.50E+01	1.98E+01	454.07	483.29	663.13	0.754	43.21	3403972
49	1.0	43.1	3.70	1.45E-02	3.24E+02	1.50E+01	1.99E+01	469.06	503.18	687.90	0.750	42.99	3404426
50	1.0	42.6	3.69	1.39E-02	3.35E+02	1.50E+01	2.00E+01	484.03	523.20	712.75	0.747	42.77	3404895
51	1.0	42.1	3.69	1.34E-02	3.45E+02	1.49E+01	2.02E+01	498.98	543.35	737.70	0.743	42.56	3405379
52	1.0	41.6	3.69	1.28E-02	3.54E+02	1.50E+01	2.03E+01	513.93	563.65	762.78	0.739	42.36	3405878
53	1.0	41.1	3.69	1.22E-02	3.63E+02	1.50E+01	2.05E+01	528.90	584.12	788.00	0.736	42.16	3406392
54	1.0	40.5	3.69	1.17E-02	3.70E+02	1.50E+01	2.07E+01	543.92	604.78	813.40	0.732	41.97	3406921
55	1.0	40.0	3.69	1.12E-02	3.76E+02	1.51E+01	2.09E+01	559.00	625.65	839.00	0.729	41.78	3407465
56	1.0	39.5	3.69	1.07E-02	3.82E+02	1.52E+01	2.11E+01	574.16	646.75	864.84	0.726	41.60	3408024
57	1.0	39.0	3.69	1.02E-02	3.86E+02	1.53E+01	2.13E+01	589.42	668.09	890.93	0.723	41.42	3408598
58	1.0	38.5	3.69	9.66E-03	3.90E+02	1.54E+01	2.16E+01	604.80	689.70	917.32	0.720	41.25	3409187
59	1.0	38.0	3.68	9.17E-03	3.93E+02	1.55E+01	2.19E+01	620.33	711.61	944.03	0.717	41.08	3409792
60	1.0	37.5	3.68	8.70E-03	3.95E+02	1.57E+01	2.22E+01	636.02	733.83	971.10	0.714	40.92	3410413
61	1.0	37.0	3.68	8.24E-03	3.96E+02	1.59E+01	2.26E+01	651.90	756.40	998.56	0.711	40.76	3411049
62	1.0	36.5	3.68	7.80E-03	3.96E+02	1.61E+01	2.29E+01	667.99	779.33	1026.43	0.709	40.60	3411701
63	1.0	36.0	3.68	7.37E-03	3.95E+02	1.63E+01	2.33E+01	684.30	802.66	1054.77	0.706	40.45	3412369
64	1.0	35.5	3.68	6.95E-03	3.93E+02	1.66E+01	2.37E+01	700.87	826.41	1083.59	0.703	40.30	3413053
65	1.0	35.0	3.68	6.55E-03	3.91E+02	1.68E+01	2.42E+01	717.71	850.60	1112.94	0.701	40.16	3413754
66	1.0	34.4	3.67	6.16E-03	3.88E+02	1.71E+01	2.47E+01	734.85	875.27	1142.85	0.698	40.02	3414471
67	1.0	33.9	3.67	5.78E-03	3.85E+02	1.75E+01	2.52E+01	752.32	900.44	1173.36	0.696	39.88	3415206
68	1.0	33.4	3.67	5.43E-03	3.80E+02	1.78E+01	2.57E+01	770.12	926.15	1204.51	0.694	39.74	3415959
69	1.0	32.9	3.67	5.08E-03	3.75E+02	1.82E+01	2.63E+01	788.30	952.42	1236.33	0.691	39.61	3416729
70	1.0	32.4	3.67	4.75E-03	3.70E+02	1.86E+01	2.69E+01	806.87	979.28	1268.87	0.689	39.49	3417517
71	1.0	31.9	3.67	4.44E-03	3.64E+02	1.90E+01	2.75E+01	825.85	1006.77	1302.16	0.687	39.36	3418324
72	1.0	31.4	3.66	4.14E-03	3.57E+02	1.94E+01	2.81E+01	845.28	1034.92	1336.25	0.685	39.24	3419150
73	1.0	30.9	3.66	3.85E-03	3.50E+02	1.99E+01	2.88E+01	865.17	1063.76	1371.17	0.683	39.12	3419995
74	1.0	30.4	3.66	3.58E-03	3.42E+02	2.04E+01	2.96E+01	885.56	1093.33	1406.98	0.681	39.01	3420860
75	1.0	29.9	3.66	3.32E-03	3.34E+02	2.09E+01	3.03E+01	906.47	1123.66	1443.71	0.679	38.89	3421746
76	1.0	29.4	3.66	3.07E-03	3.26E+02	2.15E+01	3.11E+01	927.92	1154.79	1481.41	0.677	38.78	3422652
77	1.0	28.9	3.65	2.84E-03	3.17E+02	2.20E+01	3.20E+01	949.95	1186.75	1520.13	0.675	38.68	3423580
78	1.0	28.3	3.65	2.62E-03	3.08E+02	2.26E+01	3.28E+01	972.58	1219.59	1559.91	0.673	38.57	3424530
79	1.0	27.8	3.65	2.41E-03	2.98E+02	2.33E+01	3.37E+01	995.85	1253.33	1600.80	0.671	38.47	3425503
80	1.0	27.3	3.65	2.21E-03	2.89E+02	2.39E+01	3.47E+01	1019.77	1288.04	1642.85	0.670	38.37	3426499
81	1.0	26.8	3.65	2.03E-03	2.79E+02	2.46E+01	3.57E+01	1044.39	1323.73	1686.12	0.668	38.27	3427518
82	1.0	26.3	3.64	1.86E-03	2.69E+02	2.53E+01	3.67E+01	1069.73	1360.47	1730.66	0.666	38.18	3428563
83	1.0	25.8	3.64	1.69E-03	2.58E+02	2.61E+01	3.78E+01	1095.82	1398.29	1776.53	0.665	38.09	3429632
84	1.0	25.3	3.64	1.54E-03	2.48E+02	2.69E+01	3.90E+01	1122.71	1437.24	1823.77	0.663	38.00	3430728
85	1.0	24.8	3.64	1.40E-03	2.38E+02	2.77E+01	4.01E+01	1150.42	1477.37	1872.46	0.662	37.91	3431851
86	1.0	24.3	3.63	1.27E-03	2.27E+02	2.86E+01	4.14E+01	1179.00	1518.73	1922.65	0.660	37.82	3433001
87	1.0	23.8	3.63	1.15E-03	2.17E+02	2.95E+01	4.26E+01	1208.47	1561.37	1974.41	0.659	37.74	3434180
88	1.0	23.3	3.63	1.04E-03	2.06E+02	3.04E+01	4.40E+01	1238.88	1605.35	2027.80	0.657	37.66	3435389
89	1.0	22.8	3.63	9.34E-04	1.96E+02	3.14E+01	4.54E+01	1270.27	1650.73	2082.90	0.656	37.58	3436628
90	1.0	22.3	3.62	8.39E-04	1.85E+02	3.24E+01	4.68E+01	1302.68	1697.56	2139.78	0.655	37.50	3437898

	A	B	C	D	E	F	G	H	I	J	K	L	M
91	1.0	21.7	3.62	7.51E-04	1.75E+02	3.35E+01	4.83E+01	1336.16	1745.90	2198.52	0.653	37.43	3439201
92	1.0	21.2	3.62	6.70E-04	1.65E+02	3.46E+01	4.99E+01	1370.75	1795.83	2259.20	0.652	37.35	3440537
93	1.0	20.7	3.62	5.96E-04	1.55E+02	3.58E+01	5.16E+01	1406.51	1847.42	2321.90	0.651	37.28	3441908
94	1.0	20.2	3.61	5.29E-04	1.45E+02	3.70E+01	5.33E+01	1443.49	1900.74	2386.73	0.650	37.21	3443314
95	1.0	19.7	3.61	4.68E-04	1.36E+02	3.83E+01	5.51E+01	1481.74	1955.86	2453.76	0.648	37.15	3444758
96	1.0	19.2	3.61	4.12E-04	1.26E+02	3.96E+01	5.70E+01	1521.33	2012.88	2523.12	0.647	37.08	3446239
97	1.0	18.7	3.60	3.62E-04	1.17E+02	4.10E+01	5.90E+01	1562.32	2071.88	2594.90	0.646	37.02	3447761
98	1.0	18.2	3.60	3.17E-04	1.09E+02	4.25E+01	6.11E+01	1604.78	2132.96	2669.24	0.645	36.96	3449323
99	1.0	17.7	3.60	2.77E-04	1.00E+02	4.40E+01	6.33E+01	1648.78	2196.22	2746.25	0.644	36.90	3450928
100	1.0	17.2	3.59	2.40E-04	9.23E+01	4.56E+01	6.56E+01	1694.41	2261.78	2826.07	0.643	36.84	3452577
101	1.0	16.7	3.59	2.08E-04	8.46E+01	4.73E+01	6.80E+01	1741.75	2329.76	2908.87	0.642	36.78	3454271
102	1.0	16.2	3.59	1.79E-04	7.73E+01	4.91E+01	7.05E+01	1790.90	2400.30	2994.79	0.641	36.73	3456013
103	1.0	15.6	3.58	1.54E-04	7.03E+01	5.11E+01	7.32E+01	1841.95	2473.53	3084.02	0.640	36.67	3457804
104	1.0	15.1	3.58	1.32E-04	6.38E+01	-6.09E+00	-3.38E+00	1835.86	2470.15	3077.67	0.639	36.62	3459646
105	1.0	14.9	3.57	1.13E-04	5.43E+01	-5.75E+00	-2.93E+00	1830.11	2467.23	3071.89	0.638	36.57	3461481
106	1.0	14.9	3.57	9.64E-05	4.63E+01	-5.42E+00	-2.50E+00	1824.69	2464.73	3066.66	0.637	36.51	3463312
107	1.0	14.9	3.57	8.26E-05	3.95E+01	-5.15E+00	-2.13E+00	1819.54	2462.60	3061.88	0.636	36.46	3465136
108	1.0	14.9	3.56	7.07E-05	3.37E+01	-4.91E+00	-1.82E+00	1814.63	2460.78	3057.50	0.635	36.41	3466956
109	5.0	14.9	3.54	3.27E-05	1.55E+01	-4.16E+00	-8.40E-01	1793.81	2456.58	3041.80	0.631	36.14	3476029
110	5.0	14.9	3.53	1.52E-05	7.17E+00	-3.81E+00	-3.89E-01	1774.76	2454.63	3029.03	0.626	35.87	3484998
111	5.0	14.9	3.51	7.16E-06	3.34E+00	-3.64E+00	-1.82E-01	1756.56	2453.73	3017.66	0.621	35.60	3493872
112	5.0	14.9	3.49	3.39E-06	1.57E+00	-3.55E+00	-8.57E-02	1738.80	2453.30	3007.01	0.617	35.33	3502655
113	5.0	14.9	3.47	1.62E-06	7.44E-01	-3.50E+00	-4.07E-02	1721.29	2453.09	2996.75	0.612	35.06	3511349
114	5.0	14.9	3.46	7.77E-07	3.55E-01	-3.47E+00	-1.95E-02	1703.93	2453.00	2986.73	0.607	34.79	3519955
115	5.0	14.9	3.44	3.76E-07	1.71E-01	-3.45E+00	-9.42E-03	1686.70	2452.95	2976.90	0.602	34.51	3528475
116	5.0	14.9	3.42	1.84E-07	8.28E-02	-3.43E+00	-4.58E-03	1669.57	2452.93	2967.20	0.598	34.24	3536908
117	5.0	14.9	3.41	9.03E-08	4.04E-02	-3.41E+00	-2.24E-03	1652.52	2452.91	2957.64	0.593	33.97	3545256
119	5.0	14.9	3.38	2.23E-08	9.85E-03	-3.38E+00	-5.50E-04	1618.67	2452.91	2938.85	0.583	33.42	3561696
120	5.0	14.9	3.36	1.12E-08	4.92E-03	-3.36E+00	-2.75E-04	1601.87	2452.90	2929.63	0.579	33.15	3569790
121	5.0	14.9	3.35	5.66E-09	2.47E-03	-3.35E+00	-1.39E-04	1585.14	2452.90	2920.51	0.574	32.87	3577799
122	5.0	14.9	3.33	2.88E-09	1.25E-03	-3.33E+00	-7.05E-05	1568.48	2452.90	2911.51	0.569	32.60	3585725
123	5.0	14.9	3.32	1.48E-09	6.38E-04	-3.32E+00	-3.61E-05	1551.90	2452.90	2902.61	0.564	32.32	3593567
124	5.0	14.9	3.30	7.64E-10	3.28E-04	-3.30E+00	-1.86E-05	1535.39	2452.90	2893.81	0.559	32.04	3601327
125	5.0	14.9	3.29	3.97E-10	1.69E-04	-3.29E+00	-9.64E-06	1518.95	2452.90	2885.12	0.554	31.77	3609004
126	5.0	14.9	3.27	2.08E-10	8.82E-05	-3.27E+00	-5.03E-06	1502.57	2452.90	2876.54	0.550	31.49	3616598
127	5.0	14.9	3.26	1.10E-10	4.63E-05	-3.26E+00	-2.65E-06	1486.27	2452.90	2868.05	0.545	31.21	3624111
128	5.0	14.9	3.25	5.84E-11	2.44E-05	-3.25E+00	-1.40E-06	1470.03	2452.90	2859.67	0.540	30.93	3631543
129	5.0	14.9	3.23	3.12E-11	1.30E-05	-3.23E+00	-7.48E-07	1453.86	2452.90	2851.39	0.535	30.66	3638893
130	5.0	14.9	3.22	1.68E-11	6.96E-06	-3.22E+00	-4.02E-07	1437.75	2452.90	2843.21	0.530	30.38	3646162
131	5.0	14.9	3.21	9.12E-12	3.75E-06	-3.21E+00	-2.17E-07	1421.70	2452.90	2835.13	0.525	30.10	3653351
132	5.0	14.9	3.20	4.98E-12	2.04E-06	-3.20E+00	-1.18E-07	1405.72	2452.90	2827.15	0.520	29.82	3660459
133	10.0	14.9	3.17	1.51E-12	6.13E-07	-3.17E+00	-3.57E-08	1374.00	2452.90	2811.51	0.511	29.26	3674516
134	10.0	14.9	3.15	4.68E-13	1.88E-07	-3.15E+00	-1.10E-08	1342.52	2452.90	2796.26	0.501	28.69	3688256
135	10.0	14.9	3.13	1.49E-13	5.94E-08	-3.13E+00	-3.50E-09	1311.26	2452.90	2781.39	0.491	28.13	3701682
136	10.0	14.9	3.10	4.89E-14	1.92E-08	-3.10E+00	-1.14E-09	1280.22	2452.90	2766.89	0.481	27.56	3714794
137	10.0	14.9	3.08	1.64E-14	6.41E-09	-3.08E+00	-3.81E-10	1249.40	2452.90	2752.77	0.471	26.99	3727596
138	10.0	14.9	3.06	5.68E-15	2.19E-09	-3.06E+00	-1.31E-10	1218.78	2452.90	2739.01	0.461	26.42	3740090
139	10.0	14.9	3.04	2.01E-15	7.68E-10	-3.04E+00	-4.62E-11	1188.36	2452.90	2725.61	0.451	25.85	3752278
140	10.0	14.9	3.02	7.32E-16	2.77E-10	-3.02E+00	-1.67E-11	1158.13	2452.90	2712.56	0.441	25.27	3764162
141	10.0	14.9	3.00	2.73E-16	1.02E-10	-3.00E+00	-6.21E-12	1128.09	2452.90	2699.87	0.431	24.70	3775743
142	10.0	14.9	2.99	1.05E-16	3.88E-11	-2.99E+00	-2.37E-12	1098.22	2452.90	2687.53	0.421	24.12	3787024
143	10.0	14.9	2.97	4.11E-17	1.51E-11	-2.97E+00	-9.25E-13	1068.53	2452.90	2675.54	0.411	23.54	3798006
144	10.0	14.9	2.95	1.65E-17	6.03E-12	-2.95E+00	-3.71E-13	1039.01	2452.90	2663.88	0.401	22.96	3808692
145	10.0	14.9	2.94	6.83E-18	2.47E-12	-2.94E+00	-1.52E-13	1009.64	2452.90	2652.57	0.390	22.37	3819082
146	10.0	14.9	2.92	2.89E-18	1.04E-12	-2.92E+00	-6.43E-14	980.43	2452.90	2641.59	0.380	21.79	3829178
147	10.0	14.9	2.91	1.26E-18	4.46E-13	-2.91E+00	-2.78E-14	951.37	2452.90	2630.94	0.370	21.20	3838982
148	10.0	14.9	2.89	5.59E-19	1.97E-13	-2.89E+00	-1.23E-14	922.45	2452.90	2620.62	0.360	20.61	3848496
149	10.0	14.9	2.88	2.55E-19	8.91E-14	-2.88E+00	-5.60E-15	893.67	2452.90	2610.63	0.349	20.02	3857721
150	10.0	14.9	2.86	1.19E-19	4.13E-14	-2.86E+00	-2.61E-15	865.03	2452.90	2600.96	0.339	19.43	3866657
151	10.0	14.9	2.85	5.71E-20	1.96E-14	-2.85E+00	-1.24E-15	836.51	2452.90	2591.62	0.329	18.83	3875308
152	10.0	14.9	2.84	2.80E-20	9.57E-15	-2.84E+00	-6.08E-16	808.11	2452.90	2582.59	0.318	18.23	3883673
153	10.0	14.9	2.83	1.41E-20	4.78E-15	-2.83E+00	-3.05E-16	779.83	2452.90	2573.88	0.308	17.64	3891754
154	10.0	14.9	2.82	7.25E-21	2.44E-15	-2.82E+00	-1.56E-16	751.67	2452.90	2565.49	0.297	17.04	3899552
155	10.0	14.9	2.81	3.82E-21	1.28E-15	-2.81E+00	-8.22E-17	723.61	2452.90	2557.41	0.287	16.44	3907069
156	10.0	14.9	2.80	2.07E-21	6.87E-16	-2.80E+00	-4.43E-17	695.65	2452.90	2549.64	0.276	15.83	3914305
157	10.0	14.9	2.79	1.14E-21	3.78E-16	-2.79E+00	-2.44E-17	667.80	2452.90	2542.18	0.266	15.23	3921261
158	10.0	14.9	2.78	6.47E-22	2.13E-16	-2.78E+00	-1.38E-17	640.04	2452.90	2535.03	0.255	14.62	3927939
159	10.0	14.9	2.77	3.75E-22	1.23E-16	-2.77E+00	-7.97E-18	612.37	2452.90	2528.19	0.245	14.02	3934340
160	10.0	14.9	2.76	2.23E-22	7.25E-17	-2.76E+00	-4.72E-18	584.79	2452.90	2521.65	0.234	13.41	3940463
161	10.0	14.9	2.75	1.36E-22	4.39E-17	-2.75E+00	-2.86E-18	557.28	2452.90	2515.41	0.223	12.80	3946311
162	10.0	14.9	2.74	8.43E-23	2.72E-17	-2.74E+00	-1.78E-18	529.86	2452.90	2509.48	0.213	12.19	3951884
163	10.0	14.9	2.74	5.37E-23	1.72E-17	-2.74E+00	-1.13E-18	502.51	2452.90	2503.85	0.202	11.58	3957183
164	10.0	14.9	2.73	3.50E-23	1.12E-17	-2.73E+00	-7.35E-19	475.23	2452.90	2498.51	0.191	10.96	3962208
165	10.0	14.9	2.72	2.34E-23	7.43E-18	-2.72E+00	-4.89E-19	448.01	2452.90	2493.48	0.181	10.35	3966960
166	10.0	14.9	2.72	1.60E-23	5.05E-18	-2.72E+00	-3.34E-19	420.86	2452.90	2488.75	0.170	9.74	3971440
167	10.0	14.9	2.71	1.12E-23	3.52E-18	-2.71E+00	-2.33E-19	393.76	2452.90	2484.31	0.159	9.12	3975649
168	10.0	14.9	2.70	7.98E-24	2.51E-18	-2.70E+00	-1.66E-19	366.71	2452.90	2480.16	0.148	8.50	3979586
169	10.0	14.9	2.70	5.84E-24	1.83E-18	-2.70E+00	-1.21E-19	339.72	2452.90	2476.32	0.138	7.89	3983253
170	10.0	14.9	2.69	4.38E-24	1.37E-18	-2.69E+00	-9.08E-20	312.77	2452.90	2472.76	0.127	7.27	3986651
171	10.0	14.9	2.69	3.35E-24	1.04E-18	-2.69E+00	-6.95E-20	285.86	2452.90	2469.50	0.116	6.65	3989778
172	10.0	14.9	2.69	2.63E-24	8.16E-19	-2.69E+00	-5.44E-20	259.00	2452.90	2466.54	0.105	6.03	3992637
173	10.0	14.9	2.68	2.11E-24	6.53E-19	-2.68E+00	-4.36E-20	232.16	2452.90	2463.87	0.094	5.41	3995227
174	10.0	14.9	2.68	1.73E-24	5.35E-19	-2.68E+00	-3.57E-20	205.36	2452.90	2461.49	0.084	4.79	3997549
175	10.0	14.9	2.68	1.45E-24	4.48E-19	-2.68E+00	-3.00E-20	178.59	2452.90	2459.40	0.073	4.16	3999602
176	10.0	14.9	2.68	1.25E-24	3.84E-19	-2.68E+00	-2.57E-20	151.84	2452.90	2457.60	0.062	3.54	4001388
177	10.0	14.9	2.67	1.10E-24	3.37E-19	-2.67E+00	-2.26E-20	125.11	2452.90	2456.09	0.051	2.92	4002907
178	10.0	14.9	2.67	9.86E-25	3.03E-19	-2.67E+00	-2.03E-20	98.40	2452.90	2454.88	0.040	2.30	4004158
179	10.0	14.9	2.67	9.07E-25	2.78E-19	-2.67E+00	-1.87E-20	71.70	2452.90	2453.95	0.029	1.67	4005142

	N	O	P	Q	R	S	T
1							
2							
3							
4							
5							
6							
7							
8							
9							
10	r	Alt	Alt	Theta	Theta	Time	Time
11	(km)	(m)	(km)	(Rad)	(Deg)	(sec)	(min)
12	4002.9	600906.5	600.9	0.1	4.0	647.0	10.8
13							
14							
15							
16							
17							
18							
19							
20	r	Alt	Alt	Theta	Theta	Time	Time
21	(km)	(m)	(km)	(Rad)	(Deg)	(sec)	(min)
22	3397.8	-4200	-4.20	0.00	0.00	0.0	0.00
23	3397.8	-4181	-4.18	0.00	0.00	1.0	0.02
24	3397.9	-4142	-4.14	0.00	0.00	2.0	0.03
25	3397.9	-4084	-4.08	0.00	0.00	3.0	0.05
26	3398.0	-4008	-4.01	0.00	0.00	4.0	0.07
27	3398.1	-3914	-3.91	0.00	0.00	5.0	0.08
28	3398.2	-3801	-3.80	0.00	0.01	6.0	0.10
29	3398.3	-3671	-3.67	0.00	0.01	7.0	0.12
30	3398.5	-3524	-3.52	0.00	0.01	8.0	0.13
31	3398.6	-3359	-3.36	0.00	0.01	9.0	0.15
32	3398.8	-3176	-3.18	0.00	0.02	10.0	0.17
33	3399.0	-2976	-2.98	0.00	0.02	11.0	0.18
34	3399.2	-2760	-2.76	0.00	0.02	12.0	0.20
35	3399.5	-2526	-2.53	0.00	0.03	13.0	0.22
36	3399.7	-2276	-2.28	0.00	0.03	14.0	0.23
37	3400.0	-2010	-2.01	0.00	0.04	15.0	0.25
38	3400.3	-1726	-1.73	0.00	0.04	16.0	0.27
39	3400.6	-1427	-1.43	0.00	0.05	17.0	0.28
40	3400.9	-1112	-1.11	0.00	0.05	18.0	0.30
41	3401.2	-781	-0.78	0.00	0.06	19.0	0.32
42	3401.6	-434	-0.43	0.00	0.06	20.0	0.33
43	3401.9	-71	-0.07	0.00	0.07	21.0	0.35
44	3402.3	307	0.31	0.00	0.08	22.0	0.37
45	3402.7	700	0.70	0.00	0.08	23.0	0.38
46	3403.1	1109	1.11	0.00	0.09	24.0	0.40
47	3403.5	1533	1.53	0.00	0.10	25.0	0.42
48	3404.0	1972	1.97	0.00	0.11	26.0	0.43
49	3404.4	2426	2.43	0.00	0.12	27.0	0.45
50	3404.9	2895	2.90	0.00	0.12	28.0	0.47
51	3405.4	3379	3.38	0.00	0.13	29.0	0.48
52	3405.9	3878	3.88	0.00	0.14	30.0	0.50
53	3406.4	4392	4.39	0.00	0.15	31.0	0.52
54	3406.9	4921	4.92	0.00	0.16	32.0	0.53
55	3407.5	5465	5.46	0.00	0.17	33.0	0.55
56	3408.0	6024	6.02	0.00	0.18	34.0	0.57
57	3408.6	6598	6.60	0.00	0.20	35.0	0.58
58	3409.2	7187	7.19	0.00	0.21	36.0	0.60
59	3409.8	7792	7.79	0.00	0.22	37.0	0.62
60	3410.4	8413	8.41	0.00	0.23	38.0	0.63
61	3411.0	9049	9.05	0.00	0.24	39.0	0.65
62	3411.7	9701	9.70	0.00	0.26	40.0	0.67
63	3412.4	10369	10.37	0.00	0.27	41.0	0.68
64	3413.1	11053	11.05	0.00	0.29	42.0	0.70
65	3413.8	11754	11.75	0.01	0.30	43.0	0.72
66	3414.5	12471	12.47	0.01	0.31	44.0	0.73
67	3415.2	13206	13.21	0.01	0.33	45.0	0.75
68	3416.0	13959	13.96	0.01	0.34	46.0	0.77
69	3416.7	14729	14.73	0.01	0.36	47.0	0.78
70	3417.5	15517	15.52	0.01	0.38	48.0	0.80
71	3418.3	16324	16.32	0.01	0.39	49.0	0.82
72	3419.1	17150	17.15	0.01	0.41	50.0	0.83
73	3420.0	17995	18.00	0.01	0.43	51.0	0.85
74	3420.9	18860	18.86	0.01	0.45	52.0	0.87
75	3421.7	19746	19.75	0.01	0.47	53.0	0.88
76	3422.7	20652	20.65	0.01	0.49	54.0	0.90
77	3423.6	21580	21.58	0.01	0.51	55.0	0.92
78	3424.5	22530	22.53	0.01	0.53	56.0	0.93
79	3425.5	23503	23.50	0.01	0.55	57.0	0.95
80	3426.5	24499	24.50	0.01	0.57	58.0	0.97
81	3427.5	25518	25.52	0.01	0.59	59.0	0.98
82	3428.6	26563	26.56	0.01	0.61	60.0	1.00
83	3429.6	27632	27.63	0.01	0.64	61.0	1.02
84	3430.7	28728	28.73	0.01	0.66	62.0	1.03
85	3431.9	29851	29.85	0.01	0.69	63.0	1.05
86	3433.0	31001	31.00	0.01	0.71	64.0	1.07
87	3434.2	32180	32.18	0.01	0.74	65.0	1.08
88	3435.4	33389	33.39	0.01	0.76	66.0	1.10
89	3436.6	34628	34.63	0.01	0.79	67.0	1.12
90	3437.9	35898	35.90	0.01	0.82	68.0	1.13

	N	O	P	Q	R	S	T
91	3439.2	37201	37.20	0.01	0.85	69.0	1.15
92	3440.5	38537	38.54	0.02	0.88	70.0	1.17
93	3441.9	39908	39.91	0.02	0.91	71.0	1.18
94	3443.3	41314	41.31	0.02	0.94	72.0	1.20
95	3444.8	42758	42.76	0.02	0.97	73.0	1.22
96	3446.2	44239	44.24	0.02	1.01	74.0	1.23
97	3447.8	45761	45.76	0.02	1.04	75.0	1.25
98	3449.3	47323	47.32	0.02	1.08	76.0	1.27
99	3450.9	48928	48.93	0.02	1.11	77.0	1.28
100	3452.6	50577	50.58	0.02	1.15	78.0	1.30
101	3454.3	52271	52.27	0.02	1.19	79.0	1.32
102	3456.0	54013	54.01	0.02	1.23	80.0	1.33
103	3457.8	55804	55.80	0.02	1.27	81.0	1.35
104	3459.6	57646	57.65	0.02	1.31	82.0	1.37
105	3461.5	59481	59.48	0.02	1.35	83.0	1.38
106	3463.3	61312	61.31	0.02	1.39	84.0	1.40
107	3465.1	63136	63.14	0.03	1.43	85.0	1.42
108	3467.0	64956	64.96	0.03	1.47	86.0	1.43
109	3476.0	74029	74.03	0.03	1.51	87.0	1.45
110	3485.0	82998	83.00	0.03	1.55	92.0	1.53
111	3493.9	91872	91.87	0.03	1.60	97.0	1.62
112	3502.7	100655	100.65	0.03	1.64	102.0	1.70
113	3511.3	109349	109.35	0.03	1.68	107.0	1.78
114	3520.0	117955	117.96	0.03	1.72	112.0	1.87
115	3528.5	126475	126.47	0.03	1.75	117.0	1.95
116	3536.9	134908	134.91	0.03	1.79	122.0	2.03
117	3545.3	143256	143.26	0.03	1.83	127.0	2.12
119	3561.7	159696	159.70	0.03	1.91	137.0	2.28
120	3569.8	167790	167.79	0.03	1.95	142.0	2.37
121	3577.8	175799	175.80	0.03	1.99	147.0	2.45
122	3585.7	183725	183.72	0.04	2.03	152.0	2.53
123	3593.6	191567	191.57	0.04	2.07	157.0	2.62
124	3601.3	199327	199.33	0.04	2.11	162.0	2.70
125	3609.0	207004	207.00	0.04	2.15	167.0	2.78
126	3616.6	214598	214.60	0.04	2.19	172.0	2.87
127	3624.1	222111	222.11	0.04	2.23	177.0	2.95
128	3631.5	229543	229.54	0.04	2.26	182.0	3.03
129	3638.9	236893	236.89	0.04	2.30	187.0	3.12
130	3646.2	244162	244.16	0.04	2.34	192.0	3.20
131	3653.4	251351	251.35	0.04	2.38	197.0	3.28
132	3660.5	258459	258.46	0.04	2.42	202.0	3.37
133	3674.5	272516	272.52	0.04	2.46	207.0	3.45
134	3688.3	286256	286.26	0.04	2.49	217.0	3.62
135	3701.7	299682	299.68	0.04	2.53	227.0	3.78
136	3714.8	312794	312.79	0.04	2.57	237.0	3.95
137	3727.6	325596	325.60	0.05	2.61	247.0	4.12
138	3740.1	338090	338.09	0.05	2.65	257.0	4.28
139	3752.3	350278	350.28	0.05	2.68	267.0	4.45
140	3764.2	362162	362.16	0.05	2.72	277.0	4.62
141	3775.7	373743	373.74	0.05	2.76	287.0	4.78
142	3787.0	385024	385.02	0.05	2.80	297.0	4.95
143	3798.0	396006	396.01	0.05	2.83	307.0	5.12
144	3808.7	406692	406.69	0.05	2.87	317.0	5.28
145	3819.1	417082	417.08	0.05	2.91	327.0	5.45
146	3829.2	427178	427.18	0.05	2.94	337.0	5.62
147	3839.0	436982	436.98	0.05	2.98	347.0	5.78
148	3848.5	446496	446.50	0.05	3.02	357.0	5.95
149	3857.7	455721	455.72	0.05	3.05	367.0	6.12
150	3866.7	464657	464.66	0.05	3.09	377.0	6.28
151	3875.3	473308	473.31	0.05	3.12	387.0	6.45
152	3883.7	481673	481.67	0.06	3.16	397.0	6.62
153	3891.8	489754	489.75	0.06	3.20	407.0	6.78
154	3899.6	497552	497.55	0.06	3.23	417.0	6.95
155	3907.1	505069	505.07	0.06	3.27	427.0	7.12
156	3914.3	512305	512.30	0.06	3.30	437.0	7.28
157	3921.3	519261	519.26	0.06	3.34	447.0	7.45
158	3927.9	525939	525.94	0.06	3.38	457.0	7.62
159	3934.3	532340	532.34	0.06	3.41	467.0	7.78
160	3940.5	538463	538.46	0.06	3.45	477.0	7.95
161	3946.3	544311	544.31	0.06	3.48	487.0	8.12
162	3951.9	549884	549.88	0.06	3.52	497.0	8.28
163	3957.2	555183	555.18	0.06	3.55	507.0	8.45
164	3962.2	560208	560.21	0.06	3.59	517.0	8.62
165	3967.0	564960	564.96	0.06	3.63	527.0	8.78
166	3971.4	569440	569.44	0.06	3.66	537.0	8.95
167	3975.6	573649	573.65	0.06	3.70	547.0	9.12
168	3979.6	577586	577.59	0.07	3.73	557.0	9.28
169	3983.3	581253	581.25	0.07	3.77	567.0	9.45
170	3986.7	584651	584.65	0.07	3.80	577.0	9.62
171	3989.8	587778	587.78	0.07	3.84	587.0	9.78
172	3992.6	590637	590.64	0.07	3.87	597.0	9.95
173	3995.2	593227	593.23	0.07	3.91	607.0	10.12
174	3997.5	595549	595.55	0.07	3.94	617.0	10.28
175	3999.6	597602	597.60	0.07	3.98	627.0	10.45
176	4001.4	599388	599.39	0.07	4.01	637.0	10.62
177	4002.9	600907	600.91	0.07	4.05	647.0	10.78
178	4004.2	602158	602.16	0.07	4.08	657.0	10.95
179	4005.1	603142	603.14	[illegible]	4.12	667.0	[illegible]

ASC_DELV.XLS

DELTA V'S DURING ASCENT BURN

0.508	Mass Delpetion Rate (kg/sec)
1500.0	Thrust (N)

time (sec)	mass (kg)	Acel (m/s^2)	Delta V (m/s)
0	56.800	26.408	26.408
1	56.292	26.647	53.055
2	55.784	26.889	79.945
3	55.276	27.137	107.081
4	54.768	27.388	134.470
5	54.260	27.645	162.115
6	53.752	27.906	190.021
7	53.244	28.172	218.193
8	52.735	28.444	246.637
9	52.227	28.721	275.358
10	51.719	29.003	304.360
11	51.211	29.290	333.651
12	50.703	29.584	363.235
13	50.195	29.883	393.118
14	49.687	30.189	423.307
15	49.179	30.501	453.808
16	48.671	30.819	484.627
17	48.163	31.144	515.771
18	47.655	31.476	547.248
19	47.147	31.816	579.063
20	46.639	32.162	611.225
21	46.131	32.516	643.742
22	45.623	32.878	676.620
23	45.115	33.249	709.869
24	44.606	33.627	743.496
25	44.098	34.015	777.511
26	43.590	34.411	811.922
27	43.082	34.817	846.739
28	42.574	35.233	881.972
29	42.066	35.658	917.630
30	41.558	36.094	953.724
31	41.050	36.541	990.265
32	40.542	36.999	1027.264
33	40.034	37.468	1064.732
34	39.526	37.950	1102.682
35	39.018	38.444	1141.126
36	38.510	38.951	1180.077
37	38.002	39.472	1219.549
38	37.494	40.007	1259.556
39	36.985	40.556	1300.113
40	36.477	41.121	1341.234
41	35.969	41.702	1382.936

time (sec)	mass (kg)	Acel (m/s^2)	Delta V (m/s)
42	35.461	42.300	1425.236
43	34.953	42.914	1468.150
44	34.445	43.547	1511.698
45	33.937	44.199	1555.897
46	33.429	44.871	1600.768
47	32.921	45.564	1646.332
48	32.413	46.278	1692.610
49	31.905	47.015	1739.625
50	31.397	47.776	1787.400
51	30.889	48.561	1835.962
52	30.381	49.374	1885.335
53	29.873	50.213	1935.548
54	29.365	51.082	1986.631
55	28.856	51.981	2038.612
56	28.348	52.913	2091.525
57	27.840	53.879	2145.404
58	27.332	54.880	2200.284
59	26.824	55.920	2256.204
60	26.316	56.999	2313.203
61	25.808	58.121	2371.324
62	25.300	59.289	2430.613
63	24.792	60.504	2491.116
64	24.284	61.769	2552.886
65	23.776	63.089	2615.975
66	23.268	64.467	2680.442
67	22.760	65.906	2746.348
68	22.252	67.411	2813.759
69	21.744	68.986	2882.745
70	21.235	70.636	2953.381
71	20.727	72.368	3025.749
72	20.219	74.186	3099.936
73	19.711	76.099	3176.034
74	19.203	78.112	3254.146
75	18.695	80.235	3334.381
76	18.187	82.476	3416.857
77	17.679	84.846	3501.703
78	17.171	87.357	3589.060
79	16.663	90.020	3679.080
80	16.155	92.851	3771.931
81	15.647	95.866	3867.798
82	15.139	99.084	3966.882
83	14.631	102.525	4069.406

Interpolate to find time at end of burn	0.269		
Use average of 82 and 83 second accelarations	0.508	100.804	53.442
	0.530		4020.324

Delta V total at Wt.=14.9 (in m/s)

Delta V for Ascent, Ignoring Atmospheric Drag Forces

MACH.XLC

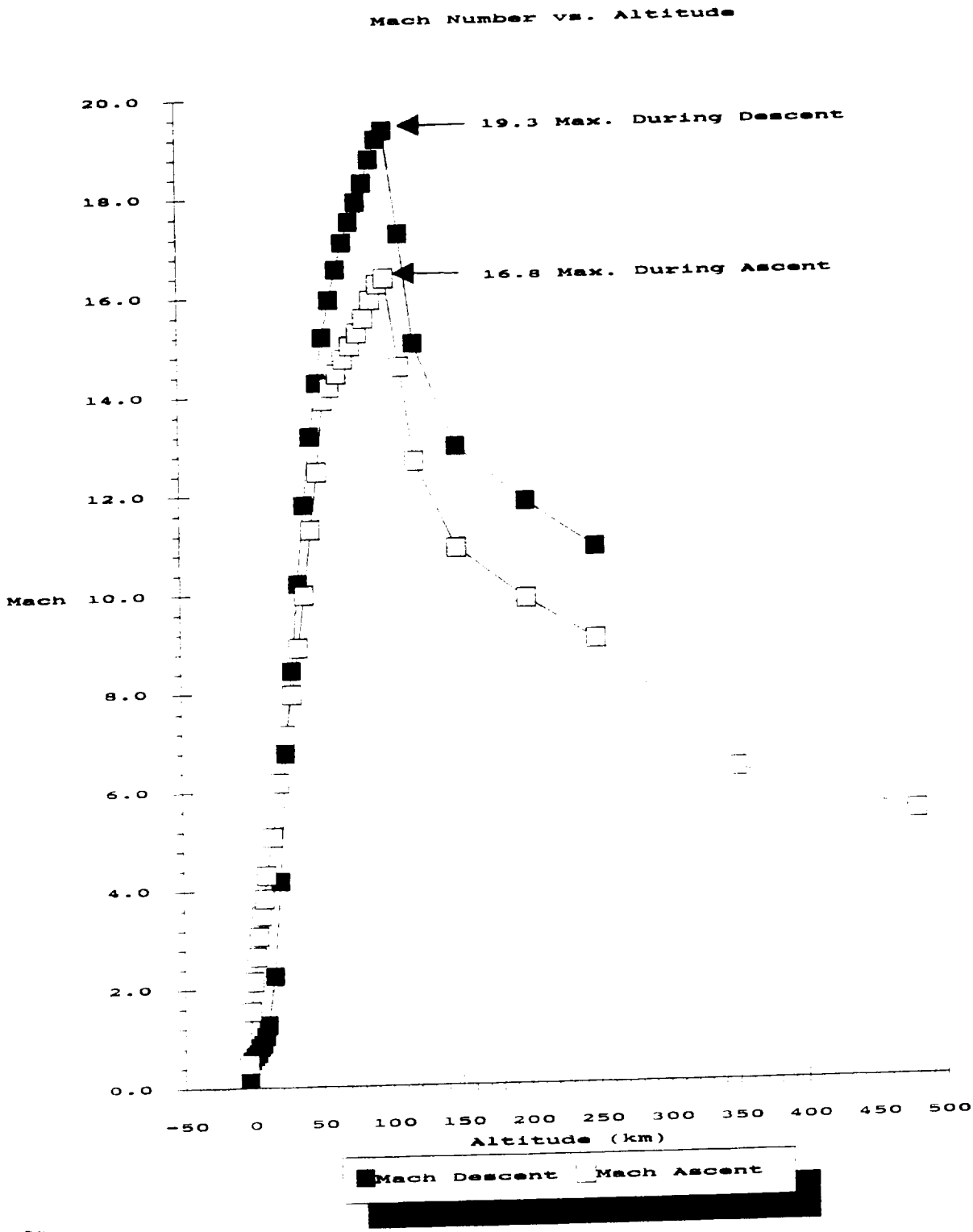

MACH_&_Q.XLS Descent Mach Numbers and Dynamic Pressures

Alt	Density	Speed of	Descent			Ascent		
(km)	(kg/m^3)	Sound(m/s)	V	Mach	q inf	V	Mach	q inf
			(m/s)		(N/m^2)	(m/s)		(N/m^2)
-4	1.35E-02	255	44	0.2	13	119	0.5	96
-2	1.18E-02	253	140	0.6	116	391	1.5	902
0	1.02E-02	252	160	0.6	131	540	2.1	1487
2	8.89E-03	251	174	0.7	135	663	2.6	1954
4	7.72E-03	249	203	0.8	159	763	3.1	2247
6	6.67E-03	248	217	0.9	157	865	3.5	2495
8	5.74E-03	247	254	1.0	185	944	3.8	2558
10	4.91E-03	246	311	1.3	237	1055	4.3	2732
15	3.34E-03	244	548	2.2	502	1236	5.1	2551
20	2.28E-03	240	1002	4.2	1145	1481	6.2	2500
25	1.53E-03	236	1596	6.8	1949	1686	7.1	2175
30	9.99E-04	235	1985	8.4	1968	1872	8.0	1750
35	6.49E-04	234	2387	10.2	1849	2083	8.9	1408
40	4.19E-04	233	2747	11.8	1581	2322	10.0	1130
45	2.74E-04	230	3031	13.2	1259	2595	11.3	923
50	1.76E-04	227	3234	14.2	920	2826	12.4	703
55	1.13E-04	222	3368	15.2	641	3084	13.9	537
60	7.12E-05	217	3453	15.9	424	3072	14.2	336
65	4.43E-05	212	3505	16.5	272	3058	14.4	207
70	2.72E-05	207	3535	17.1	170	3048	14.7	126
75	1.64E-05	203	3551	17.5	103	3402	16.8	95
80	9.75E-06	199	3560	17.9	62	3035	15.3	45
85	5.74E-06	195	3563	18.3	36	3030	15.5	26
90	3.32E-06	190	3563	18.8	21	3022	15.9	15
95	1.88E-06	186	3561	19.1	12	3018	16.2	9
100	1.02E-06	184	3555	19.3	6	3007	16.3	5
110	2.75E-07	206	3550	17.2	2	2997	14.5	1
120	8.72E-08	236	3545	15.0	1	2985	12.6	0
130	3.52E-08	252						
140	1.61E-08	264						
150	8.11E-09	272	3518	12.9	0	2958	10.9	0
160	4.34E-09	277						
170	2.41E-09	281						
180	1.34E-09	288						
190	7.86E-10	291						
200	4.66E-10	294	3472	11.8	0	2894	9.8	0
210	2.81E-10	297						
220	1.71E-10	301						
230	1.06E-10	305						
240	6.60E-11	310						
250	4.17E-11	315	3421	10.9	0	2835	9.0	0
260	2.66E-11	324						
270	1.73E-11	332						
280	1.14E-11	343						
290	7.63E-12	354						
300	5.22E-12	367						
310	3.65E-12	380						
320	2.61E-12	394						
330	1.91E-12	407						
340	1.43E-12	419						
350	1.09E-12	430				2726	6.3	0
480	9.03E-14	480				2583	5.4	0

Section E:

Specialized Structures

Tim Gibson

Parachute

During the descent through the martian atmosphere, the lander will employ a parachute to deaccelerate to a velocity at which the liquid engine can prepare the lander for touchdown. The size of the parachute, measured by its reference area, the area of a circle whose diameter is equal to the distance across the fully deployed parachute, must be large enough to create enough drag so that the required final or "terminal" velocity will be attained, without too much deacceleration during the opening "jerk". It can be estimated from Air Force research (ref. 3) that the peak deacceleration during opening jerk is slightly more than 3 times that of the deacceleration calculated from a force-balance relationship. The lander is limited to a maximum acceleration of 10 earth g's. This limits maximum force-balance calculated deacceleration to under 3.33 g's.

The force-balance relationship is:

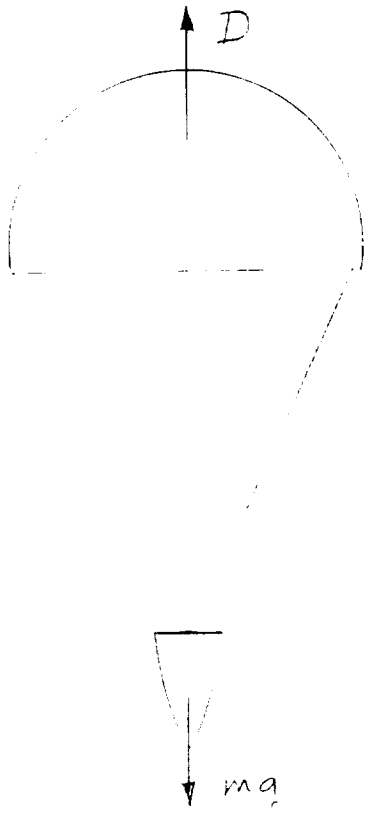

which yields: $D - mg = ma$

where: drag, $D = C_D \, {}^1/_2 \, \partial \, v^2 \, S$
drag coefficient, C_D
atmosphere density, ∂
velocity, V
reference area, S
mass of the lander, m
deacceleration, a

so, we have: $$C_D \, {}^1/_2 \, \partial \, v^2 \, S - mg = ma$$

From this, by setting a = 0, we can obtain the reference area required for a desired terminal velocity:

$$S = {}^{2 \, m \, g} / {}_{C_D \, \partial \, V^2}$$

or, the maximum force-balance deacceleration:

$$a = (CD \; 1/2 \; \partial \; v^2 \; S - mg) / {}_m$$

where V is the deployment velocity.

By starting at V = deployment velocity, and recalculating V every time interval Δt by numerically integrating the acceleration (see Appendix E.4), the maximum descent distance and time to reach terminal velocity can be determined. This method yields a maximum because the actual acceleration rate is, as mentioned earlier, higher than the force-balance method predicts. However, the maximum is desirable for determining the minimum altitude at which the parachute can be deployed safely. Low altitude parachute deployment is desirable to minimize the effect of cross winds.

Initially, the lander was to use a 2-stage parachute. The small first stage, 3.33 m diameter, limited peak deacceleration to 3.14 g's at a deployment velocity of 280.00 m/sec at 1 km altitude (fig. E.1). The larger second stage, 9.9 m in diameter, limited peak deacceleration to 2.69 g's at a deployment velocity of 88.00 m/sec (fig E.2) and attained a terminal velocity of less than 30.00 m/sec

in less than 75 m. This configuration could be deployed at less than 1 km above ground level and maintain a 3 times maximum g's value under our 10g mission limit.

The parachute is an extended skirt canopy type (fig E3) which has a higher drag than flat circular or cross-form types but has a longer opening time and correspondingly has lower peak opening forces. The canopy is fabricated of 2.60 ounce per square yard ($89\ g/m^2$) dacron cloth, per MIL-C-7350, type 1. The suspension lines are tubular braided dacron with an ultimate tensile strength of 2740N. The approximate weight of the canopy can be calculated from the surface area of 1/2 of a sphere:

$$A_{surface} = 2 \pi r^2$$

and a required storage volume (chute pack) based on a maximum packing density of $\approx 600\ kg/m^3$.

So, the mass of the chute canopy, $m_{canopy} = 89\ A_{surface} = 89\ (2 \pi r^2)$,

and the volume of the chute pack, $v_{pack} = (89)\ (2 \pi r^2) / 600 \times 10^3$.

This mass and volume dependence on the radius squared led to an optimization where the weight and size of the parachute were compared to the weight of added liquid fuel to accomplish the same deacceleration. It was determined that decreasing the parachute from 9.9 meters in diameter ($m_{canopy} = 13.7$ kg) to 4 meters in diameter ($m_{canopy} = 0.75$ kg), while adding ≈ 4 kg of fuel, would decrease mass by ≈ 8.9 kg. Also, the volume required for the chute pack went from $0.0228\ m^3$ to $0.00125\ m^3$.

Using the 4 m diameter parachute, an analysis was done (fig. E4) for the earliest possible deployment, 5 km above ground level, with the highest deployment velocity possible, V = 248.54 m/sec. Maximum force-balance deacceleration was 2.47 g's, with a distance to terminal velocity of ≈ 0.5 km. Next, an analysis was done (fig. E5) for a late deployment, -3 km altitude, with a corresponding terminal velocity of 187.4 m/sec. Maximum force-

balance deacceleration was 2.48 g's, with a distance to terminal velocity of ≈ 325 m.

FIG. E3

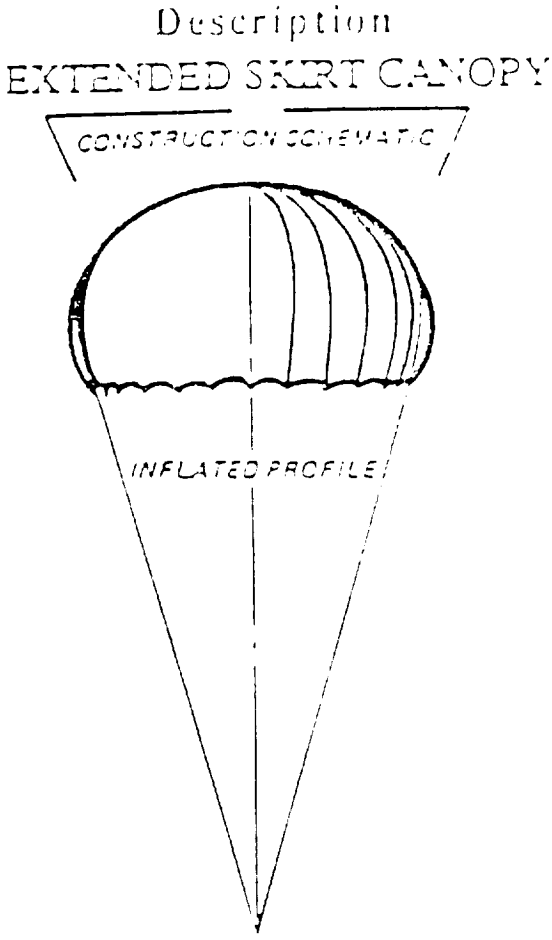

APPENDIX EA

```
      program mars
      implicit none
      real*4  cd, rho, s, g, m, v, vterm, t, h, a, vnew, accel
      real*4  deltat
      integer*4  i
c
      cd = 1.0
      deltat = 0.1
      rho = 0.0127
      s = 12.5664
      g = 3.73
      m = 100.0
      v = 187.4
      vterm = sqrt((2.0*m*g)/(cd*rho*s))
c
      write(6,50) vterm
50    format(1x,'v term = ', f7.3,'m/sec',/,1x,'V (m/sec)',
     *  5x,'h (meters)',5x,'accel (g s)',
     *  5x,'time (sec)')
c
      t = 0.0
      h = 0.0
      do 100 i = 1, 200
         t = t + deltat
         a = (0.5*cd*rho*(v**2)*s - m*g)/m
         h = h + v*deltat - 0.5*a*(deltat**2)
         vnew = sqrt((v**2) - 2.0*a*h)
         accel = a/9.81
         write(6,60) v, h, accel, t
60       format(1x,f7.3,7x,f7.2,10x,f7.5,8x,f5.1)
         if ( v .le. (1.00001*vterm)) go to 200
         v = vnew
      enddo
200   continue
      end
```

FIG. E1

V (m/sec)	h (meters)	accel (g s)	time (sec)
280.000	27.85	3.14891	.1
276.911	55.39	3.07227	.2
270.816	82.32	2.92355	.3
261.952	108.39	2.71320	.4
250.698	133.34	2.45618	.5
237.537	156.98	2.16995	.6
223.025	179.19	1.87222	.7
207.745	199.89	1.57901	.8
192.264	219.05	1.30315	.9
177.101	236.71	1.05366	1.0
162.700	252.94	.83567	1.1
149.412	267.85	.65093	1.2
137.489	281.57	.49855	1.3
127.079	294.26	.37586	1.4
118.233	306.07	.27919	1.5
110.917	317.15	.20451	1.6
105.024	327.65	.14782	1.7
100.398	337.68	.10549	1.8
96.855	347.37	.07435	1.9
94.202	356.78	.05178	2.0
92.258	366.01	.03563	2.1
90.861	375.09	.02423	2.2
89.874	384.08	.01629	2.3
89.189	393.00	.01082	2.4
88.720	401.87	.00710	2.5
88.403	410.71	.00461	2.6
88.193	419.53	.00295	2.7
88.055	428.33	.00187	2.8
87.966	437.13	.00117	2.9
87.909	445.92	.00072	3.0
87.873	454.71	.00044	3.1
87.850	463.49	.00027	3.2
87.836	472.28	.00016	3.3
87.828	481.06	.00009	3.4
87.823	489.84	.00005	3.5
87.820	498.62	.00003	3.6
87.818	507.41	.00002	3.7
87.817	516.19	.00001	3.8
87.817	524.97	.00001	3.9

FIG. E2

V (m/sec)	h (meters)	accel (g s)	time (sec)
88.000	8.67	2.69566	.1
85.356	17.08	2.51574	.2
80.265	25.00	2.18488	.3
73.286	32.24	1.76431	.4
65.229	38.70	1.32630	.5
56.989	44.35	.93109	.6
49.372	49.26	.61311	.7
42.953	53.54	.38056	.8
38.017	57.33	.22368	.9
34.550	60.78	.12494	1.0
32.322	64.00	.06647	1.1
31.004	67.10	.03371	1.2
30.279	70.13	.01629	1.3
29.907	73.12	.00749	1.4
29.727	76.09	.00328	1.5
29.644	79.06	.00136	1.6
29.609	82.02	.00053	1.7
29.594	84.98	.00020	1.8
29.589	87.94	.00007	1.9
29.587	90.90	.00002	2.0
29.586	93.85	.00001	2.1

FIG. E4

v term = 90.802m/sec

V (m/sec)	h (meters)	accel (g s)	time (sec)
248.540	24.73	2.46841	.1
246.118	49.23	2.41317	.2
241.337	73.25	2.30569	.3
234.372	96.58	2.15289	.4
225.501	119.03	1.96476	.5
215.086	140.45	1.75316	.6
203.546	160.73	1.53037	.7
191.323	179.80	1.30781	.8
178.860	197.63	1.09505	.9
166.568	214.25	.89924	1.0
154.806	229.69	.72492	1.1
143.868	244.05	.57427	1.2
133.971	257.43	.44746	1.3
125.253	269.93	.34324	1.4
117.773	281.70	.25941	1.5
111.520	292.84	.19329	1.6
106.424	303.48	.14208	1.7
102.372	313.71	.10307	1.8
99.226	323.63	.07381	1.9
96.835	333.31	.05220	2.0
95.056	342.81	.03646	2.1
93.757	352.19	.02515	2.2
92.826	361.47	.01714	2.3
92.169	370.69	.01153	2.4
91.713	379.86	.00766	2.5
91.401	389.00	.00503	2.6
91.191	398.12	.00326	2.7
91.051	407.22	.00209	2.8
90.960	416.32	.00132	2.9
90.900	425.41	.00082	3.0
90.863	434.49	.00050	3.1
90.839	443.58	.00031	3.2
90.824	452.66	.00018	3.3
90.815	461.74	.00011	3.4
90.810	470.82	.00006	3.5
90.807	479.90	.00004	3.6
90.805	488.98	.00002	3.7
90.804	498.06	.00001	3.8
90.803	507.14	.00001	3.9

FIG. E5

v term = 68.369m/sec

V (m/sec)	h (meters)	accel (g s)	time (sec)
187.400	18.62	2.47641	.1
184.971	37.00	2.40283	.2
180.194	54.91	2.26095	.3
173.304	72.14	2.06283	.4
164.666	88.51	1.82535	.5
154.741	103.91	1.56750	.6
144.046	118.25	1.30756	.7
133.100	131.51	1.06080	.8
122.387	143.71	.83816	.9
112.318	154.91	.64593	1.0
103.209	165.20	.48624	1.1
95.269	174.71	.35805	1.2
88.593	183.56	.25821	1.3
83.180	191.87	.18257	1.4
78.940	199.76	.12667	1.5
75.731	207.32	.08628	1.6
73.377	214.66	.05774	1.7
71.701	221.83	.03796	1.8
70.539	228.88	.02452	1.9
69.755	235.85	.01556	2.0
69.236	242.78	.00970	2.1
68.902	249.67	.00594	2.2
68.690	256.54	.00358	2.3
68.559	263.39	.00211	2.4
68.479	270.24	.00122	2.5
68.432	277.08	.00070	2.6
68.404	283.92	.00039	2.7
68.389	290.76	.00021	2.8
68.380	297.60	.00011	2.9
68.375	304.44	.00006	3.0
68.372	311.28	.00003	3.1
68.371	318.11	.00002	3.2
68.370	324.95	.00001	3.3

Heat Shield Structure

The structure of the heat shield serves to hold the insulation material in position, and serve as an aero-braking device. The 1.5 meter diameter heat shield is designed to withstand a maximum total aero-force of 6.9 kN which occurs at an altitude of 31 km and a corresponding free-stream velocity of 1985 m/sec. The structure in contact with the insulation encounters a maximum temperature of 700 F for approximately 30 seconds.

Due to its high stiffness-to-weight ratio and resistance to thermal effects, a beryllium honeycomb bonded with high-temperature thermoplastic adhesive was chosen for the heat shield structure. Four beryllium tubular braces serve to brace the structure (see fig. E6).

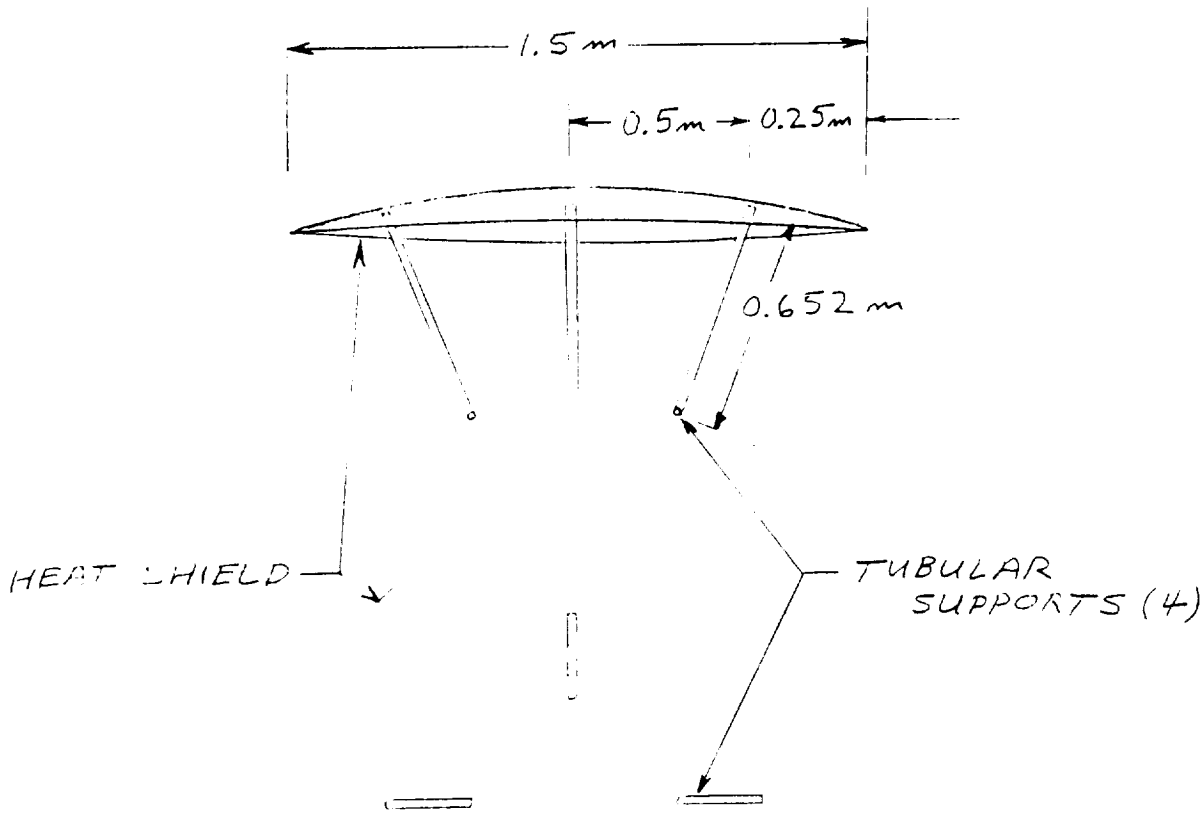

FIG. E6

In order to conservatively size the structural components simplified models (see fig. E7) were chosen which would provide an adequate safety margin and facilitate analysis.

FIG. E7

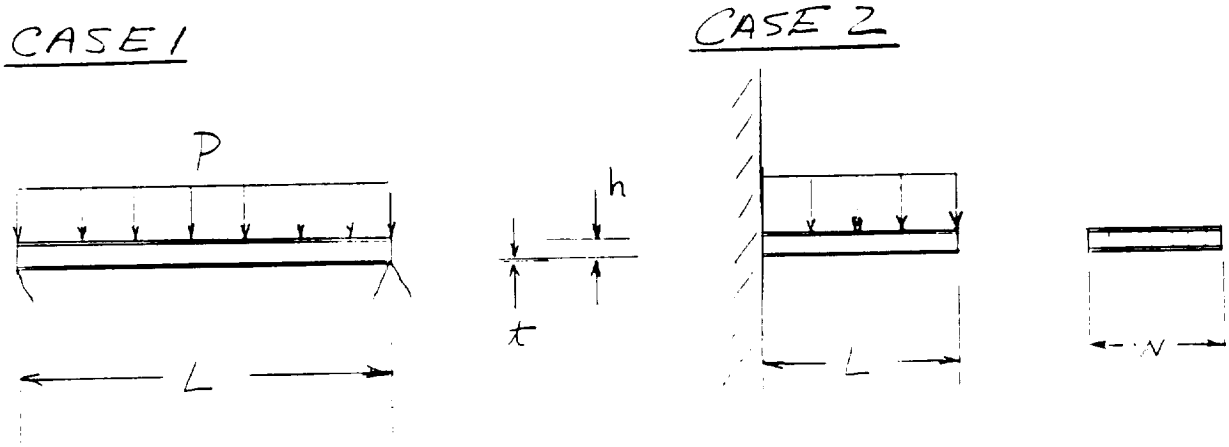

where: unsupported length, L
load per unit length, P
depth of honeycomb, h
thickness of face sheet, t
width of beam, w

From strength of materials the stress is: stress = My/I

now, $y = {}^1/_2 d + t$, but since $t \ll {}^1/_2 h$, $y = {}^1/_2 d$

and, by the parallel axis theorem $I = {}^2/_3 wt^3 + 2wt({}^1/_2 d)^2$

since ${}^2/_3 wt^3 \ll 2wt({}^1/_2 d)^2$, we have $I \approx 2wt({}^1/_2 d)^2 = {}^1/_2 wtd^2$

so, stress $\approx M(1/2)h / (1/2)wth^2 = M/wtd$

or, letting M = moment per unit width, stress = M/td

Also from strength of materials we know the maximum moment, M, of our model beams (fig. E-7) for case 1 is equal to

$$M\ (max.) = PL^2/8\ ,$$

and for case 2

$$M\ (max) = PL^2/8\ .$$

Using a maximum unsupported length of L = 1 m for case 1 and L = 0.5 m for case 2, we have:

$$M\ (max) = P/8$$

Now $stress_{crit}$ for beryllium = $stress_{yield} = 3.24 \times 10^8\ N/m$ and the distributed load,

$$P = \text{Aero-force}/\text{area} = (6.9\ Kn/\pi(.75m)^2)(1m) = 3905\ N/m$$

Rearranging, we have: $t\ d = P/8(stress_y) = 3905/8(3.244 \times 10^8)$

$$= 1.507 \times 10^{-6}$$

Taking the minimum thickness for the beryllium face sheets to be t = 0.010" = 0.000254 m, $\Rightarrow d = 1.507 \times 10^{-6}/.000254$

$$= 0.00593m = 0.23\ in$$

so, we will specify a beryllium honeycomb with a core depth, d = 0.25" = 0.00635 m. Checking, we have

$$stress_{crit} = {}^{3905}/_{8(.00635)(.000254)} = 3.03\times10^{8}\ {}^{N}/_{m^2}$$

which is over 6% under $stress_y$.

Now, in order to determine the mass of the structure the density of the honeycomb core is needed. A "rule of thumb" for estimating honeycomb

core density is $\partial_{core} = {}^{2\partial_{Be}V_{max}}/_{stress_{Be\ shear}}$

where: density of Be, $\partial_{Be} = 1826\ {}^{kg}/_{m^3}$
shear stress of Be, $stress_s \approx 0.6\ stress_y$

and the maximum shear stress, again from strength of materials, is

$$V_{max} = {}^{1}/_{2}P = 1.952.5\ N$$

so, $$P_{core} = {}^{2(1826)(1952.5)}/_{0.6(3.24\times10^{8})} = 0.0376\ {}^{kg}/_{m^3}$$

The lightest core material available is approximately 1.5 lbs/ft or 24 kg/m. Apparently the shear force is too low in this application for the "rule of thumb" approximation to be accurate. It does indicate though that it is safe to use the lightweight core. So, the mass of the structure is:

$$Mass = 2\partial_{Be}(\pi r^2 t) + \partial_{core}(\pi r^2 d)$$

$$= \pi r^2(2\partial_{Be}t + \partial_{core}d)$$

$$= \pi(.75)^2[2(1826)(.000254) + 24(.00635)] = 1.91\ kg$$

The model for the tubular braces is simple compression (see fig $E\ 3$). The force in each tube may be as high as

$$F = (1.5)({}^{max.\ aero\text{-}force}/_{\#\ of\ tubes})$$

where: max. aero-force = 6.9 kN
# of tubes = 4

so $F = (1.5)\ (6900)/4 = 2588$ N

FIG. E8

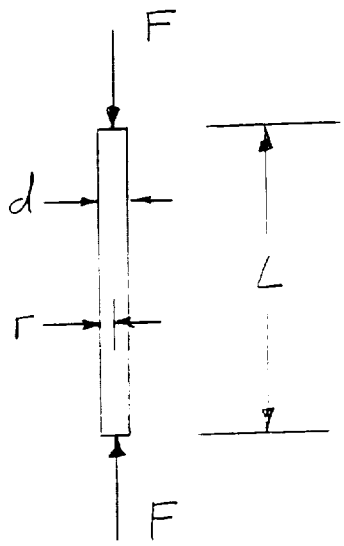

where: diameter, d
radius, r
length, L
wall thickness, t
force, F

For a thin wall tube under compression there are three design constraints:

1) stress limit: stress = $F/\pi dt$

2) Euler buckling: $F = \pi^2 EI/L^2$

3) crippling: stress = $0.3Et/r$

For a first iteration, the stress limit and Euler buckling are solved together in order to find the optimum tube dimensions, where

$I = \pi r^3 t$ for a thin-wall tube.

Now, solving 1) and 2) for the force, F, yields

$$(\text{stress})2\pi rt = \pi^2 E \pi r^3 t / L^2$$

$$\text{so} \quad r = 2(\text{stress})L^2/\pi^2 E = 2(.652)^2(3.24\times10^8)/\pi^2(2.896\times10^{11})$$

$$= 0.009817 \text{ m.}$$

This is a tube with a diameter of 0.0196 m or 0.773". Solving for the wall thickness, t = 0.0001313 m = 0.0052 in. In order to specify a tube which might be commonly available, we will use 0.75 in. (0.01875 m) diameter and 0.010 in. (0.000254 m) wall thickness beryllium tubing. Checking, we have:

1) stress limit, $F = (\text{stress})2\pi rt = 4848$ N

2) Euler buckling, $F = \pi^2 EI/L^2 = 4421$ N

3) crippling, $\text{stress} = 0.3Et/r = 23.5\times10^8$

which are all considerably over any anticipated forces. Now, the mass of

each tube is, $\text{mass/tube} = \pi dtL\partial_{Be}$

$$= \pi(.01875)(.000254)(.652)(1826) = .0178 \text{ kg}$$

So, the total for four tubes is $4(0.0178) = .0712$ kg

Therefore, the mass of the entire structure is: $1.91 + .0712 = 1.98$ kg

Soil Sample Collection

The mission requirement is to bring 1 kg of Martian soil back to the orbiting MOV (Mars Orbiting Vehicle). This will be accomplished with the use of an extendable surface sampler, which consists of a collector head attached to the end of a retractable boom. The boom is constructed from two ribbons of beryllium welded together along the edges. When extended, the two layers opened to form a rigid tube. When retracted, the boom flattens onto a storage spcol. A flat cable sandwiched between the boom layers transmits electrical power to the collector head.

The collector head is a scoop with a movable lid. To fill the scoop, the boom is extended along or into the surface. Once full, the lid closes. The boom is then elevated such that the scoop can be dumped into a container at the top of the lander (fig. E 9). The nose cap at the top of the lander's aero-shell (fig. E 10) is moved upward by a threaded driveshaft and, when free of the aero-shell, is then rotated out the way for dumping into the sample container.

Design considerations include tube buckling and bending stresses, and torque for pushing the scoop into the Martian soil, lifting the sample into the container, and opening and closing the container.

Data, Martian soil:

density, ∂ = 0.7 to 3.2 $^{g}/_{cm^3}$,
maximum penetration resistance, PR = 6 $^{N}/_{cm^2}$ cm

Scoop

Volume required for 1 kg sample, ∂ = 0.7 $^{g}/_{cm^3}$

$^{1}/_{700}$ = 0.00143 m^3 = 1430 cm^3

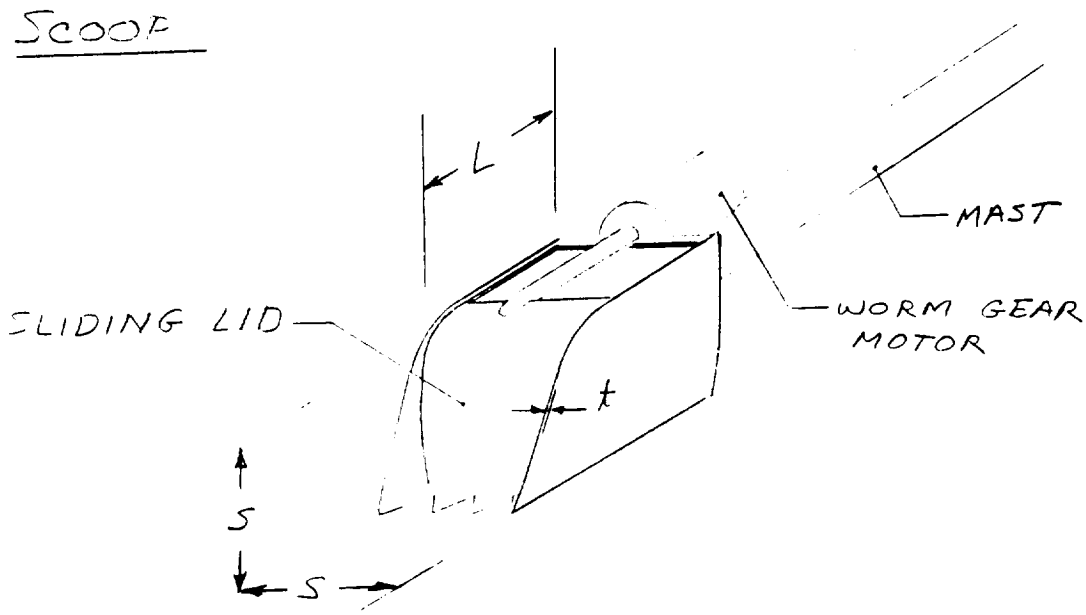

where: s = scoop side, L = scoop length, t = material thickness.

Since the collector is being driven into the soil, titanium is used as a material for the scoop due to its toughness. The worm-gear motor should have enough torque to close the lid against maximum penetration resistance. Now, the force needed to drive the scoop into the soil,

FIG. E9

SAMPLER-ARM OPERATION

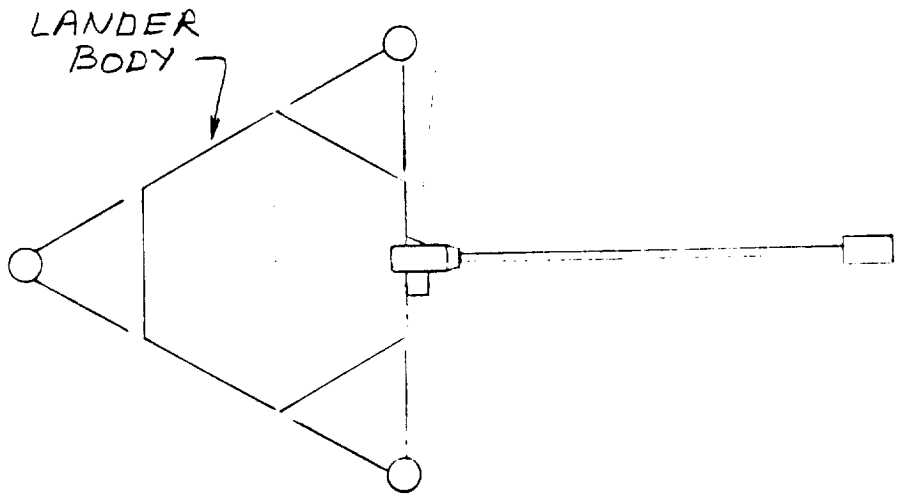

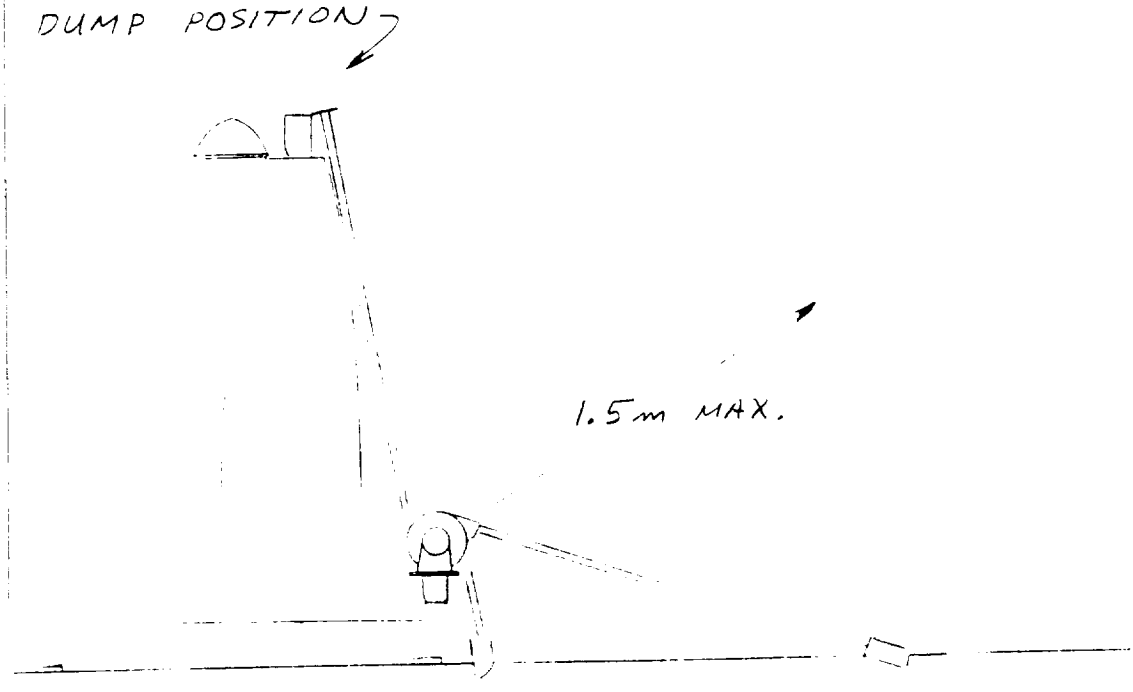

FIG. E10

CONTAINER COVER

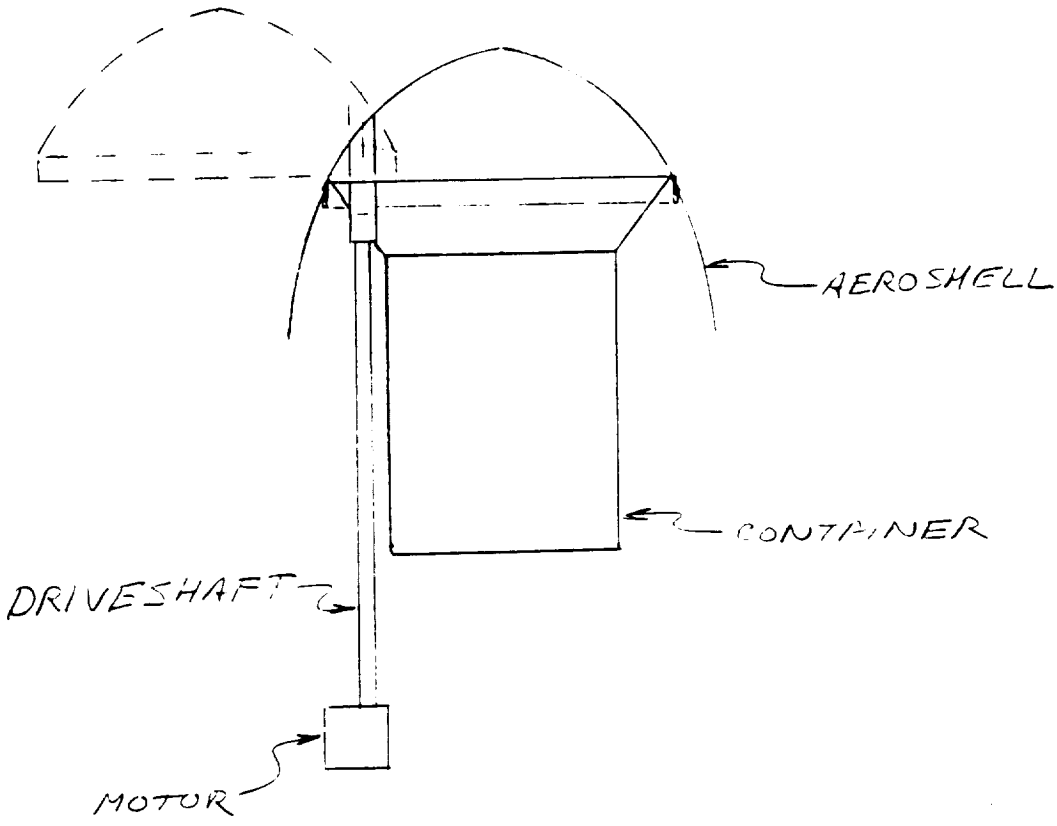

F = PR (length) (scoop cross sect. area)

where: scoop area = 4 st, and length, L = 16.5 cm, s = 10.16 cm, and t = 0.010 in = 0.0254 cm,

so, F = (PR) (L) [4 (s) (t)] = 6 (16.51) [4 (10.16) (0.0254)]
= 102.26 N

A force of F = 200 N will be used in the design of the sampler apparatus to insure an adequate safety margin.

Mast

The dimensions of the mast (boom) will be governed by maximum compressive stress, Euler buckling, and bending. The bending requirement will be to lift the scoop, sample, and mast into the "dump position."

Maximum length of mast = 1.5m

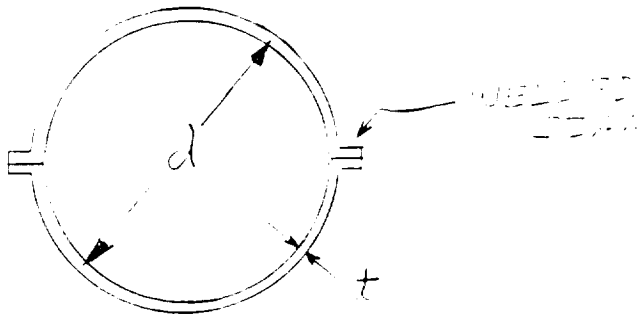

The wall thickness of the beryllium mast is taken to be 0.0508mm, which is common for the welded seam type masts.

t = 0.0508 mm = 5.08 x 10^{-5}m
= 0.002 "

In order to find the minimum diameter, maximum compressive stress is considered:

$$\text{stress}_y = F/A \quad \Rightarrow \quad F = \text{stress}_{yield} A = \text{stress}_y \pi dt$$

$$\Rightarrow \quad d = F/\text{stress}_y \pi t = 200/(3.24\times10^{8})\ \pi\ (5.08\times10^{-5})$$

$$= 0.00387 \text{ m}$$

so, $$d = 0.387 \text{ cm}$$

Now consider Euler Buckling: $F = \pi^2 EI/L^2 = \pi^2 E \pi r^3 t/L^2$

so, $r = (FL^2/\pi^3 Et)^{1/3} = (200(1.5)^2/\pi^3(2.896\times10")(5.08\times10^{-5}))^{1/3}$

$$= 0.00995 \text{ m}$$

$$d = 0.01991 \text{ m} = 1.991 \text{ cm} = 0.784 "$$

and finally bending, from strength of materials: $\text{stress} = My/I$,

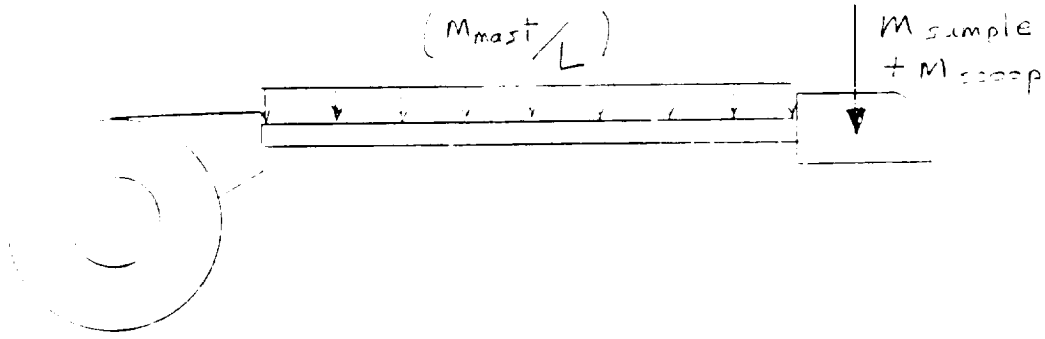

Mass of Be mast of length 1.5m,

$$m_{mast} = \pi dLt\partial_{Be} = \pi d(1.5)(5.08\times10^{-5})(1826) = 0.437d$$

Now, the moment, $M = m_{mast}(1/2 L) + m_{sample}L + m_{scoop}L$.

$m_{scoop} = 4(.1016)(.000254)(.1651)\partial_{Ti} = 4621\ {}^{kg}/_{m^3} + m_{worm\ gear\ motor}$

$m_{worm\ gear\ motor} = .45\ kg$

so $m_{scoop} = 4(.1016)(.000254)(.1651)(4621) + .45\ kg$

$= .0788\ kg + .45\ kg$

so $M = .437d(.75) + (1.5) + .5288(1.5) = .3277d + 2.2932$

and $I = \pi r^3 t = ({}^{\pi}/_{8})d^3 t$

so $stress_y = {}^{My}/_{I} = {}^{(.3277d + 2.2932)4}/_{\pi d^2(5.08x10^{-5})}$

$= {}^{(1.31d + 9.1728)}/_{(1.596x10^{-4}d^2)}$

but $stress_y = 3.24x10^8$, so, rearranging, we have

$5.171x10^4 d^2 - 1.31d - 9.1728 = 0$

or $d^2 - 2.533x10^{-5}d - 1.774x10^{-4} = 0$

solving for d:

d	F(d)
.01991	.0002185
.05	.00232
.01	-.000077653
.015	.00004722

so, for bending $0.010m < d < .015m$. The Euler buckling in compression is the limiting case, therefore the diameter is chosen to be $d = .01991$ m.

Finally, an analysis of crippling failure:

$$F_{crip}/\pi dt = 0.3E^{2t}/d$$

$$F_{crip} = 0.3\pi(2.896x10")2(5.08x10^{-5})^2 = 1408\ N$$

The apparatus is designed for a maximum of 200N, so there is no problem here.

Reel Assembly

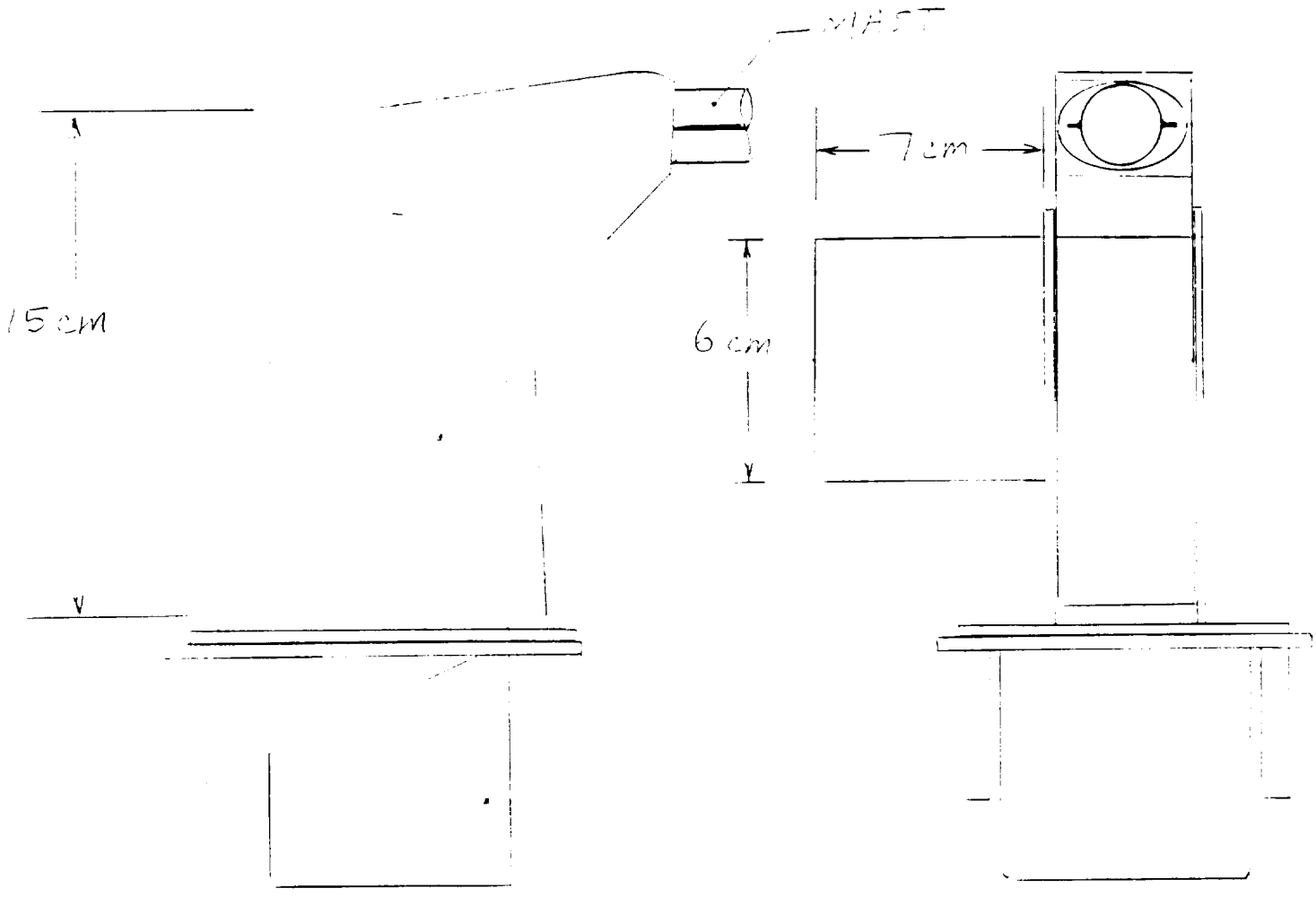

Worst case torque required would occur while forcing scoop into soil, so $T = Fr$ where $F = 200$ N

$r = 7.25$ cm $= 0.0725$ m

$T = 200(.0725) = 14.5$ Nm

$= 128.3$ in lbs

A Hurst Instrument Motor #2602-001 has a mass of 0.68 kg and delivers 250 in lbs of torque at 1 RPM, which corresponds to a scoop speed of1.5 $^{cm}/_{sec.}$ The maximum power requirement of each motor, $P \approx 54$ watts, so the electrical power requirements per sample collection are:

time for unreeling at 1.5 $^{cm}/_{sec} \approx 100$ sec, 2 (100) = 200 sec,
motors running = 3, => 32400 watt-sec,
time to rotate through boom swing ≈ 30 sec, 2 (30) = 60sec,
motors running = 3, => 9720 watt-sec,
time to rotate to dump position at 1 RPM ≈ 15 sec, 2 (15) = 30 sec,
motors running = 4, => 6480 watt-sec,
time to dump ≈ 15 sec,
motors running = 4, => 3240 watt-sec.

So, the total energy required per try ≈ 51840 watt-sec.
The lander will have 300 watts available for 10 minutes (600 sec) = 180000 watt-sec. Therefore there will easily be enough energy for at least 3 complete attempts.

References

Parachute

1) Eckstrom, C. V. and J. S. Preisser. "Flight Test of a 30-Foot Nominal Diameter Disk-Gap-Band Parachute Deployed at a Mach Number of 1.56 and a Dynamic Pressure of 11.4 Pounds Per Square Foot." TM X-1451, Sept. 1967, NASA.

2) Ewing, E. G., H. W. Bixby and T. W. Knacke. "Recovery Systems Design Guide." U.S. Air Force AFFDL-TR-78-151, December, 1978.

3) Cockrell, D. J. "The Aerodynamics of Parachutes." NATO's Advisory Group for Aerospace Research and Development AGARDograph No. 295, July, 1987.

4) Peterson, C. W. "High-Performance Parachutes." Scientific American, May 1990.

5) Gillis, C. L. "Deployable Aerodynamic Decelerators for Space Missions." AIAA Journal of Spacecraft and Rockets, Vol 6, No 8, August 1969.

Heat Shield

6) Bruhn, E. F. *Analysis and Design of Flight Vehicle Structures.* Indiana: Jacobs Publishing Inc., 1973.

7) Ugural, A. C., and S. K. Fenster. *Advanced Strength and Applied Elasticity.* New York: Elsevier Science Publishing Co., Inc., 1987.

8) Agrawal, B. N. "Design of Geosynchronous Spacecraft." Prentice-Hall, Inc., 1986.

9) Preliminary minimum sizing "rule of thumb" for honeycomb core density for shear strength at Hughes Aircraft.

10) Roark, R. S. *Formulas for Stress and Strain*, 4th ed. McGraw Hill.

11) ASME ME Magazine, Materials Reference Issue, 1988.

12) Rennie, B. B. "New Closed Tubular Extendable Booms." Proc. Second Aerosp. Mech. Symp., Herzl, G. G., ed., JPL TM 33-355, August 15, 1967.

13) Herzl, G. G. *Tubular Spacecraft Booms (Extendible, Reel Stored)*, Volume 2. California: Published by author, 1970.

14) Meyer, R. X. "Planet Mars." Class handout, Spring Quarter 1990.

15) N81-10101, 318pp, Viking '75 spacecraft design. NASA Reference Publications from UCLA Engineering Library.

16) N84-35248, 545pp, Mars exploration, Mars data; Mariner, Voyager, Viking spacecraft. NASA Reference Publications from UCLA Engineering Library.

17) "Viking Exploration of Mars." National Geographic Magazine, Vol 151, No 1, Jan, 1977.

CONCLUSIONS

We believe our conceptual design to represent the best version of the three being presented this quarter. This design has by far the lightest weight and shows much evidence of the optimization proceedures we used to improve our designs while the competing designs were busy attempting to incorperate some of the best features of our earlier models. Although our design is by no means perfect and optimized in every possible way, it certainly represents a very solid foundation upon which a final design may eventually be built. Our team has enjoyed this project very much and we all feel we have learned a great deal while working on it and we look forward to working on similiar challenging projects in the world outside of UCLA.